Field Measurement and Evaluation of Time-Dependent Losses in Prestressed Concrete Bridges

Project Number: WPI-0510735

Draft Final Report

submitted to

Florida Department' of Transportation

Dr. Moussa Issa, P.M.

by
Dr. Okey Onyemelukwe, P.L
Dr. Sashi Kunnath, Co-P.I.

University of Central Florida
Orlando, Florida 32816

February 24, 1997

TABLE OF CONTENTS

LIST OF TABLES

LIST OF FIGURES

CHAPTER 1

INTRODUCTION

1.1 Background

The Florida Department of Transportation (FDOT) is frequently confronted with contractor suggested redesigns of some of its prestressed concrete bridge projects. In which case most of the contractors call for changing the bridge girder design from its original post-tensioned continuous members to longer simple supported spans. Often, these result in deeper simple span girders with larger cross-sectional areas, moment of inertia and consequently, greater ultimate capacity. Thus, enabling the designer to eliminate the post-tensioning and change the statical scheme from continuous to simply supported.

Therefore, although the girders are designed as simple spans, the attached deck slabs remain as continuous members. The final configuration of both the deck slab and the girder acting as a unit, is in essence a hybrid between a strictly statically indeterminate structure and a determinate structure. Further investigation of this sort of design is necessary, since the time-dependent behavior of these members with respect to creep,

shrinkage and steel relaxation is drastically different for indeterminate structures when compared to simple ones.

Therefore, it is the objective in this project to conduct the following studies:

- Instrument sections of the bridge girder and deck slab for strain and temperature measurements, which will be used in determining the prestress losses in the members

- Utilize the field measured data to determine the effects of the relative shrinkage between the continuous slab and the simply supported beam.

- Reduce and process the measured data to form a useful database for future use by MOT in related projects

- Use analytical and code procedures for prestressed concrete bridge design to establish the adequacy or ramifications of the modified design. Especially, since most of these redesigns claim the simply supported system has the same structural capabilities as the continuous post-tensioned design, and that both designs should be considered equivalent.

In this report the effects of time-dependent prestress losses in prestressed concrete bridges are studied. Time-dependent behavior of concrete is an important consideration in

the design and analysis of structures, especially with respect to prestressed concrete bridges. Both prestressed concrete and conventional reinforced concrete tend to deform with time. The reasons for these continuous deformations include creep and shrinkage. These deformations directly affect the strains in the concrete, which also change with time. Therefore, creep and shrinkage must be compensated for before a member can perform at its best. Without accounting for creep and shrinkage effects, serviceability problems may arise with excessive camber, deflection, and/or flexural stresses. The change in stress due to the above mentioned phenomena are classified as part of the prestress losses, and must be accounted for in the design of prestressed concrete members.

There are two categories of prestress loss: instantaneous losses and timedependent losses. The instantaneous prestress losses are made up primarily of anchorage slip, friction, and elastic shortening. These losses occur only once and do not necessarily vary with time. The time-dependent losses consist of creep and shrinkage of concrete and relaxation of the prestressing steel. These losses vary throughout the lifetime of a member and increase rapidly at the early age of the concrete, while increase over the remaining life occurs at a decreasing rate.

Prestress losses are often accounted for by two different approaches. One method takes a known lump sum value established from similar members as the prestress loss for the member being examined. In this approach, the prestressed loss is often expressed as a percentage of the initial stress applied to the steel strands. The other method involves calculating each contribution of the loss separately, summing these components and taking

that sum as the total prestress loss. In the sections that follow, a general overview of prestressing of concrete structures will be presented. After which, more specific details as they apply to the Westbound Gandy Bridge project will be covered.

1.2 Methods for Prestressing Concrete

Prestressed concrete involves the pre-application of compressive force, transferred from the steel tendons, to the surrounding concrete. This compressive load, which is typically eccentric, is designed to counteract the service load that will be applied on the member during its lifetime. Upon application of this prestress force, the beam will bow concave upward from the casting bed and rest on its ends. This bowing action caused by the preloading is referred to as camber or "negative deflection." The stress distribution resulting from the prestress force would consist of tensile stresses toward the top of the member and compressive stresses toward its bottom. As the service loads are applied the member tends to deform downward or deflect, overcoming the initial camber. This results in the member being mainly kept in compression toward its top, and with little or no tensile stresses near the bottom. Since concrete is much stronger in compression than it is in tension, it would be beneficial to keep the member in as much compression as possible. This is precisely what prestressing does, it virtually eliminates tensile stresses that would otherwise occur under service load conditions.

Prestressed concrete offers many advantages over conventional reinforced concrete. For example, prestressed concrete allows for the use of stronger materials, such as high-strength steel (with yield strengths of 18621VIPa (270 ksi)) and high-strength concrete (with compressive strengths of 34.5 MPa (5 ksi) and above). These materials cannot be used with conventional reinforced concrete because their properties are not consistent with that type of design. The higher strength concrete and steel allow for smaller and lighter sections, than those used for conventional reinforced concrete members with the same load carrying capacity. Cracking, deflections, and service load stresses can be controlled easily using these high-strength materials with prestressed concrete.

It is theoretically possible to design a member with zero tensile stress and such a case is known as full prestressing. This case is very limiting and often leads to troublesome excessive camber after loads are applied. This excessive camber in flexural prestressed members can create uneven driving surfaces in bridges, or promote cracking in walls of buildings as well as other problems. These problems have lead to a viable alternative to full prestressing known as partial prestressing. Lying somewhere between both conventional reinforced concrete and full prestressing is partial prestressing. This midway alternative requires the use of conventional steel reinforcement in addition to prestressing steel, depending on the design, to provide additional load carrying capacity. Quite often the non-prestressed steel is also used to control the crack width that develops in the member.

Prestressed concrete is used in many different types of structures such as bridges, parking garages, and floor beams in buildings to name a few. The advantages of

prestressed concrete are vast, which explains why the use of this form of construction has continued to increase throughout the years.

There are two methods used to induce a compressive load on a prestressed concrete member. These methods are pretensioning and post-tensioning. The basic idea of pretensioning is that the steel strands are tensioned before the concrete is cast around them. With post-tensioning, the steel strands are not tensioned until after the concrete has been casted. A brief discussion of these two methods will now be presented.

1.2.1 Pretensioning

Pretensioning consists of prestressing the tendons before the concrete is casted around it. In order to achieve this, it is necessary to attach the ends of the prestressing strands to permanent abutments. Then at one abutment a jack is used to tension the strands against the other abutment. After the concrete is casted and achieves sufficient strength, the strands are then cut from the abutments allowing the prestress to be transferred to the concrete. This stress is transferred through the bond between the concrete and the prestressing steel. Some advantages to pretensioning are the ability to produce many beams within a shorter period of time and under controlled conditions. A specific method for pretensioning concrete is the long'-line method. This method prestresses strands for many members which will be casted end-to-end along a single bed. This economical method saves on labor costs and allows for reusable forms.

Pretensioning is the method predominantly used for prestressing concrete in the industry today.

1.2.2 Post-tensioning

Post-tensioning involves casting concrete around conduits which contain unstressed steel. After the concrete reaches a specified strength these strands are then tensioned, usually at the construction site. The beam is prepared with a special anchorage system at one end which allows it to be tensioned against itself. Quite often multiple beams are post-tensioned at the same time to form one continuous member. In this case the conduits are left empty during casting and the strands are shot through just before tensioning. Post-tensioning is usually done in the field. After the strands are tensioned, grout is then pumped into the conduits filling any voids that may be present. An advantage of post-tensioning is that the conduits can be easily shaped to allow for many different types of tendon profiles. Post-tensioning also allows for the combination of single members to form one continuous unit. This is achieved by passing the steel tendons through the ducts of each of the members and tensioning the strands, thus causing these members to act as one. [1]

Pretensioning and post-tensioning of prestressed concrete offer many different alternatives to the designer. In most situations, the design itself will dictate which of these options is more viable.

1.3 Prestress Losses

1.3.1 Introduction

In our discussion so far about prestressed concrete there has been little detail on the variation of prestress force during the lifetime of the member. This is important because the constant prestressing force first applied does not remain constant during the lifetime of the structure. The loss of prestress, which is broken down into instantaneous and time-dependent losses, accounts for this variation in force and stress in the strand. The instantaneous prestress loss represent losses felt just before or immediately after the transfer of the prestressing force to the concrete. Conversely, the time-dependent prestress losses are those that are constantly varying throughout the lifetime of the member. It is important to accurately account for both of these types of losses. Failure to do so will affect serviceability conditions more so than the ultimate capacity of the member. Camber, deflection, and cracking are examples of service conditions that can be affected by incorrectly computing the prestress losses. Such errors would have little effect on the ultimate strength of a flexural member unless the steel tendons are unbonded or if their final stress after losses is less than $0.5f_{pu}$, where f_{pu}, is equal to the ultimate strength of the prestressing strand.[2]

1.3.2 Instantaneous Losses

The instantaneous prestress loss which occurs just before, or at transfer of prestress from the strands to the concrete consists of three main constituents: frictional losses, anchorage slip, and elastic shortening of the concrete. Depending on the method of prestressing being used some of these losses may not be applicable. A brief description of these losses and when they apply follows.

1.3.2.1 Anchorage Seating Loss and Frictional Losses

Upon transfer of the prestress force to the anchorage seat, some slippage is caused due to the deformation of the connection holding the steel strands. This causes the stressed tendons to loosen and lose some stress. Typically the anchorage slip can be compensated for by overstressing the steel strands. Anchorage slip is typically applicable to post-tensioning although in pretensioning a comparable condition occurs with the connections at the abutment.

The loss of prestress due to friction occurs between the steel tendons and its duct or ducts. Hence, this type of loss is often associated with post-tensioning. The loss is comprised of two parts: the wobble effect and the curvature effect. These effects deal with the friction due to the misalignment of the ducts, and accidental curvature of the steel tendons, respectively. The frictional loss varies with the length of the member. The frictional loss can also be compensated for by overstressing the tendons. In general,

frictional losses only apply to post-tensioned members and are often neglected for pretensioned members because its effect is usually very small.'

Anchorage seat and friction loss are mechanical types of loss. These losses are the difference between the jacking load and the applied load. The anchorage seat and frictional losses can be calculated and either partially or fully compensated for by overstressing.[4]

1.3.2.2 Elastic Shortening

Elastic shortening of concrete deals directly with the relationship between the prestressing steel strands, and the surrounding concrete which is bonded to it. The transfer of the prestressing force to the steel strands causes them to shorten, which in turn causes the bonded concrete to shorten as well. Elastic shortening is usually calculated at the prestressing steel centroid and is accounted for differently depending on the method of prestressing used.

For a pretensioned member, elastic shortening usually varies with length with a maximum occurring at the midspan. In post-tensioned members, the loss is dependent upon whether the strands are all tensioned at the same time or in a sequential order. If the strands are all tensioned at once, there is no loss from elastic shortening. On the other hand, if the strands are stressed at different times elastic shortening loss will occur and must be accounted for.

These instantaneous losses, made up of anchorage slip, friction, and elastic shortening, reduce the jacking stress and subsequent force to some lower value. The reduced force is often referred to as the initial prestress force. This force will be considered the actual force applied to the member. However, the initial prestress force does not remain constant, it will be reduced by the time-dependent prestress losses.

1.3.3 Time-Dependent Prestress Losses

The prestressing force is continually changing throughout the lifetime of a structure. This change is not only because of the variation of service loads, but because of the time-dependent prestress losses. These losses, as their name suggests, are time variant. As time proceeds the rate of increase of these losses continues at a decreasing rate. The time-dependent losses are primarily made up of three components. These are creep and shrinkage of the concrete, and relaxation of the prestressing steel after its application to the concrete. It is very difficult to determine each individual contribution of these losses to the time-dependent loss as a whole because they are all inter-related. Hence, a variation in one directly causes a change in the others and vice-versa.

1.3.3.1 Creep

Creep is the continual straining of concrete under sustained loading for a period of time. The phenomenon of creep is not only a problem for prestressed concrete, but for all types of concrete members that have a constant load for a duration of time. This excess

deformation due to creep is caused in addition to the immediate elastic straining created by the application of the load. As time of loading increases the effect of creep gradually diminishes. These creep strains created are usually more significant than the elastic strains. Unlike elastic strains, only a portion of the creep strains are recoverable.

The creep of concrete due to the prestress in turn reduces the stress in the steel, which causes prestress loss. Creep is directly effected by the shrinkage of concrete and the relaxation of the steel, both which will be explained later. These three time-dependent mechanisms are inter-related and work together to create prestress loss over time.'

Creep is influenced by many factors. Some of these factors include; amount and duration of sustained loading, age at time of loading, water-to-cement ratio of the concrete mixture, aggregate modulus of elasticity and aggregate-paste ratios, the size of the concrete member, and amount of steel reinforcement present. Most of these effects would be considered in determining the prestress losses in the Gandy Bridge Project.

1.3.3.2 Shrinkage

Shrinkage is the time-varying loss of excess water in a concrete member. Like creep, shrinkage is not just a problem for prestressed members but all concrete members in general. When the concrete for a member is poured it usually contains water above what is necessary for chemical hydration of the cement to enhance its workability. This excess water slowly evaporates throughout time.

Shrinkage causes the member to shorten, which in turn leads to loss of some stress in the prestressed steel tendons. If a member was totally immersed in a 100 percent relative humidity environment over its life, there would be no shrinkage loss. But since such a condition is highly irregular over the life of a member, shrinkage must be accounted for.

Shrinkage of concrete is affected by many different factors. Some of these factors include the materials used in the concrete design and mix. These include; the type of aggregate used, the water-to-cement ratio, the type of admixtures and cement used. The physical properties of the member may also affect the amount and rate of shrinkage occurring. The strength of the concrete used, the amount of steel reinforcement used, and the volume-to-surface area ratio are some of these physical properties. The existing environmental conditions such as ambient temperature and relative humidity play a part in determining the shrinkage that will occur.

1.3.3.3 Steel Relaxation

Steel relaxation is the decrease of stress in a tendon while the length remains relatively constant. This differs from creep of concrete, which is change in strain under a constant stress. The tendon length is assumed constant when considering the prestress loss from steel relaxation. In reality this is not the case, the length is affected by the other time-dependents losses, namely creep and shrinkage of the concrete a well as changes in the applied loads.

Steel relaxation is not the only loss that affects the stress in the steel tendons. Elastic shortening, creep, and shrinkage of the concrete also change the stress in the prestressing steel. This inter-dependence between the steel relaxation, elastic shortening, and the other time-dependent losses further complicates the calculations of the individual components of the total loss.

There are a few conditions that influence steel relaxation. The amount of prestress applied to the steel tendons, the type and strength of the tendons used, and the time the stress was applied are the primary conditions of importance. Another factor that is considered in accounting for the loss due to steel relaxation is the method of prestressing used to tension the member. For pretensioned members, there is steel relaxation occurring before the strands are applied to the concrete as well as after. The steel relaxation for these two time periods are accounted for differently. For post-tensioned members, the steel relaxation loss begins immediately after the strands are stressed against the concrete.

As described in the previous paragraphs, the time-dependent losses, namely creep and shrinkage of concrete and steel relaxation, are difficult to account for individually since they are all inter-related. However, these time-dependent losses all continue through time at a decreasing rate. Neglecting these losses may not lead to catastrophic failure, but would directly influence serviceability conditions.

1.4 Westbound Gandy Bridge Project

This report studies the effects of time-dependent prestress losses in prestressed concrete girders by instrumenting an actual bridge. Strain measurements, taken from these girders, are used to deduce the actual prestress loss. The strain readings were obtained by using embedded vibrating wire strain gauges.

The Westbound Gandy Bridge in Pinellas and Hillsborough Counties of Florida, is the actual bridge used in this case study. The original design for the Approach span consisted of 25 typical units made up primarily of 4-span continuous post-tensioned girders of 144 ft. The re-design consists of 31 typical units made up primarily of 3-simply supported spans of 144 ft. The new bridge configuration is primarily composed of 43.9 meter (144 foot) pretensioned modified AASHTO Type VI concrete girders. According to the Value Engineering Report', this girder is 15.25 cm (6 inches) deeper than the Florida Bulb-T, and has 18% additional area, but a 44% greater moment of inertia and 64% greater ultimate capacity. These girders are set on the bridge as three span simply supported units. Composite action is then achieved with a continuous slab over these spans. This hybrid structural configuration is lacking in performance data, especially with respect to prestress losses, camber, and deflection. To investigate these conditions four strategically located girders were chosen for instrumentation in this project. Three locations along the span were picked for the placement of a series of gauges. These points are at the midspan, quarter-span and 1.52 meters (5 feet) from the end support.

Therefore, all instrumented girders have gauges at their midspans as well as gauges at either the quarter-span or 1.52 meters (5 feet) from the end support.

At each of the location selected along the span, series of gauges were placed throughout the cross-section. Some of the cross-sectional points chosen had physical significance, such as the steel, concrete, and composite section centroids. Additional points between those already mentioned were picked to account for the variation between them.

Data collection began in December 1995 at the Hardaway Prestress Plant in Tampa, Florida, where the beams were casted. The beams were placed at the bridge site in April 1996 by Misener Marine Construction Company, where data collection is still on going, and is currently scheduled to continue for another two years.

This report will deal with the data collected from the studied beams just after they were cast and stressed, through their placement upon the bridge, and before the composite slab was poured. The data from this period in all covers 150 days.

The format and content of the rest of the body of this report is presented next. Chapter 2, Girder and Bridge Instrumentation, entails all instrumentation aspects of the girder and bridge studied, what equipment was used and how it was installed, what gauge locations were chosen and why, and other important experimental details. Chapter 3, Code Treatment of Prestress Losses, illustrates how various Codes treat prestress losses. Chapter 4, Data Analysis and Experimental Results, explains how results were obtained, separates the immediate losses from the time-dependent losses, contains various plots of

prestress loss, and compares Code results with those obtained. Chapter 5, Effects of Prestress Loss on Bridge Design, examines the effects of prestress losses within the girder cross-sections, utilizes percent comparison with Codes, calculates tendon and concrete stresses, investigates the relationship of relative humidity and ambient temperature with prestress losses, and compares actual camber readings to those calculated using the prestress loss of Chapter 4.

1.5 Unit Conversion

The calculations done throughout this research report were done using the English system of units such as feet, pounds, and ksi. The final results were than converted into the SI system of units, centimeters, Newton, and Mega-Pascal. The three primary conversion factors used throughout this report are as follows:

$$1 \text{ in} = 2.54 \text{ cm}$$

$$1 \text{ lb} = 4.448 \text{ N}$$

$$1 \text{ ksi} = 6.895 \text{ MPa}$$

The dimensions and results are reported in SI units, with the English equivalent occurring in parentheses. It is important to note that calculations were done in English system of units and then converted to SI units, although the SI units are presented as the primary unit.

CHAPTER 2

GIRDER AND BRIDGE INSTRUMENTATION

2.1 Introduction

The Westbound Gandy Bridge is made up of many different span lengths, of which the most frequent occurring span length is 43.9 m (144 feet). Since this length is most prevalent, girders this length were selected for this study. Each of these 43.9 meter (144 foot) girders have the shape of the AASHTO Type VI girder with some modifications. Four of these Modified AASHTO Type VI girders were selected for instrumentation in this project.

2.1.1 Bridge Configuration

The design of the bridge calls for three simply-supported pretensioned girders with a continuous reinforced concrete deck, to form composite action over the three spans. A typical cross-section of the bridge consists of four girders, two of which are interior, and two of which are exterior. This bridge configuration and typical cross-section can be seen in Figure 2-1 and 2-2, respectively. In order to see the variation of the loading effects after the slab is casted, for the interior spans versus the exterior spans, two of each type were chosen for instrumentation. These four girders are representative of the entire three

span system since loading is symmetric, and are labeled in Figure 2-1, as Beams 1 through Beam 4.

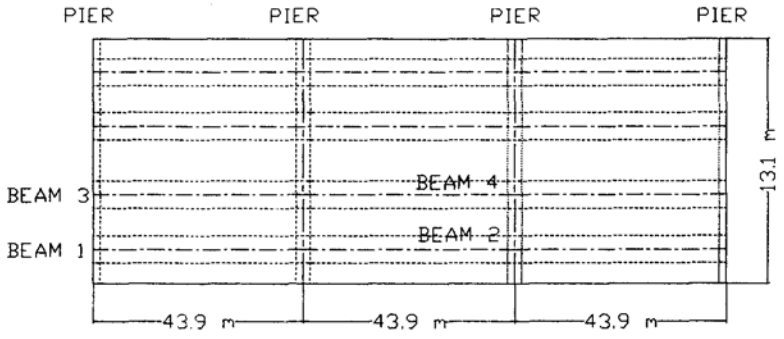

Figure 2-1 Bridge Configuration of the Westbound Gandy Bridge in Tampa, Florida.

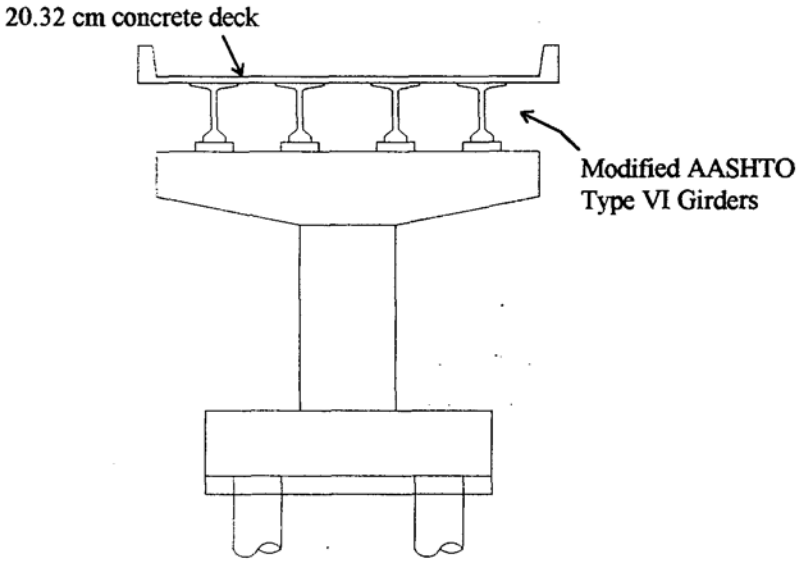

Figure 2-2 Cross-section of the Westbound Gandy Bridge.

2.1.2 Modified AASHTO Type VI

As mentioned earlier, the girder type investigated in this project is the Modified AASHTO Type VI. This girder is derived from the Standard Type VI Bridge Girders suggested by AASHTO. In Figure 2-3 both the Standard AASHTO and the Modified AASHTO Type VI girders are presented with their properties in Table 2-1. The Modified Type VI is 15.2 cm (6 in) taller, and has a maximum top flange width 47.5 cm (18 in) wider, when compared to that of the Standard Type VI as well as other dimensional changes. These changes allow for an increase in the gross moment of inertia of the section, I., of 21 % while only increasing the self weight of the member by less than 2 %.

The design of the Modified AASHTO Type VI girder used on the Westbound Gandy Bridge consists of, 64 - 1.27 cm ($^{1}/2$ inch) oversized or special 1862 MPa (270 ksi -seven-wire low relaxation prestressing strands pulled at 150.3 IN (33.8 kips) each. These 1.27 cm ($^{i}/2$ inch) oversized or special strands have an area per strand of 1.08 cm^2 (0.167 in 2), which is larger than the area of standard strands this size at, 0.987 cm^2 (0.153 in^2). Of the 64 strands used ,50 are straight and 14 are draped using a two point depressed configuration. In addition to these strands, there are 2 - 0.95 cm ($^{3}/_{g}$ inch 270) ksi strands in the top flange stressed at 44.5 kN (10 kips) each. These two strands are used as hanger bars for the shear reinforcement, and should not be considered part of the initial prestressing force applied. Since there is no conventional steel reinforcement used in the girders, they may be considered as fully prestressed. Figure 2-4. shows the end and midspan cross- sections of the girder with tendons, and Figure 2-5 shows the tendon profile of the Modified AASHTO Type VI girder used on the bridge.

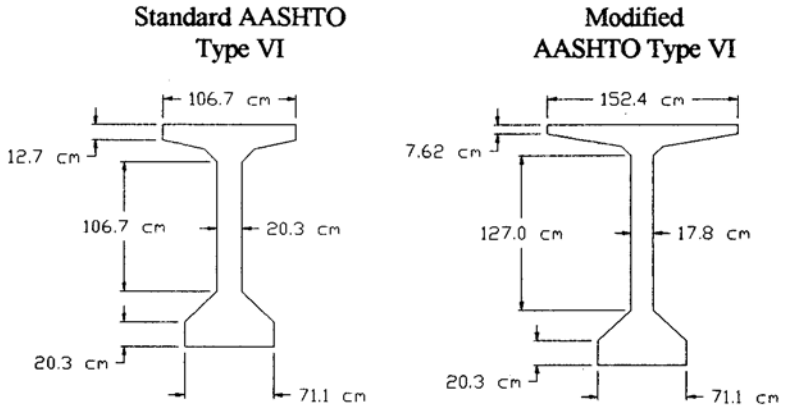

Figure 2-3 Standard and Modified AASHTO Type VI Girder Cross-sections.

Table 2-1 Properties for the Standard and Modified Type VI Girders

AASHTO Type VI	Height		Area		I_c		Girder Weight (w_0 = 0.145kpf)	
	cm	in	cm^2	in^2	m^4	in^4	kN/m	kpf
Standard	182.9	72	7,000	1,085	0.3052	733,320	191.2	1.092
Modified	198.1	78	7,129	1,105	0.3894	935,544	194.9	1.113

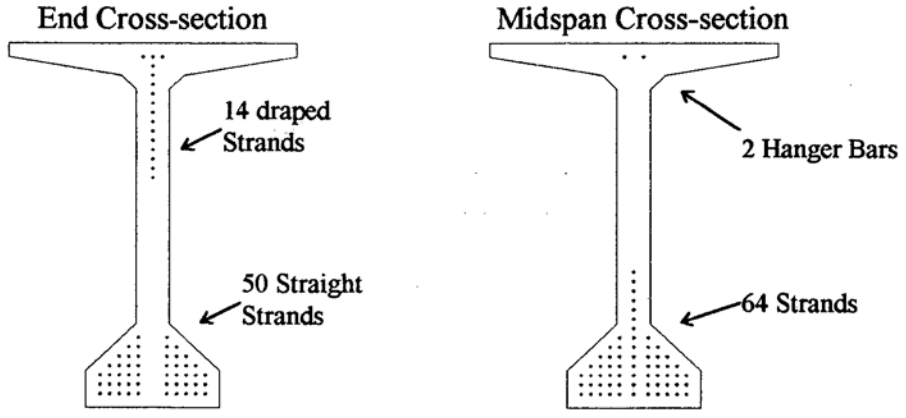

Figure 2-4 Ends and Midspan cross-sections with tendons.

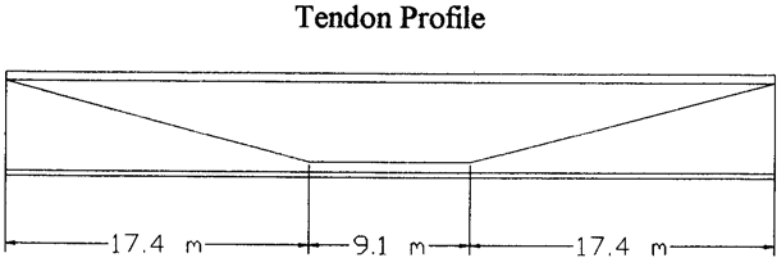

Figure 2-5 Tendon profile for Modified Type VI girder for Westbound Gandy bridge.

2.2 Equipment Used for Instrumentation

2.2.1 Strain Gauges

In order to monitor the strain readings in the four girders investigated, a strain measuring device had to be selected. In addition to strains created by the applied loads, temperature variations also induce strains in concrete members. Therefore, the gauge selected must have the capacity to measure temperature readings as well as strain. This will allow for the extraction of the temperature effects from the overall strain. Also, the gauge must be such that it can be embedded in the concrete, in order to achieve the strain readings from deep within the girder.

The strain measuring device selected was Model VCE-4200 Vibrating Wire Embedded Strain Gauge, manufactured by Geokon Inc., Lebanon, New Hampshire. A schematic of this gauge can be seen in Figure 2-b. This strain gauge is suggested by Geokon Inc. for long term measurements in concrete bridges. It also meets the

requirements necessary for this study, that is, this vibrating wire strain gauge has the capacity to measure both temperature and strain within the concrete.

Strain measurements are obtained using the vibrating wire principle. These strain gauges contain a steel wire that is tensioned between its two ends, which are embedded in the concrete. When changes of strain occur, relative movement between these two ends

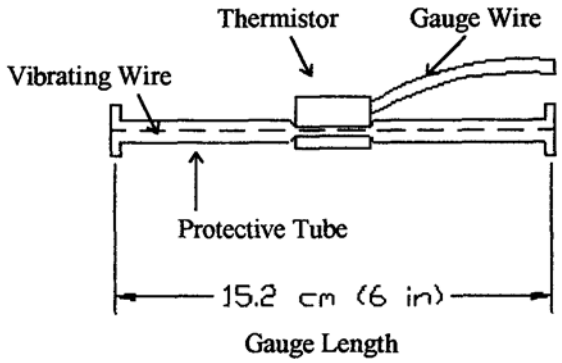

Figure 2-6 Model VCE-4200 Vibrating Wire Strain Gauge from Geokon Inc.[8]

cause a change in the tensioned wire. This change of tension corresponds to a change in frequency, which can be transformed to micro-strain- through a conversion factor.

In addition to the vibrating wire, each gauge contains a thermistor. This thermistor allows for temperature readings to be obtained. Changes in temperature directly correspond to changes in resistance output given by the thermistor.[8]

2.2.2 Other Equipment Used

In addition to the strain gauges, there are many other pieces of equipment necessary to collect and store, strain and temperature readings. The strain gauges work in conjunction with multiplexers to convey strain and temperature readings to a data acquisition system. There are limits on how much data can be stored within the storage module of the data acquisition system. Therefore, data must be collected periodically or else newer data may displace the older data.

The collection of data can be done in two ways for this project. One way is by directly connecting a computer to the data acquisition system and collecting. Another alternative is accessing a cellular phone module, which is located within the data acquisition system this access can be achieved from a remote location by using computer equipped with a modem, and then collecting. In order to collect data by either approach, it is necessary to have the Micro-10 software from Geokon Inc. installed on the receiving computer used.

Environmental conditions are also important when considering prestress losses in concrete structures. Of particular importance are the readings of the ambient temperature and the relative humidity. These factors directly influence the prestress losses and are important. In this study, these readings are obtained using a Campbell Scientific HIVIP 35C relative humidity and temperature probe, and stored by the data acquisition system.

The use of all the equipment mentioned requires a constant power source. Therefore, connected to the data acquisition system is a 12-volt rechargeable battery. This power source allows for data to be collected and stored in the storage module. It also

allows the cellular phone module to be turned on for set time intervals, for data collection via a modem. Since, these activities tend to drain the battery, a recharging device must be used. The battery is recharged in this project via a 20 watt solar panel which is connected to it.

2.3 Girder Instrumentation

2.3.1 Gauge Placement Along Girder Span

The choice of the locations along the span in which to place the vibrating wire strain gauges are important, especially, since it is necessary to determine the prestress loss variation with length. Three points of importance were selected along the span of the girders. These points consisted of the midspan, quarter-span, and 1.52 m (5 ft) from the end support. The midspan and the quarter-span are located at 21.95 m (72 ft) and 10.97 m (36 ft) from the end support, respectively. Two of these three points were chosen for each of the beams instrumented.

There are many reasons for these points to be selected along the span. The midspan was chosen because it is where the maximum camber occurs after the prestress is applied. It is also where the maximum deflection occurs after all loads are applied. The choice of the location at 1.52 m (5 ft) from the end support was made because a very small moment is felt at this location. It is also significant because it is beyond the transfer length of the girders. Beyond the transfer length, the concrete will

have absorbed the full application of the prestressing force. The final location at the quarter-span was chosen to better define the prestress loss variation along the span it provides an intermediate point between the losses in the area of the large moment at the midspan, and that of the small moment at 1.52 m (5 ft) from the support.

Of these points only two locations were selected for each of the four girders instrumented. The distribution is as follows: the midspan of all four girders, 1.52 m (5 ft) from one end support of both Beam 1 and Beam 4, and quarter-span point of Beam 2 and Beam 3. Beams 1 and 2 are exterior girders and Beams 3 and 4 are interior girders, when placed on the bridge. Figure 2-7 clearly depicts this distribution.

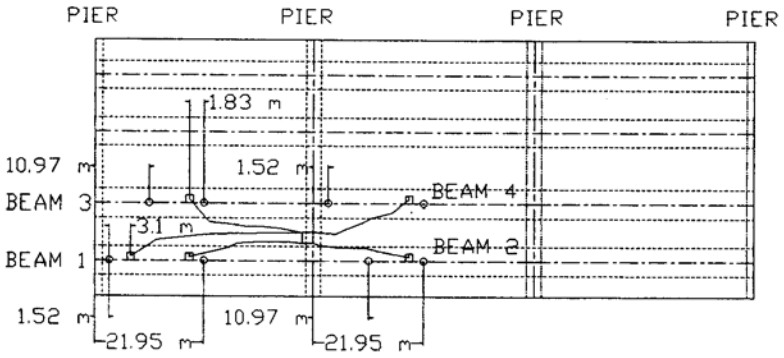

Figure 2-7 Instrumented locations along the studied girders.

2.3.2 Gauge Placement Across Girder Cross-section

Since there are three independent locations instrumented along the span, there will be three cross-sections to be considered. Each of these cross-sections will have its own local properties, as well as global properties which are uniform throughout. It is then

necessary to determine which points within each cross-section are significant, when considering prestress losses. Once these points are found, vibrating wire strain gauges can be placed at these locations. The midspan is considered the most important cross-section for obvious reasons. Therefore, it is logical that this cross-section would contain the most strain gauges. Each midspan cross-section contains eight vibrating wire strain gauges within it (Beam 1 has an additional three gauges see Section 2.3.3). A typical instrumented midspan cross-section can be seen in Figure 2-8. The locations 7.62 cm (3 in) and 190.5 cm (75 in) from the

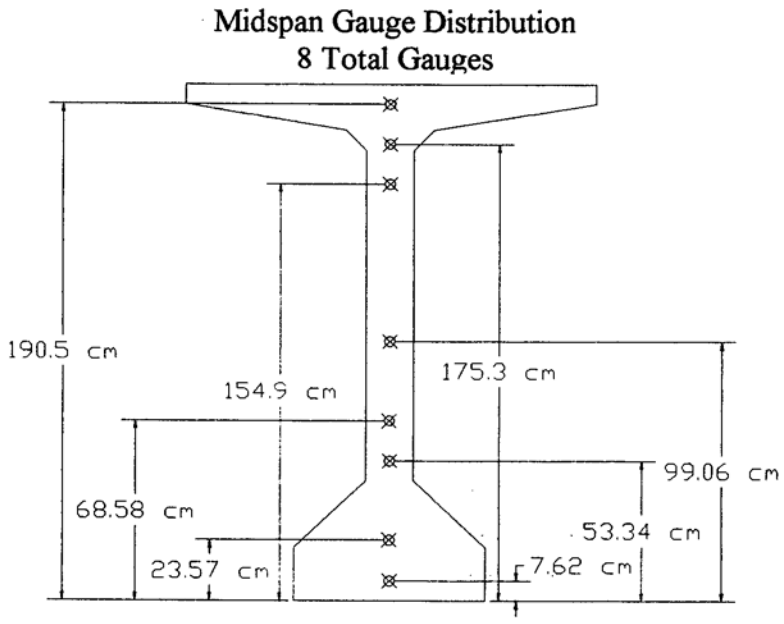

Figure 2-8 Midspan gauge distribution for all Beams studied.

bottom of the girder were selected, because they are the closest you can get to the outermost fibers, without invading the 7.62 cm (3 in) concrete cover zone requirement

ACI Code 3 8R-89, Section 7.7.3.1.[9] The location of 23.57 cm (9.28 in) represents the steel centroi of all the prestressing strands within the cross-section. The choice of 99.06 cm (39 in) as made because this point is very close to the girder concrete centroid. The composite section concrete centroid will occur at about 154.9 cm (61 in), after the deck is placed, so this point was also chosen. The points 53.34 cm (21 in), 65.58 cm (27 in), and 175.3 cm (6 in) were picked to show the loss variation between the selected points of significance.

The uarter-span and 1.52 m (5 ft) from the support, each have 6 vibrating wire strain gauge located throughout their respective cross-sections (Beam 1 has an additional three gauges at the 1.52 m (5 ft) from the support see Section 2.3.3). Each of these cross-sectio s contain the gauges placed at 7.62 cm (3 in), 175.3 cm (69 in), and 190.5 cm (75 in), whic are similar to the midspan cross-section. The centroid of the steel in the bottom flange or the straight tendons is 18.80 cm (7.4 in) for both cross-sections, and a gauge was paced at this point also. An additional gauge was placed at the steel centroid of the drape strands for both cross-sections. This location is 84.07 cm (33.1 in) at the quarter-span and 147.1 cm (57.9 in) at the point located 1.52 m (5 ft) from the support. These two cross-sections can be seen in Figures 2-9 for the quarter-span, and Figure 2-10 for the point 1.52 m (5 ft) from the end support.

2.3.3 Gauge .Placement Along Strand

In addition to the cross-sectional variation of prestress, another area of interest was how the stress would vary directly along the strands. For this an additional 6

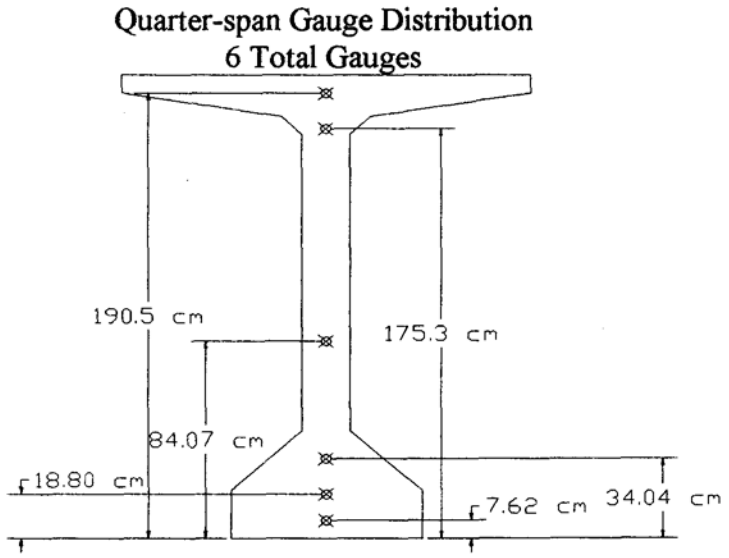

Figure 2-9 Quarter-span gauge distribution for Beams 2 and 3.

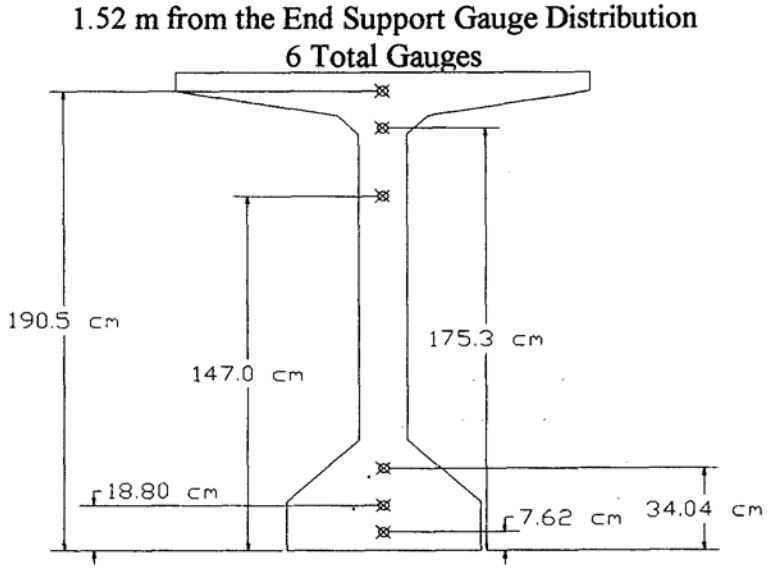

Figure 2-10 Gauge distribution for Beams 1 and 4 at 1.52 m from the end support.

vibrating wire strain gauges were placed in Beam 1. Three gauges were placed at 22.86 cm (9 in) from the bottom at the midspan, and the other three were placed at 17.78 cm (7 in) from the bottom at the point 1.52 m (5 ft) from the support. This gauges were directly attached to the steel tendons at these locations, to secure them from shifting during casting.

2.4 Composite Slab Instrumentation

2.4.1 Introduction

The girders of the Westbound Gandy Bridge are covered with a 20.32 cm (8 in) continuous reinforced concrete deck slab over each three-span unit. This deck causes the girder-deck combination to act as a single unit. Although this concrete deck is not prestressed, it would be interesting to see how and if the prestress losses occurring in the girders below it, would effect the slab's stress distribution. Figure 2-11 contains a top view of the instrumented deck. Table 2-2 contains information about the depth, location, and orientation of each gauge labeled in Figure 2-11.

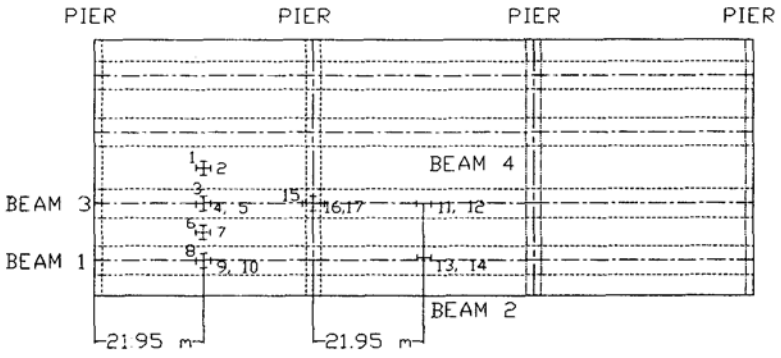

Figure 2-11 Slab gauge distribution for Westbound Gandy Bridge.

Table 2-2 Detailed information about composite slab gauges.

Slab Gauge #	Depth (measured from top of beam)		Location	Orientation (with respect to beam direction)
1	7.62 cm	3.0 in	Midspan of Slab between Beam 3 and North Beam	Perpendicular
2	10.16 cm	4.0 in	Midspan of Slab between Beam 3 and North Beam	Parallel
3	11.43 cm	4.5 in	Midspan of Beam 3	Perpendicular
4	10.16 cm	4.0 in	Midspan of Beam 3	Parallel
5	1.27 cm	0.5 in	Midspan of Beam 3	Parallel
6	13.97 cm	5.5 in	Midspan of Slab between Beam 1 and 3	Perpendicular
7	11.43 cm	4.5 in	Midspan of Slab between Beam 1 and 3	Parallel
8	10.80 cm	4.25 in	Midspan of Beam 1	Perpendicular
9	10.16 cm	4.0 in	Midspan of Beam 1	Parallel
10	2.54 cm	1.0 in	Midspan of Beam 1	Parallel
11	10.16 cm	4.0 in	Midspan of Beam 4	Parallel
12	0.76 cm	0.3 in	Midspan of Beam 4	Parallel
13	12.7 cm	5.0 in	Midspan of Beam 2	Parallel
14	1.27 cm	0.5 in	Midspan of Beam 2	Parallel
15	13.97 cm	5.5 in	At support between Beam 3 and 4	Perpendicular
16	12.7 cm	5.0 in	At support between Beam 3 and 4	Parallel
17	1.27 cm	0.5 in	At support between Beam 3 and 4	Parallel

2.4.2 Gauge Placement Along the Slab Longitudinal Axis

The choice of points along the slab in which gauges were placed was important, especially, since the results obtained would have to work in conjunction with those from the girders. The midspan of each girder would be a natural place, allowing a complete stress distribution from the bottom portion of the girder to the top portion of the slab to be determined directly. Other locations of interest are the points of maximum positive and negative moment in the continuous deck.

2.4.3 Gauge Placement Across Depth of Slab

In the case of the girder, the gauges were placed parallel with the span of the girder, in order, to obtain stresses in the axial direction. In the concrete deck, however; it is important to obtain stress distributions in both the longitudinal and perpendicular directions of the slab. This is necessary because applied loads create moments, which in turn induce stresses in both directions within the deck.

The gauges were placed at approximately two depth locations within the slab. These two depths are 0 and 10.16 cm (4 in), measured from the top of the girder. The gauges placed at 0 represents the location where the interface between the girder and the slab occurs. There should be a stress discontinuity occurring at this location. The point at 10.16 cm (4 in) was chosen because it is the mid-depth of the-20.32 cm (8 in) thick slab. And in addition to this, it allows for a determination of the stress distribution between this point and the 0 cm point.

2.5 Installation of Strain Gauges

2.5.1 Girder Strain Gauges

Effective installation of the vibrating wire strain gauges was imperative for this research project to be successful. The strain gauges had to be installed securely, such that, they would not shift during the casting of the beams. This was achieved by attaching the gauges to two Number 3 steel rebars. These two rebars were separated by a distance slightly smaller than the width of the gauge, and welded together by two pieces of steel. The location of gauges were marked with chalk on the rebars, and then the gauges were attached with steel tie wire. Finally, the gauge-rebar combination was tied securely to the prestressed steel tendons to keep it in place.

Each of these strain gauges have a wire with a connector attached to its end. It was very important to keep the connectors dry, so that they would not be damaged during casting of the concrete. This was achieved by running the wires along the rebar and placing the wires in several plastic bags above the top flange of the beam. After casting and vibration of the concrete, the wires were removed from the bag and connected to the multiplexers. Then, these multiplexers were connected to the data acquisition system before data collection began. The photographs shown in Figures 2-12(a-d) depict the gauge installation process for the girders and bridge instrumentation perceptively. In fact, the pictures in these two figures give a complete history of the bridge instrumentation process from start, to placement of the slab or bridge deck..

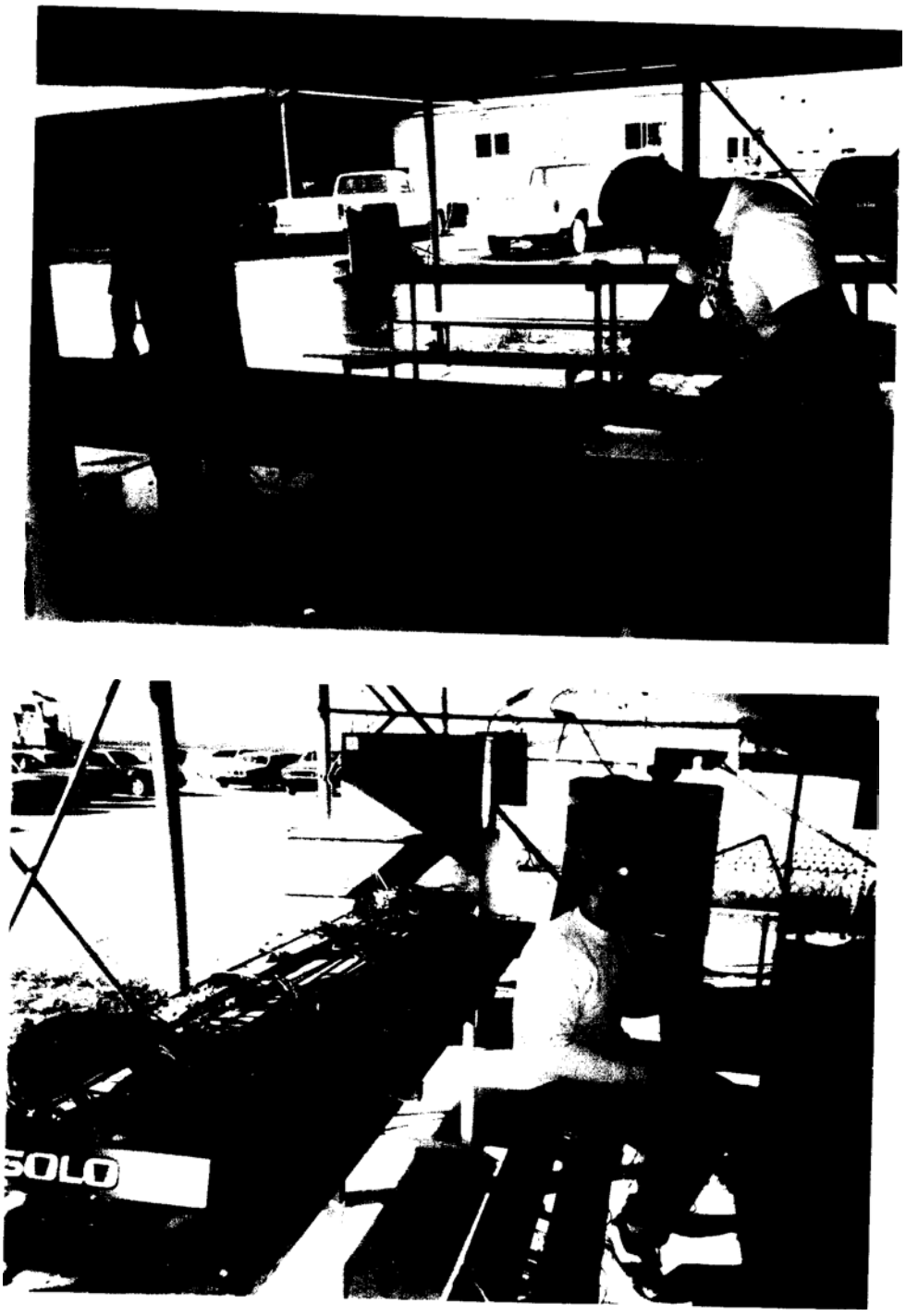

Figure 2-12a Preparation of strain gauges for placement in girders.

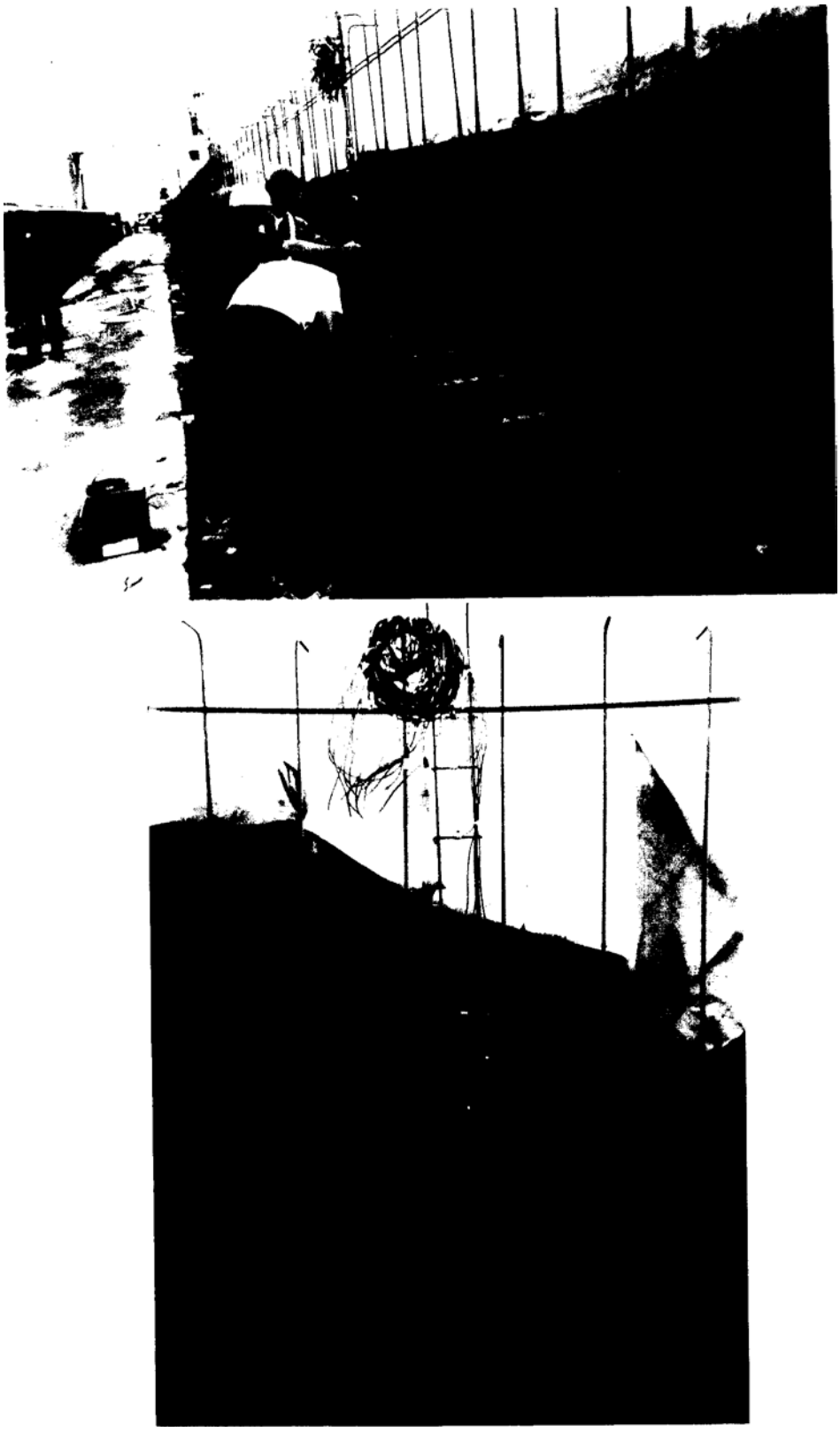

Figure 2-12b Shows placement of strain gauge within the girders.

Figure 2-12c Attachment of strain gauges along the steel strands.

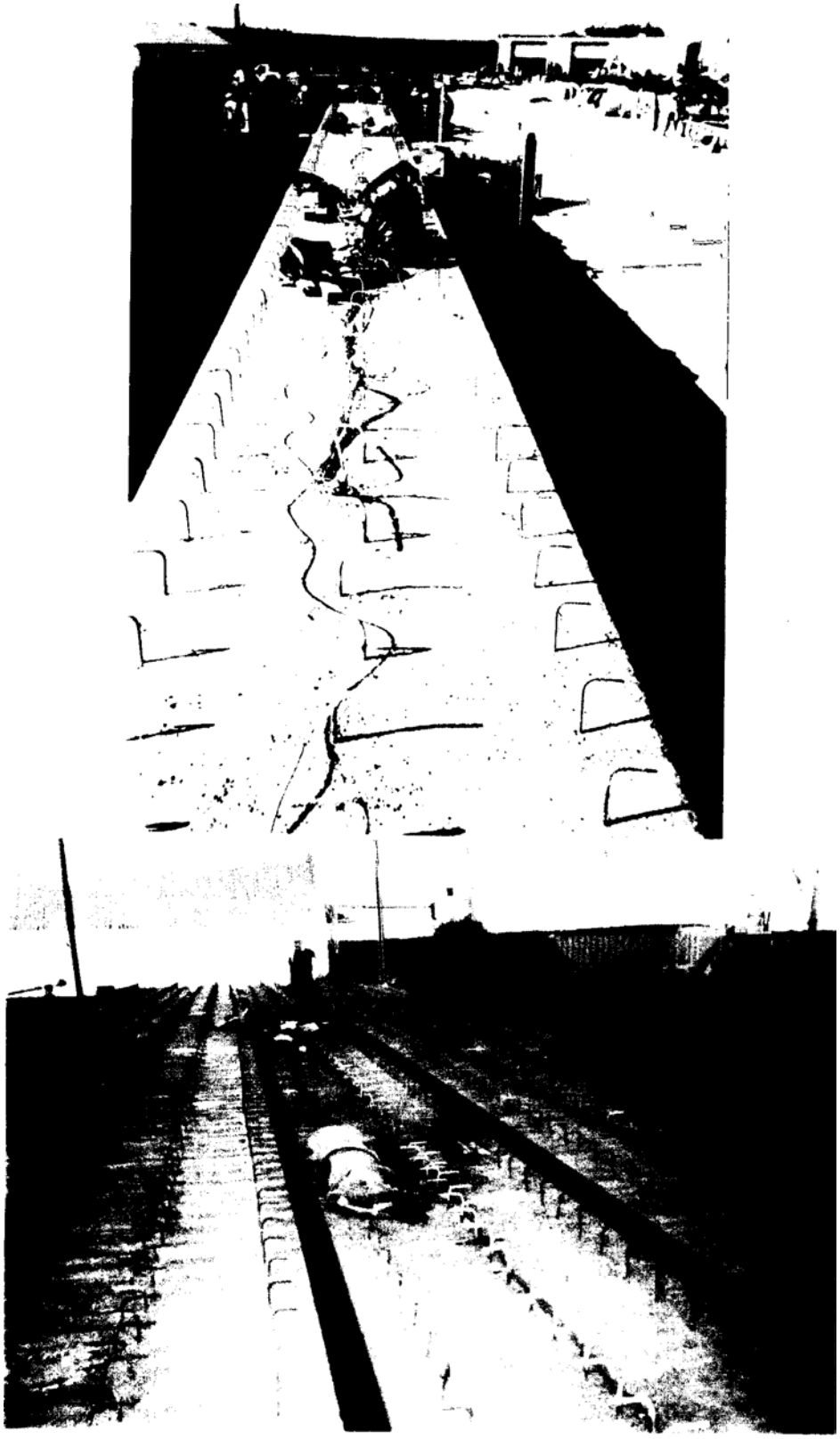

Figure 2-12d The instrumented girders in the staging area awaiting shipment to the bridge site.

2.5.2 Slab Strain Gauges

Instrumentation of the slab gauges promoted a different kind of problem, because the slab forms and steel reinforcement were in place before the gauges could be installed. The strain gauges could not be placed any time earlier, because they could be damaged during the placement of the steel reinforcement for the slab. Hence, the strain gauges were then attached to the steel rebar after the slab reinforcement was in place at the specified locations using steel tie wire.

The connecting wire lengths were increased, by cutting and soldering longer wires to them. Since the wires could not be placed earlier it was necessary for all the wires to be feed below the steel reinforcement in the slab. This is because during casting the workers walk directly on the reinforcement, and if the wires were caught between the feet of the workers and the rebar, the wire could possibly be damaged.

To enable connection of the gauges to the multiplexers which were attached to the web (see Section 2.6), it was necessary to cut holes in the bottom of the forms, and to pass the wires through, to the multiplexers.

2.6 Equipment Attachment to Bridge

Once the girders were moved to the bridge ¯all equipment had to be permanently secured to the bridge. The multiplexers were directly attached to the web of the girders. A schematic of this can be seen in Figure 2-13. These multiplexers were attached with

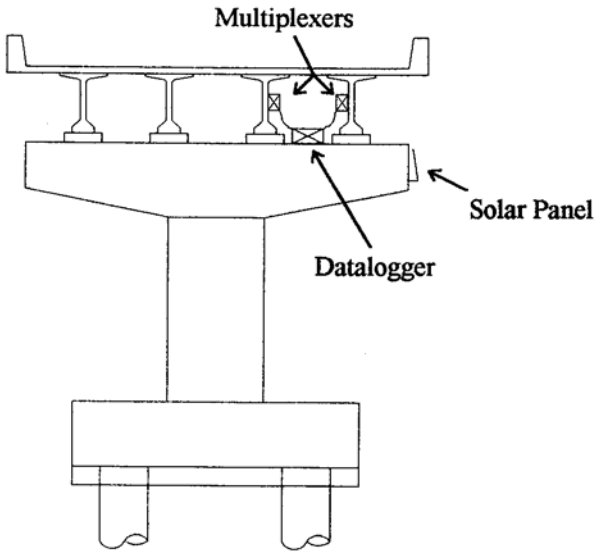

Figure 2-13 Bridge cross-section with equipment.

5.72 cm (2-$^{1}/_{4}$ in) concrete bolts and a hammer drill. The strain gauge wires and multiplexer wires connected to the data acquisition system required some sag, which had to be accounted for. Using 1.27 cm ($^{1}/2$ in) clips the wires were bolted to the web of the adjacent girders.

The location of the data acquisition system was important because it had to be easily accessed in case of a problem. The location selected was the pier between the four instrumented beams. Along side of the datalogger is the 12-volt battery, both of which are bolted using concrete bolts. This location allows for the datalogger to be accessed by a ladder placed a the footer.

It was important to get the solar panel in an area where it would be directly exposed to sunlight, in order to allow it to recharge the battery effectively. The relative

humidity and ambient temperature probe, and cellular phone antenna had to be in a location where their readings or waves would not be inhibited. Hence, all of these three pieces of equipment were attached to the outside of the pier. The wires from all these three pieces of equipment are directly connected to the data acquisition system. Figure 214(a-c) shown pictures of the equipment attachments at the bridge site.

2.7 Shrinkage Cylinders

In a bid to separate the components of the time-dependent prestress loss, it is important to get as much information about the concrete as possible. It was decided that five 15.24 cm by 30.48 cm (6 by 12 in) cylinders would be casted for the purpose of determining shrinkage strains in concrete. These cylinders were made from the same concrete batch as used for the girders, and exposed to the same environmental conditions as the girders.

Each of these shrinkage cylinders are instrumented with similar vibrating wire strain gauges that were used in the girders and the deck. The gauge was placed in the center of the cylinder mold, and held in place by three steel tie wires to allow measurement of axial strain. These tie wires pass through small holes in the mold, and are taped to the outside of the mold to hold it in place. A slit on the top of the mold was left so the wire could be connected to the multiplexer.

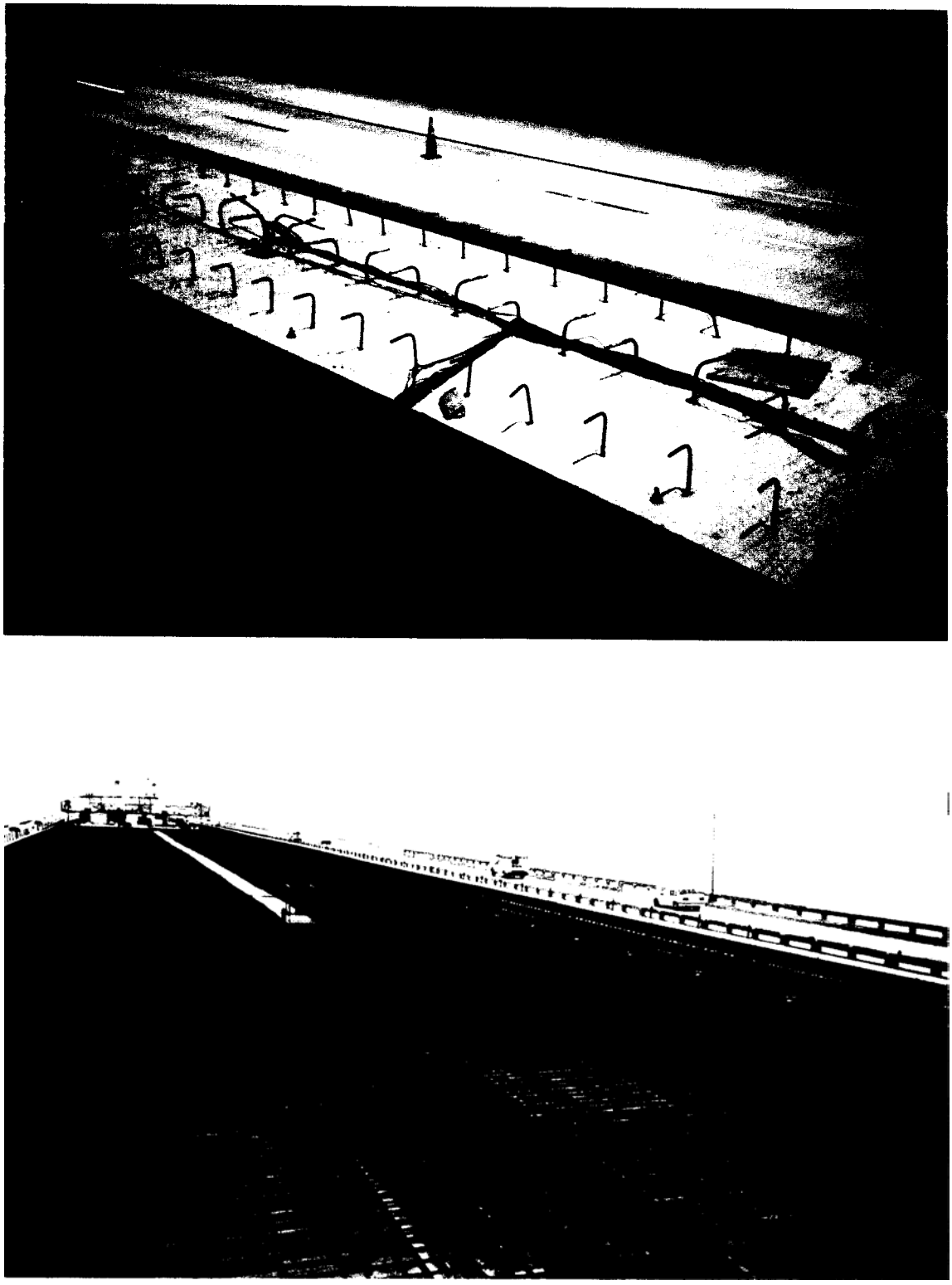

Figure 2-14a Placement of girder on bridge pier and bridge deck with

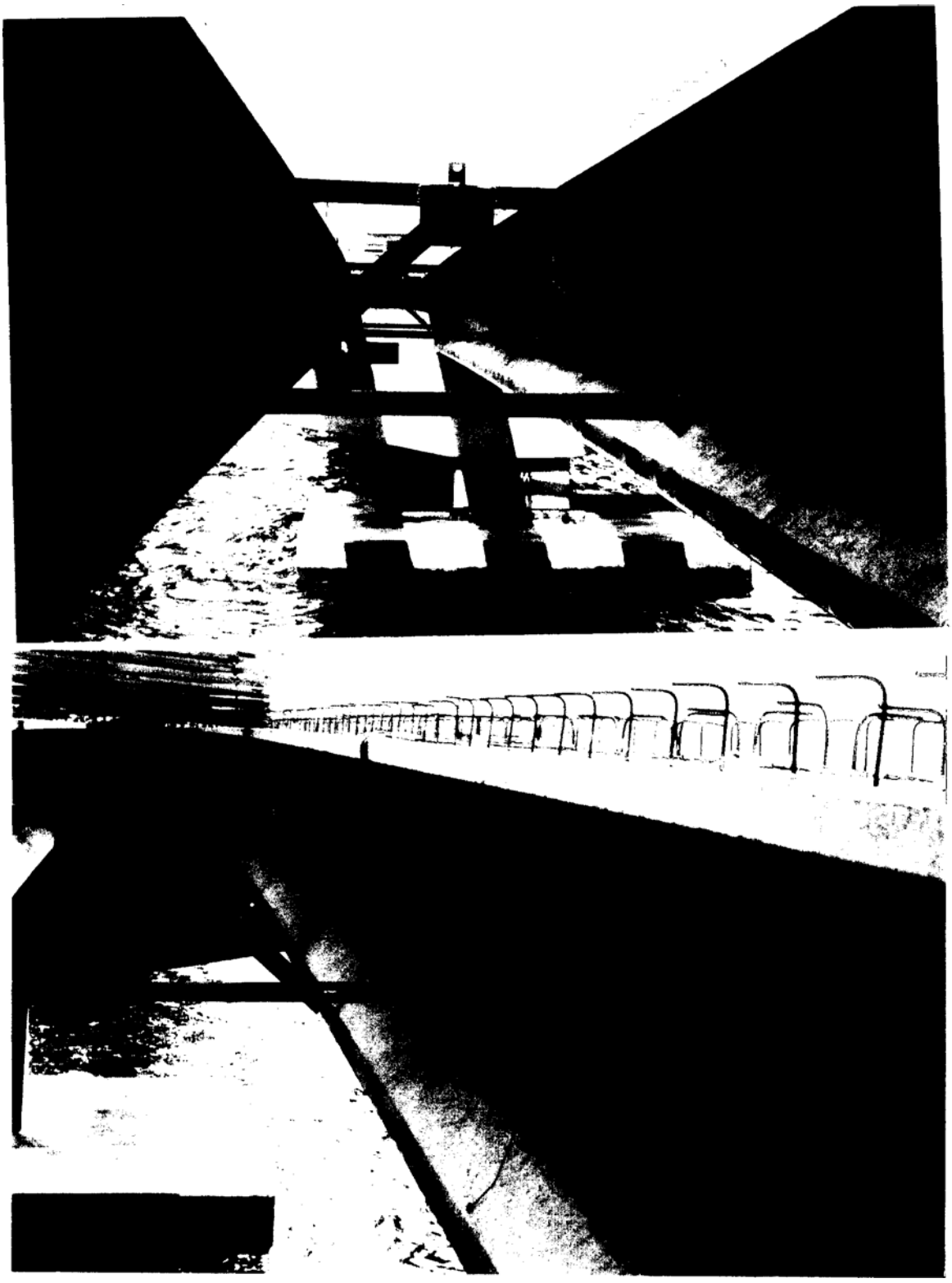

Figure 2-14b Multiplexers attached to girder web with slack in the connecting wires.

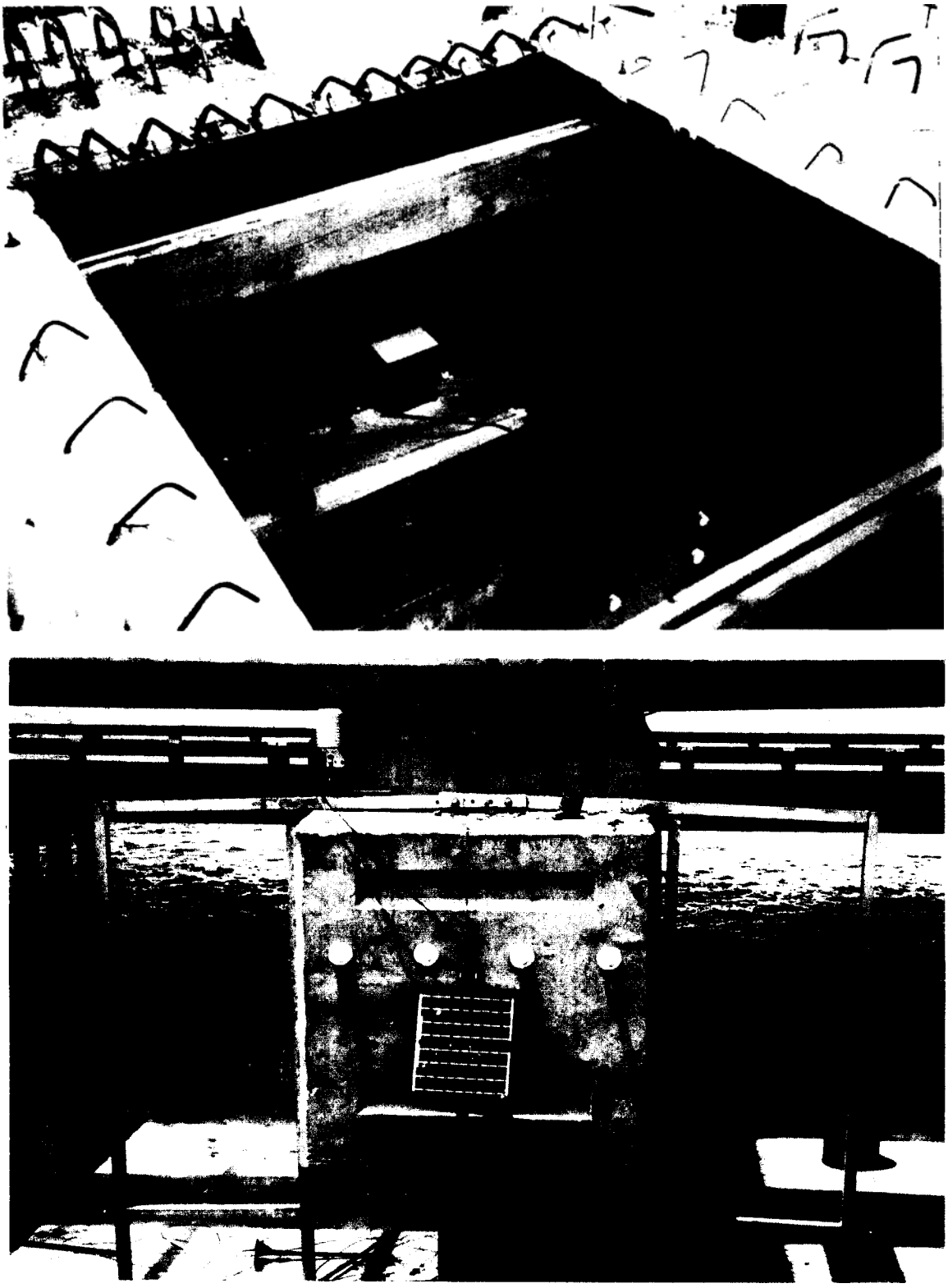

Figure 2-14c Location of data acquisition system and battery (top) and solar panel, cellular phone antenna, and relative humidity probe (bottom).

The girders and cylinders were casted at the same time. The cylinders were exposed to the same conditions as the girders from conception, to the bridge site. Once at the bridge site, the cylinders were placed on an adjacent pier to that where the data logger is located. The wires from the cylinders are attached to the side of the girders, similarly, to those of the multiplexers and girder gauge wires. The photograph in Figure 2-15a shows the preparation of a typical shrinkage cylinder mold before casting. In Figure 215b. The shrinkage cylinders are depicted on top of the girder in the stage area, and at their final location when moved to the bridge site.

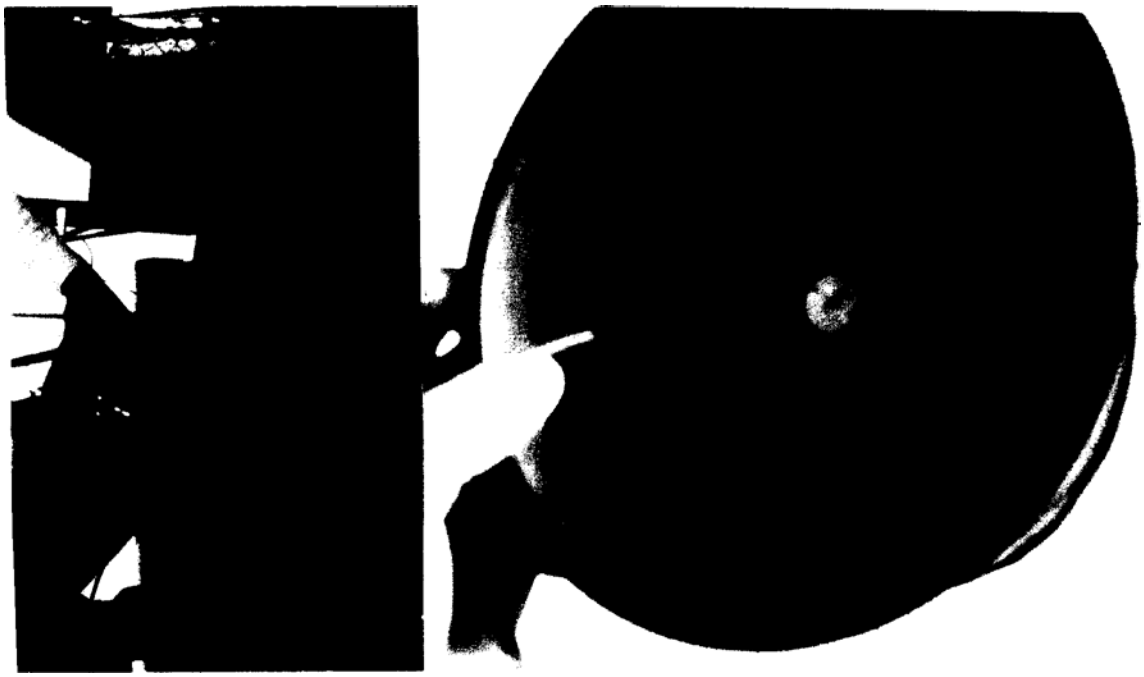

Figure 2-15a A Preparation of shrinkage cylinder mold with strain gauge.

Figure 2-15b Shrinkage cylinders on top of the girder and at the bridge site.

2.8 Modulus of Elasticity

2.8.1 Introduction

The modulus of elasticity of any material directly relates the stress to the strain according to Hooke's Law, which is a = E·s. The symbols a, E, and s, are the stress, modulus of elasticity, and strain for a given material, respectively. For concrete, this linear relationship holds true initially, but becomes nonlinear after a certain point.

2.8.2 ACI 318-89R Definition of E,

The American Concrete Institute Building Code Requirements for Reinforced Concrete of 1989, Revised in 1992 (ACI 318-89R), defines the modulus of elasticity of material as; the ratio of the normal stress to its strain for either tensile or compressive stresses under the proportional limit of that material as described in Section 2.1 of the Code. For concrete, the 89R Code states in Section 8.5 Commentary that the modulus of elasticity of concrete, E, is the slope of the line drawn from 0 to $0.45fi_c$ on a stress strain curve, where f,' is defined as the 28 day compressive strength of concrete. It also states that measured E,- values may range from 80 to 120 percent of the calculated value.

The equation suggested by the ACI to determine E,, is based on w, and f_c'. Where w,, is -the specific weight of the concrete in lb/ft^3 and f,-' is in psi. For w,, ranging from 90 to 155 lb/ft^3 the equation for E, in Section 8.5 of the Code is as follows:

$$Ec = w_c^{1.5} 33\sqrt{f'_c} \qquad (2.1)$$

And this is the equation typically used in design.

2.8.3 Experimental Determination of E,

The actual modulus of concrete tends to deviate as a function of time from the equation suggested by ACI. A more accurate modulus for concrete could give a better representation of what the actual prestress losses are. , With this in mind, an additional twenty test cylinders, 15.24 cm by 30.48 cm (6 by 12 in) were cast from the concrete batch used, so that the modulus of concrete could be determined experimentally.

The experiments would be performed at the CEEFL (the Civil and Environmental Engineering Field Lab) at the University of Central Florida. The equipment used was a compressive strength machine manufactured by SATEC Systems, Inc., Grove City, Pennsylvania, and a strain measuring box borrowed from the Florida Department of Transportation Structures Laboratory, Tallahassee, Florida. The strain gauges used were attached to the outside of the cylinder being tested. From the testing, the following measurements of the compressive strength and elastic modulus were recorded. Table 2-3 contains the experimental results from this testing. Due to some inconsistencies in the laboratory results, it was determined that perhaps a more sophisticated experimentally setup could achieve more reliable results. This setup would include an automatic data acquisition system that remove the human error aspect of trying to obtain the readings manually. In this report, another method of calculating E., is used in order to avoid including large experimental errors in

Table 2-3 Experimental results using concrete collected during casting of Beams 1 and 4.

Experiment Results for f_c' and E_c Conducted at CEEFL, UCF				
Time	f_c'		E_c	
Days	MPa	psi	GPa	ksi
1	27.983	4058.5	30.097	4365.1
2	35.981	5218.5	23.772	3447.8
3	39.170	5680.9	29.275	4245.9
5	43.603	6323.9	36.215	5252.4
7	45.777	6639.1	27.625	4006.5

the values obtained. The elastic modulus is an essential component in this study and is needed to be computed as a function of time.

2.8.4 CEB-FIP Model Code 1990 Method for Determining E,(t)

In the text "Concrete Structures: Stresses and Deformations," by Ghali and Farve[10], it suggests a few different methods for determining the time-dependent modulus of elasticity of concrete. The method used here is that which was suggested by the CEB-FIP Model Code 1990." This committee suggests the following equation for determining the 28 day modulus of elasticity:

$$E_c(28) = 21500\left(\frac{f_{cm}}{f_{cm0}}\right)^{\frac{1}{3}} \qquad (2.2)$$

In Equation 2.2, f,. is the mean compressive strength at 28 days in MPa, and f_{cmo} is equal to 10 MPa. The mean compressive strength, $f_{cm}$is related to the characteristic strength, f_{ck}, as follows:

$$f_{cm} = f_{ck} + \Delta f \qquad (2.3)$$

In Equation 2.3, the quantity Of is equal to 8 MPa. The characteristic strength, f .k is obtained performing compression tests on 15.0 by 30.0 cm (6 by 12 in) cylinders stored in water at 20 ± 2 °C and tested 28 days after casting. So Equation 2.2 can now be rewritten as follows:

$$E_c = 21500\left[\frac{(f_{ck} + \Delta f}{f_{cm0}}\right]^{\frac{1}{3}} \qquad (2.4)$$

The time-dependent modulus E,(t) is estimated by the following equation:

$$E_c(t) = \beta_E(t)E_c(28) \qquad (2.5)$$

where

$$\beta_E = \sqrt{\exp\left[s\left(1-\sqrt{\frac{28}{t}}\right)\right]} \qquad (2.6)$$

In Equation 2.6, the time t is measured in days, and s is a coefficient depending on the type of cement used. For rapid hardening high strength cements, s is equal to 0.2, as it was taken for this project.

2.8.5 Calculating E,(t) and Comparing to Design

In order for Equation 2.6 to be effective, it is necessary to have a reliable source of f_{ck}. The closest quantity available to f_{ck} is f_c' at 28 days. The Quality Control personnel at the Hardaway Company in Tampa, Florida, measured compressive strength, at time of transfer, 7, and 28 days after the concrete was casted. For each beam, two tests were performed for each day mentioned. The only values needed here are those for f,.' at 28 days. Since Beams 1 and 4 were casted on the same day using the same concrete batch, their compressive strengths were averaged to come up with one value. Similarly, the procedure was done for the compressive strengths of Beams 2 and 3. The results obtained can be seen in Table 2-4. It is interesting to note that the original design was done on the assumption of f_c' of 44.8 MPa (6500 psi), but the strength achieved in the field was are much greater. With the quantities in Table 2-4, it is now possible to obtain values of $E_c(t)$. These values will be included in Table 2-5 and compared to those from the original design.

Table 2-4 Values of the 28 day Compressive for the Girders (Courtesy of Hardaway Company, Prestress Division, Tampa, Florida).

f_c' Values that will used as f_{ck} in Equation 2.4 for $E_c(28)$			
Beam 1 and Beam 4		Beam 2 and Beam 3	
MPa	psi	MPa	psi
57.316	8313	54.879	7959

Now that all the parameters have been established the calculation of $E_c(t)$ can proceed. The calculated values E_c' for Beams 1 and 4, and Beams 2 and 3, versus the design calculated values are shown in Table 2-5. As mentioned earlier, the results using another method, the ACI Committee 209 method for determining $E_c(t)$ can be found in Appendix A. The actual design was based on the CEB-FIP Method, hence it was used over the ACI Committee Method in this study.

These E_c values according to CEB-FIP were used in determining the prestress loss of the members analyzed in this project. Additional days, which were between those values reported in Table 2-5, were calculated and used in the loss calculations as well.

Table 2-5 Design $E_c(t)$ versus $E_c(t)$ calculated by CEB-FIP Model Code 1990 Method.

Design and Calculated Values for f_c' and E_c						
Time	Design		Beams 1 and 4		Beams 2 and 3	
	E_c		E_c		E_c	
Days	GPa	ksi	GPa	ksi	GPa	ksi
3	29.138	4226.0	27.814	4033.9	37.465	3983.3
7	30.892	4480.3	30.909	4482.8	30.521	4426.5
14	31.637	4588.4	32.774	4753.2	32.362	4693.6
28	32.03	4656.4	34.160	4654.3	33.731	4892.6
40	32.151	4662.8	34.722	5035.8	34.286	4972.6
60	32.246	4676.7	35.259	5113.8	34.817	5049.6
80	32.293	4683.5	35.584	5160.8	35.137	5096.0
100	32.322	4687.7	35.806	5193.1	35.357	5127.9
120	32.341	4690.5	35.972	5217.1	35.520	5151.6
400	32.409	4700.0	36.766	5332.3	36.305	5265.4
2000	32.432	4703.7	37.308	5410.9	36.840	5343.0
10000	32.437	4704.4	37.553	5446.4	37.082	5378.0

CHAPTER 3

CODE TREATMENT OF PRESTRESS LOSS

3.1 Introduction

There are several different methods for determining the prestress loss of a member. The accepted methods are defined by various legal bodies. The American Association of State Highway and Transportation Officials (AASHTO) is the legal body that sets the standards for bridge design. For prestressed concrete, the Prestressed Concrete Institute (PCI) suggests the methods of design, for both prestressed and precast concrete. The standards for both prestressed and conventional concrete are specified by the American Concrete Institute (ACI).

These bodies have different methods for determining the prestressed loss for various types of members. Although, the ACI and PCI methods stem from the same article and will be combined as one. In the sections that follow, a brief overview of how these bodies determine prestress loss will be presented and discussed. At the end, a spreadsheet program will be used to calculate the results for the methods presented.

The units specified for the equations in this chapter are based on the English system of units. It is the results of these equations that are then converted to SI units through the conversion factors of Section 1.5.

3.2 AASHTO-LRFD Method for Determining Prestress Loss

3.2.1 Introduction

The AASHTO-LRFD[12] method defines the prestress loss for both pretensioning and post-tensioning in Section 5.9.5. The prestress loss is broken into an instantaneous portion and a time-dependent portion. The AASHTO-LRFD method offers two options for determining the time-dependent prestress loss. The first is a lump sum based on the type of member being examined, the 28 day compressive strength of that member, and the partial prestressing ratio. The other option is a refined calculation of each of the components of the time-dependent loss.

3.2.2 Total Prestress Loss

The AASHTO-LRFD in Section 5.9.5.1 defines the total prestress loss for pretensioned members that are constructed and prestressed in a single stage as follows:

$$\Delta f_{pT} = \Delta f_{pES} + \Delta f_{pSR} + \Delta f_{pCR} + \Delta f_{pR} \quad (3.1)$$

and for post-tensioned members:

$$\Delta f_{pT} = \Delta f_{pF} + \Delta f_{pA} + \Delta f_{pES} + \Delta f_{pSR} + \Delta f_{pCR} + \Delta f_{pR} \quad (3.2)$$

The variables in Equations 3.1 and 3.2 are defined in ksi as follows:

Δf_{pT} = total loss

Δf_{pF} = loss due to friction

Δf_{pA} = loss due to anchorage set

Δf_{pES} = loss due to elastic shortening

Δf_{pSR} = loss due to shrinkage

Δf_{pCR} = loss due to creep of concrete

Δf_{pR} = loss due to relaxation of steel

It also states that the portion of steel relaxation loss occurring before transfer of stress to the concrete may be deducted from the total relaxation loss.

3.2.3 Instantaneous Losses

In Section 5.9.5.2 of the AASHTO-LRFD, it discusses the methods for determining the instantaneous losses. These losses are comprised of anchorage set, friction, and elastic shortening.

3.2.3.1 Anchorage Set Loss

In Section 5.9.5.1 of the AASHTO-LRFD, it states that the anchorage set loss is the larger of two possible slips. The first slip is what is measured while the anchorage is restraining the stress in the prestressing steel, before and at transfer. The other slip, is the amount suggested by the manufacturer of the anchor system. The commentary to this section recommends possible values-of slip, depending on the type of equipment used, if none are available.

3.2.3.2 Frictional Losses

In Section 5.9.5.2.2 of AASHTO-LRFD, for pretensioned members that have draped strands the frictional losses should be considered at the hold-down devices. For post-tensioned members, the frictional losses between the duct and the prestressing strands can be determined as follows:

$Af_{pF} = f_{pj}(1 - e^{-(Kx+\mu\alpha)})$ (3.3) The variables in Equations 3.3 are as follows:

f_p; = stress in the prestressing steel at jacking in ksi

x = length of a prestressing tendon from the jacking end to any point under consideration in ft.

K = wobble friction coefficient (ft^{-1})

μ= coefficient of friction (1/Rad)

α = sum of the absolute values of angular change of prestressing steel path from jacking end

e = base of the Napieran logarithms

This section also contains a table of values that can be used for K and μ depending on the type of tendon and sheathing used.

3.3.2.3 Elastic Shortening

In Section 5.9.5.2.3 of AASHTO-LRFD, the methods for determining the elastic shortening for both pretensioned and post-tensioned members are presented. The elastic

shortening loss for pretensioned members is as

$$\Delta f_{pES} = \frac{E_p}{E_{ci}} f_{cgp} \qquad (3.4)$$

The variables in Equations 3.4 are defined as follows:

fcgp = sum of concrete stresses at the center of gravity of prestressing tendons due to the prestressing force at transfer and the self-weight of the member at the sections of maximum moment (ksi)

E_p = modulus of elasticity of prestressing steel (ksi)

E_{ci} = modulus of elasticity of concrete at transfer (ksi)

It also suggests that for the usual design of pretensioned members, that f_{cgp} be calculated at an assumed stress of $0.65f_{pu}$ for stress relieved strands and high strength bars and $0.70f_{pu}$ for low relaxation strands.

For post-tensioned members, the elastic shortening loss is computed differently and is as follows:

$$\Delta f_{pES} = \frac{N-1}{2N} \frac{E_p}{E_{ci}} f_{cgp} \qquad (3.5)$$

The variables in Equations 3.5 are defined as follows:

N = number of identical prestressing tendons

f_{cgp} = sum of concrete stresses at the center of gravity of prestressing tendons due to the prestressing force after jacking and the self-weight of the member at the sections of maximum moment (ksi)

It also states that the elastic shortening results in Equation 3.5 can be lower if stage stressing and retensioning procedures are used.

3.2.4 Lump Sum Approximation for Time-Dependent Losses

In Section 5.9.5.3 of the AASHTO-LRFD Code, it suggests the use of an approximate method for determining the total of all the time-dependent losses. This method can be used for pretensioned members, if the compressive strength at transfer is greater than or equal to 24.1 MPa (3.5 ksi). It may also be used for post-tensioned members, if the members are non-segmental with spans up to 48.8 m (160 ft), and if the stress transfer occurs between 10 and 30 days after casting. In addition to the above criteria the following material conditions must also be true for both types of tensioning: the member must be constructed from normal weight concrete and be either steam or moist cured, and the prestressing strands or bars used within in the member must have normal or relaxation properties. Average exposure conditions and temperatures must be felt by the member during its lifetime.

This approximate method is a function of f.' and PPR. Table 3-1 gives a listing of the applicable equations when using this procedure. The variable PPR is the partial prestressing ratio and is defined in Section 5.5.4.2 of the AASHTO-LRFD Code as follows:

$$PPR = \frac{A_{ps}F_{py}}{A_{ps}F_{py} + A_sF_y} \qquad (3.6)$$

The variables in Equation 3.6 are defined as follows:

A_B = area of non-prestressed tension reinforcement (in 2)

A_{pg} =area of prestressing steel (in 2)

F_y = specified yield strength of reinforcing bars (ksi)

F_{py} = yield strength of prestressing steel (ksi)

Table 3-1 Equations used for lump sum prestress loss calculation according to AASHTO LRFD

Type of Beam Section	Level	For Wires or Strands with f =235 250, or 270 ksi	For Bars with f_{pu} = 145 or 160 ksi
Rectangular Beams, Solid Slab	Upper Bound Average	29.0 + 4.0 PPR 26.0 + 4.0 PPR	19.0 + 6.0 PPR
Box Girder	Upper Bound Average	21.0 + 4.0 PPR 19.0 + 4.0 PPR	15.0
I-Girder	Average	$33.0\left[1.0-0.15\frac{f_c'-6.0}{6.0}\right]+6.0PPR$	19.0 + 6.0 PPR
Single T Double T. Hollow Core and Voided Slab	Upper Bound Average	$39.0\left[1.0-0.15\frac{f_c'-6.0}{6.0}\right]+6.0PPR$ $33.0\left[1.0-0.15\frac{f_c'-6.0}{6.0}\right]+6.0PPR$	$33.0\left[1.0-0.15\frac{f_c'-6.0}{6.0}\right]+6.0PPR$

The values obtained from equations of Table 3-1 can be reduced if low relaxation strands are used. Box girders can be reduced by 27.6 MPa (4.0 ksi). Rectangular beams, solid slabs, and I-girders can be reduced by 41.4 MPa (6.0 ksi). Single T's, double T's, hollow core, and voided slabs can be reduced by 55.2 MPa (8.0 ksi).

3.2.5 Detailed Estimates of the Time-Dependent Losses

In Section 5.9.5.4 of the AASHTO-LRFD Code, methods for determining the individual components of the time-dependent prestress loss are discussed. Creep, and shrinkage of concrete, and steel relaxation make up the total time-dependent prestress loss. The methods in this section can be applied to non-segmental prestressed members that have spans less than 76.2 m (250 ft), normal density concrete, and at time of prestress have a compressive strength of 24.1 MPa (3.5 ksi).

3.2.5.1 Shrinkage

In Section 5.9.5.4.2 of the AASHTO-LRFD Code, the shrinkage prestress loss is only a function of one variable for both pretensioned and post-tensioned members. The average annual ambient relative humidity, H, in percent, is that variable. The shrinkage loss is as follows:

$$\Delta f_{pSR} = (17.0 - 0.150H) \quad (3.7)$$

$$\Delta f_{pSR} = (13.5 - 0.123H) \quad (3.8)$$

Equation 3.7 applies for pretensioned members, and Equation 3.8 applies to posttensioned members.

3.2.5.2 Creep

In Section 5.4.5.4.3 of the AASHTO-LRFD Code, the creep loss is considered the same for both pretensioned and post-tensioned members. And is defined as follows:

$$\Delta f_{pCR} = 12.0 f_{cgp} - 7.0 f_{cdp} \geq 0 \quad (3.9)$$

The variables in Equation 3.9 are defined as follows:

$f_{g,}$ = concrete stress at the center of gravity of prestressing steel at transfer (ksi)

Δf_{cdp} = change in concrete stress at the center of gravity of prestressing steel due to permanent loads, except the load acting at the time prestressing force is applied.

3.2.5.3 Steel Relaxation

In Section 5.9.5.4 of AASHTO-LRFD Code, the steel relaxation loss is broken into two portions for pretensioned members. The first portion is the steel relaxation that begins after the strands are stressed, and ends upon transfer of the stress from the steel to the concrete. This steel relaxation loss calculated at transfers is as follows:

$$\Delta f_{pR1} = \frac{\log(24.0t)}{10.0}\left[\frac{f_{pj}}{f_{py}} - 0.55\right] f_{pj} \quad (3.10)$$

$$\Delta f_{pR1} = \frac{\log(24.0t)}{40.0}\left[\frac{f_{pj}}{f_{py}} - 0.55\right] f_{pj} \quad (3.11)$$

Equation 3.10 applies for stress-relieved strands and Equation 3.11 applies for low-relaxation strands. The variables in Equations 3.10 and 3.11 are as follows:

t = time estimated in days from stressing to transfer (Days)

f_{pj} = initial stress in the tendon at the end of stressing just before transfer(ksi)

f_{py} = specified yield strength of prestressing steel (ksi)

The second portion of the steel relaxation loss that applies for pretensioned members, takes place after the stress is transferred. The steel relaxation loss in post-tensioned members occurs only at this stage. The equations for this is as follows:

$$\Delta f_{pR2} = 20.0 - 0.4\Delta f_{pFS} - 0.2(\Delta f_{pSR} + \Delta f_{pCR}) \quad (3.12)$$

$$\Delta f_{PR2} = 20.0 - 0.3\Delta f_{pF} - 0.4\Delta f_{pES} - 0.2(\Delta f_{pSR} + \Delta f_{pCR}) \quad (3.13)$$

Equation 3.12 is for pretensioned members with stress-relieved strands and Equation 3.13 for post-tensioned members with stress-relieved strands. All variables are defined as before. If low relaxation prestressing steel is used the value of MpR2 can be taken as 30% of those obtained using Equations 3.12 or 3.13.

3.3 ACI-PCI Method

3.3.1 Introduction

In Section 18.6 of the ACI 318R-89'[3] Code, are given the types of loss that should be accounted for in prestress concrete design. It also only gives equations for determining frictional losses in post-tensioned tendons. In the Commentary to this section, it suggests using the ACI-ASCE Committee 423 Report 14 for estimating the prestress losses. This same report is the premise for the method described in Section 4.5 of the PCI Handbook." Since the report is the basis for both the ACI and PCI procedures, they have been combined here as one method. Applicable sections from both the ACI and PCI will be presented in this section.

3.3.2 Sources of Loss from ACI Code

In Section 18.6.1 of the ACI Code, definitions of the types of losses that should be estimated when the effective prestress is being determined are given. There are many different types of losses and these lead to the eventual reduction of the jacking stress to effective prestress. The sources of loss that most be allowed for are as follows: anchorage seat loss, elastic shortening, creep, and shrinkage of concrete, relaxation of tendon stress, and friction loss due to intentional or unintentional curvature of the tendons in post-tensioning.

3.3.3 Typical Range of Total Loss According to PCI

The PCI handbook in Section 4.5.2, suggests typical ranges of total prestress loss depending on the type of concrete being used. For normal weight concrete members the total loss may lie between 173 to 345 MPa (25 to 50 ksi). For sand-lightweight concrete members the total loss may be between 207 to 3791VIPa (30 to 55 ksi).

3.3.4 Frictional Loss According to ACI

In Section 18.6.2 of the ACI Code, the equations for calculating the friction loss in post-tensioned members are presented. The PCI Handbook suggests that this loss can be ,ompensated for by overstressing, and presents no method for calculating this (see Section 3.3.5). The ACI equations are as follows:

$$P_s = P_x e^{(Kl_x + \mu\alpha)} \quad \text{if}(Kl_x+\mu\alpha) \geq 0.3 \qquad (3.14)$$

$$P_s = P_x (1+Kl_x + \mu\alpha) \qquad \text{if } (K1_x + \mu\alpha) < 0.3 \qquad (3.15)$$

The variables in Equation 3.15- and 3.16 are defined as follows:

P_s = prestressing force at jacking end

P_x = prestressing tendon force at any point x

K = wobble friction coefficient

μ = curvature friction coefficient

α = total angular change of prestressing tendon profile in radians from tendon jacking end to any point x

The Commentary to this section of the ACI Code contains suggested values for p and a, based on the type of prestressing medium being used.

3.3.5 Equations for Determining Prestress Loss According to PCI

In Section 4.5.3 of the PCI Handbook, the equations for determining prestress losses are presented. It is interesting to note that the PCI Handbook suggests that because anchorage seat and frictional losses are mechanical losses, that they can be made up for by overstressing. Because of this argument those two types of losses are not considered in the total loss equation of Section 4.5.3 of the PCI Handbook. The equation for total loss of prestress is as follows:

$$T.L.= ES + CR + SH + RE \qquad (3.16)$$

The variables in Equation 3.16 are defined as follows:

T.L. = total loss (psi)

ES = elastic shortening

CR = creep of concrete

SH = shrinkage of concrete

RE = relaxation of tendons

The equation for elastic shortening is very similar to that which is suggested by the AASHTO-LRFD and is as follows:

(3.17)

The variables for Equation 3.17 are as follows:

K_{rg} = 1.0 for pretensioned members

Es = E_p in AASHTO

F_{cir} = f_{cgp} in AASHTO

$$f_{cir} = K_{cir}\left(\frac{P_i}{A_g} + \frac{P_i e}{I_g}\right) - \frac{M_g e}{I_g} \qquad (3.18)$$

The variables in Equation 4.16 are defined as follows:

K_{cir} = 0.9 for pretensioned members

P_i = initial prestress force after anchorage seating loss

e = eccentricity of center of gravity of tendons with respect to the center of gravity of concrete at the cross-section considered

A_g = area of gross concrete section at the cross-section considered

I_g = moment of inertia of gross concrete section at the cross-section considered

M_g = bending moment due to dead weight of prestressed member and any other permanent dead loads in place at time of prestressing

The equation for creep is similar to that of the AASHTO-LRFD, except that it incorporates more variables, and it is as follows:

$$CR = \frac{K_{cr} E_s}{E_c}(f_{cir} - f_{cds}) \tag{3.19}$$

The variables in Equation 3.19 are defined as follows:

K_{cr} = 2.0 for normal weight concrete or 1.6 for sand-lightweight concrete

f_{cds} = stress in concrete at center of gravity of tendons due to all superimposed permanent dead loads that are applied to the member after it has been prestressed

E_c = modulus of elasticity of concrete at 28 days

$$f_{cds} = \frac{M_{sd} e}{I_s} \tag{3.20}$$

The variables in Equation 3.20 are defined as follows:

M.,= moment due to all superimposed permanent dead loads applied after prestressing

The equation for shrinkage is dependent on many variables and is as follows:

$$SH = (8.2 \times 10^{-6}) K_{sh} E_s \times (1\text{-}0.06\ V/S)(100\text{-}R.H.) \tag{3.21}$$

The variables in Equation 3.21 are defined as follows:

K_{sh} = 1.0 for pretensioned members

V/ S = volume to surface ratio

R.H. = percent relative humidity

The equation for steel relaxation uses values selected based on the type of tendon used, and on the ratio of initial prestress after immediate losses, f_{pi}, to the ultimate strength of the tendon, f_{pu}. The equation is as follows:

$$RE = [K_{re} - J(SH + CR + ES)]C \quad (3.22)$$

The values K,., and J are functions of the type of tendon used and can be found in Table 3-2.The values of C, which is a function of the ratio f_{pi}/f_{pu}, are found in Table 3-3.

Table 3-2 Values of K_{re} and J.

Type of Tendon	K_{re}	J
270 Grade stress-relieved strand or wire	20,000	0.15
250 Grade stress-relieved strand or wire	18,500	0.14
240 or 235 Grade stress-relieved wire	17,600	0.13
270 Grade low-relaxation strand	5,000	0.040
250 Grade low-relaxation wire	4,630	0.037
240 or 235 grade low-relaxation wire	4,400	0.035
145 or 160 stress-relieved bar	6,000	0.05

Table 3-3 Values of C

f_{Pi}/f_{pu}	Stress-relieved strand or wire	Stress-relieved bar or low relaxation strand or wire
0.80		1.28
0.79		1.22
0.78		1.16
0.77		1.11
0.76	1.45	1.05
0.75	1.36	1.00
0.74	1.27	0.95
0.73	1.27	0.90
0.72	1.18	0.85
0.71	1.09	0.80
0.70	1.00	0.75
0.69	0.94	0.70
0.68	0.89	0.66
0.67	0.83	0.61
0.66	0.78	0.57
0.65	0.73	0.53
0.64	0.68	0.49
0.63	0.63	0.45
0.62	0.58	0.41
0.61	0.53	0.37
0.60	0.49	0.33

3.4 Spreadsheet Prestress Loss Results

The equations from the AASHTO and ACI-PCI were incorporated into a spreadsheet, and calculated for each girder section considered in this project. These sections are the midspan and the 1.52 m (5 ft) from the end support of Beams 1 and 4, and the midspan, and quarter-span of Beams 2 and 3. The results for all of these sections are similar. These results will be presented here in this section for the beams being investigated. The midspan had to be done for both sets of beams because the time at transfer times, and the concrete compressive strengths were different. These results are presented in Table 3-4 and Table 3-5 of this report.

Table 3-4 Spreadsheet results for the midspan of all beams studied.

Results for Midspan of Beams 1 and 4 in MPa					
Code	ES	CR	SH	RE	TL
ACI-PCI	116.9	204.6	30.7	53.8	406.1
AASHTO	123.3	228.9	39.6	25.6	417.5
Results for Midspan of Beams 2 and 3 in MPa					
Code	ES	CR	SH	RE	TL
ACI-PCI	126.4	207.2	30.7	52.9	417.1
AASHTO	133.2	228.9	39.6	22.4	424.3

Table 3-5 Spreadsheet results for quarter-span and 1.52 m from the end support of the beams studied.

Results for Quarter-span of Beams 2 and 3 in MPa					
Code	ES	CR	SH	RE	TL
ACI-PCI	123.4	202.2	30.7	53.6	410.3
AASHTO	129.4	222.3	39.6	23.4	414.9
Results for 1.52 m from End Support of Beams 1 and 4 in MPa					
Code	ES	CR	SH	RE	TL
ACI-PCI	116.9	204.6	30.7	54.0	406.2
AASHTO	123.3	228.9	39.6	26.6	417.5

The total loss values are higher for Beams 2 and 3, than Beams 1 and 4 at the midspans. The results for the quarter-span of Beams 2 and 3, and the 1.52 m (5 ft) from the end support of Beams 1 and 4, will be shown in Table 3-5. These results, for all points examined, will be plotted and compared with those obtained experimentally.

Chapter 4

DATA ANALYSIS AND EXPERIMENTAL RESULTS

4.1 Introduction

The thousands and thousands of strain readings collected from the datalogger on the Westbound Gandy Bridge, are used to determine the prestress losses within the girders. However, it is not practical to use every reading for this task of determining the losses. Portions of the readings have various fluctuations that are not consistent with adjacent measurements. In order to have smooth data to work with, the raw data was filtered to eliminate large fluctuations in the measured values.

The data file is first collected as a ANSI -DOS based file with each entry separated by commas and each row representing the readings taken at a particular time. This file is then brought into Microsoft Excel, and each data reading is placed in a separate cell. This allows the data to be easily manipulated.

A typical example of the raw data collected and imported into Microsoft Excel is shown in Table 4-1. This represents only a small portion of the file because the full version is very large. The first column represents the datalogger number. The year, Julian date, and hour of collection, which is represented in military time, are in columns 2, 3, 4,

and 5, respectively. The sixth column is the battery voltage, which needs to be greater than 12 Volts, in order, for data to be stored and collected properly at time of collection. The remaining columns are used to report the data in pairs of strain and temperature. In which, the first column in the pair is the strain reading in microstrain (10^6 - the actual strain) and the second column is the temperature reading in °F for each gauge. This sequence continues until the last two columns of collected data. The last two, represent the ambient temperature in °F and relative humidity in percent(not shown in Table 4-1).

Figure 4-1 is a plot of the raw data collected from the gauge at the steel centroid, of the section at the midspan of Beam 3. This plot contains the microstrain and internal temperature versus time for December 31, 1995. Figure 4-2 shows the ambient temperature and relative humidity measured for the same time interval shown in Figure 41. The measurements used for these plots are raw and continuous for the interval shown. Raw in the sense that the readings are as measured, and before any filtering have been included. This is done to illustrate that high fluctuations do occur due to extraneous vibrations, and are not considered useful data. One suggested reason why these fluctuations occur, is because, sudden electric noise from adjacent equipment could cause such a disturbance.

Table 4-1 Example of the raw collected

Col_1	Col_2	Col_3	Col_4	Col_5	Col_6	Strain	Temp	Strain
113	1995	355	12/21/95	1300	12.632	2445.9	67.334	2474.2
113	1995	355	12/21/95	1400	12.631	2447.5	67.605	2465.2
113	1995	355	12/21/95	1500	12.631	2447.5	68.424	2461.3
113	1995	355	12/21/95	1600	12.631	2445.2	69.69	2455.4
113	1995	355	12/21/95	1700	12.638	2439.2	71.137	2448
113	1995	355	12/21/95	1800	12.625	2432.6	72.548	2440.1
113	1995	355	12/21/95	1900	12.624	2425.8	73.662	2434.4
113	1995	355	12/21/95	2000	12.624	2419.1	74.875	2427.8
113	1995	355	12/21/95	2100	12.619	2411.5	76.158	2421
113	1995	355	12/21/95	2200	12.625	2404.2	77.409	2416
113	1995	355	12/21/95	2300	12.618	2397.5	78.668	2415.5
113	1995	356	12/22/95	0	12.618	2397.1	78.49	2421.8
113	1995	356	12/22/95	100	12.618	2402.7	77.297	2430.4
113	1995	356	12/22/95	200	12.618	2410.1	75.767	2439.3
113	1995	356	12/22/95	300	1_2.619	2418.9	74.029	2448.1
113	1995	356	12/22/95	400	12.612	2428.1	72.262	2457
113	1995	356	12/22/95	500	12.619	2456.4	70.577	2465.7
113	1995	356	12/22/95	600	12.611	2445.4	69.081	2475.3
113	1995	356	12/22/95	700	12.612	2451.3	67.113	2482.9
113	1995	356	12/22/95	800	12.612	2455.1	65.548	2486.6

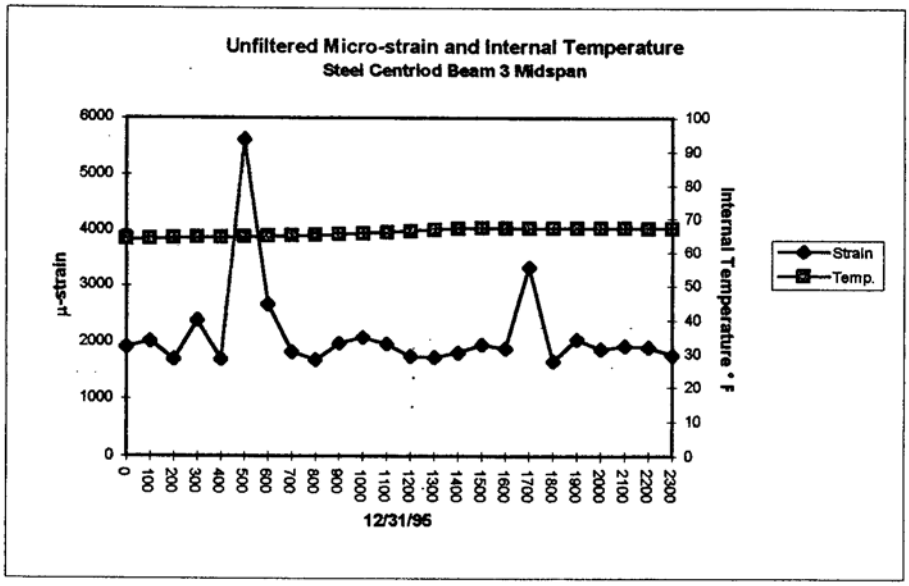

Figure 4-1 Unfiltered data plotted for December 31, 1995.

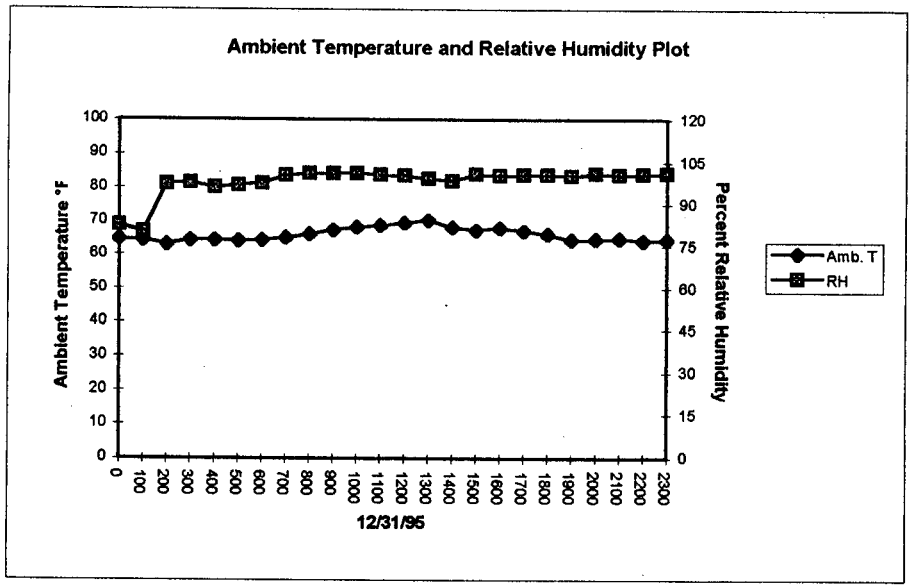

Figure 4-2 Unfiltered data plotted for December 31, 1995.

4.2 Determination of Prestress Loss from Measured Data

The strain and temperature measurements used for determining the prestress losses, were taken from the most consistent data at the particular days of interest. The difference between the strain readings are what is important, because, our concern is determining the change in prestress throughout the member with time.

The measured strain reading is made up of many different components which induce strain. In order to determine the change in strain and corresponding stress that belongs to prestress loss, it is necessary to extract these other components. These components consist of temperature effects and weight effects. The temperature effects are

created within the concrete and the steel of the vibrating wire in the strain gauge itself. The weight effects are felt by the member immediately upon cutting of the steel strands from the abutments. These effects must be removed to determine strain change due to prestress loss.

However to start with, it is necessary to determine a datum or reference to relate the change in the strain to, so that all changes refer back to the same point. Since we are dealing with two types of prestress losses (instantaneous and time-dependent), it becomes essential that there has to be two different reference points. The instantaneous loss, which is considered all elastic shortening, has its reference point as the last reading before the prestressing strands were cut. The last point used in determining the elastic shortening is the first reading taken after all the strands have been cut (3 hours after the first strand was cut). This point is also used as the new reference or datum for determination of the time dependent prestress losses.

The change in concrete strain due to prestress, $\epsilon_{prestress}$, is determined by the following equation:

$$\Delta\epsilon_{\text{ Prestress}} - \Delta\epsilon_{\text{Total}} - \epsilon_{\text{Temp.}} - \epsilon_{\text{Weight Effects}} \qquad (4\text{-}1)$$

Equation 4-1 extracts the prestress strain difference from the overall change in strain. Each of the components of this equation will be explained in detail in the following paragraphs.

The change in total strain, D£Totai, is the difference between the strain readings, after temperature corrections of the steel in the vibrating wire strain gauges have been accounted for. This temperature correction is represented in the following equation:

$$\Delta\epsilon_{Total} = (\epsilon_t - \epsilon_0) + (T_t - T_{t-1}) \times 6.78 \quad (4\text{-}2)$$

In Equation 4-2, ϵ and T represent the strain reading in microstrain and the internal temperature, respectively. The subscripts, t and 0, represent the readings at any time t and at a reference point 0. The subscript t-1 is the temperature reading used for the previous determination of the $\Delta\epsilon_{Prestress}$. The 6.78 multiplied with the internal temperature change is the coefficient of expansion of the steel used for the vibrating wire in the strain gauge. This number was recommended by Geokon Inc. and has the units of micro-strain/°F.

The strain created from the change of internal temperature within the concrete is ETomp. This strain can have large effects on the overall strain, in a concrete member, and must be removed to extract $\Delta\epsilon_{Prestress}$. The equation for ϵ_{Temp} is as follows:

$$\epsilon_{Temp} = 5.5 \times (T_t - T_{t-1}) \quad (4\text{-}3)$$

In Equation 4-3, the 5.5 multiplied with the internal temperature change is the coefficient of expansion of concrete and has the units of micro-strain/°F. All the other terms in Equation 4-3 are defined as before.

Another portion of the total strain that must be removed is the strain that is created from the weight effects, £weigt Eff tr. The weight effects need to be considered immediately after the strands are cut. At this time the members camber upward, and the force due to the self weight is pulling against it. The standard equation for determining the stress

created by the weight effects can be converted to strain through its relationship with the Young's Modulus. The stress equations due to weight effect is as follows:

$$f_{Top} = \frac{-12 \times M_0 \times (y - c_{Conc})}{I_{Conc}} \quad \text{for } y \geq c_{Conc} \qquad (4\text{-}4)$$

$$f_{Bottom} = \frac{12 \times M_0 \times (c_{Conc} - y)}{I_{Conc}} \quad \text{for } y < c_{Conc} \qquad (4\text{-}5)$$

Equation 4-4 and Equation 4-5 represent the stress in the top and bottom portions of the member, with respect to the neutral axis, respectively. These portions are separated by the concrete centroid, c_{Conc} with units of inches. M_o is in k-ft and is the moment created by the self weight of the member. I_{Conc} is the moment of inertia of the concrete section in in^4. Both Equation 4.4 and Equation 4.5 will yield stresses in ksi.

The initial prestress force and stress is based upon the force applied to the area of steel present. In determining the prestress losses of a member, it is usually customary to calculate them is terms of equivalent steel throughout the cross-section. This then makes it necessary to convert the strain changes in the concrete to equivalent stress changes in the steel. It is assumed that changes in the concrete strains and the prestressing steel, are equivalent because of the strong bond between them. The change in steel stress is obtained by multiplying the change of strain extracted from the gauges in the concrete by the modulus of elasticity of the prestressing steel. The equation for this is as follows:

$$\Delta f_{prestress} = E_s - \Delta \epsilon_{\ Prestress} \qquad (4\text{-}6)$$

For the Westbound Gandy bridge the modulus of the prestressing steel, E_s, is 28,000 ksi

4.3 Ambient Temperature and Relative Humidity

Ambient temperature and relative humidity are considered important factors when examining the time-dependent behavior of prestressed concrete. This is especially true when studying shrinkage of concrete, as mentioned in Section 1.3.3.2 of this report. Shrinkage in turn affects the concrete creep and steel relaxation also.

In the case of the Westbound Gandy Bridge project all beams were investigated not cast on the same day. Beams 1 and 4, were cast five days before Beams 2 and 3, under different environmental conditions. Figures 4-3 and 4-4 contain the ambient temperature and relative humidity plots for Beams 1 and 4, and Beams 2 and 3, respectively. The points on these plots cover the same time intervals, selected for determination of the change in prestress force. An average of the conditions on each day was computed and plotted.

4.4 Immediate Prestress Loss

4.4.1 Introduction

In the case of the Modified AASHTO Type VI pretensioned prestress girders used on the Westbound Gandy bridge, it is assumed that all of the immediate prestress loss is elastic shortening. Anchorage slip and frictional losses were considered negligible in comparison to elastic shortening. The steel relaxation before the strands were cut was also considered negligible.

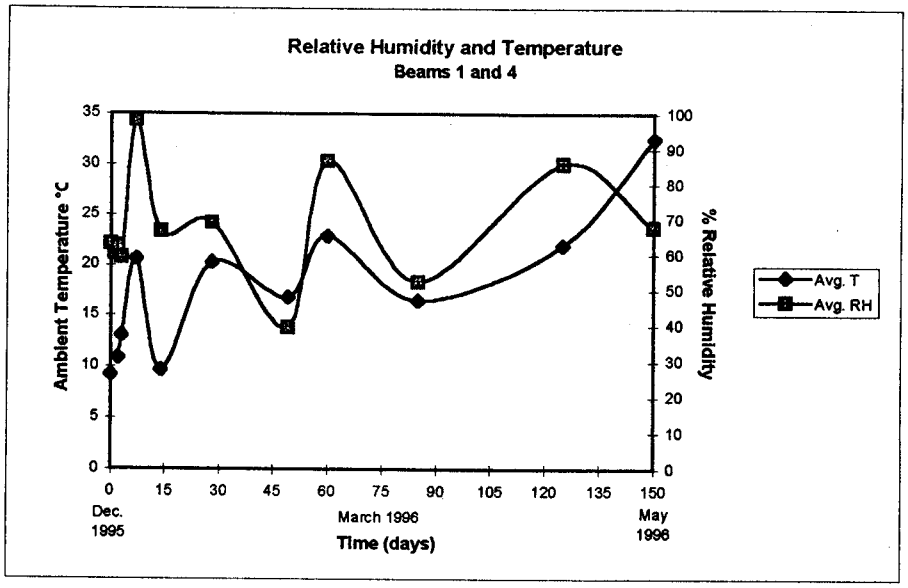

Figure 4-3 Relative Humidity and ambient temperature for Beams 1 and 4.

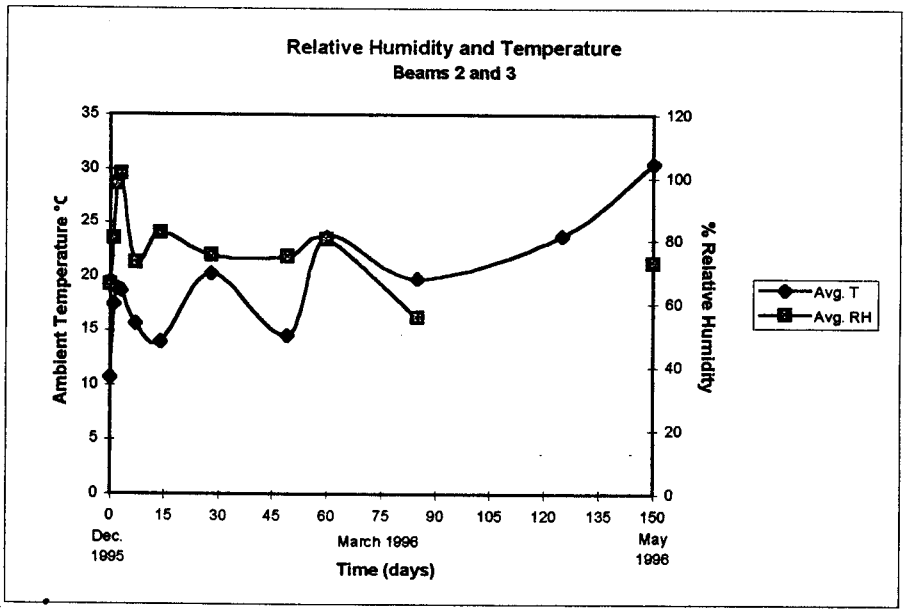

Figure 4-4 Relative Humidity and ambient temperature for Beams 2 and 3.

The portion of the prestress loss associated with elastic shortening is said to occur simultaneously, with the application of the prestress from the steel strands to the concrete. The cutting of the strands take place approximately over a 3-hour period. Since this loss is considered a one time loss, it has an absolute start and end point. Therefore, the beginning reference point was selected just before the strands were cut. The end reference point used in the analysis was chosen at the time the cutting was finished. With this simple assumption, elastic shortening loss can be determined for all locations where data was available. Initial data for Beam 2 is unavailable and is not considered in this analysis.

4.4.2 At Midspan

The elastic shortening results obtained for midspans of Beams l, 4, and 3, can be seen in Figures 4-5, 4-6, and 4-7, respectively. The differences between Beams 1 and 4, and Beam 3, is the age of the concrete when the prestressing strands were cut, and the ambient conditions (temperature and relative humidity). At the time the strands were cut, the age of concrete for Beams 1 and 4 were five days old, while Beam 3 was three days old. Also included on the plots are the elastic shortening results calculated by the ACIPCI and AASHTO equations of Chapter 3. In examining these plots there are clear trends, ranging from small changes in the top flange, to gradually larger changes toward the bottom flange. The elastic shortening results are larger for Beam 3, than those of Beams 1 and 4. A possible reason for this may be that the gauges were shifted during casting of the beams, causing their position not to be parallel with the span.

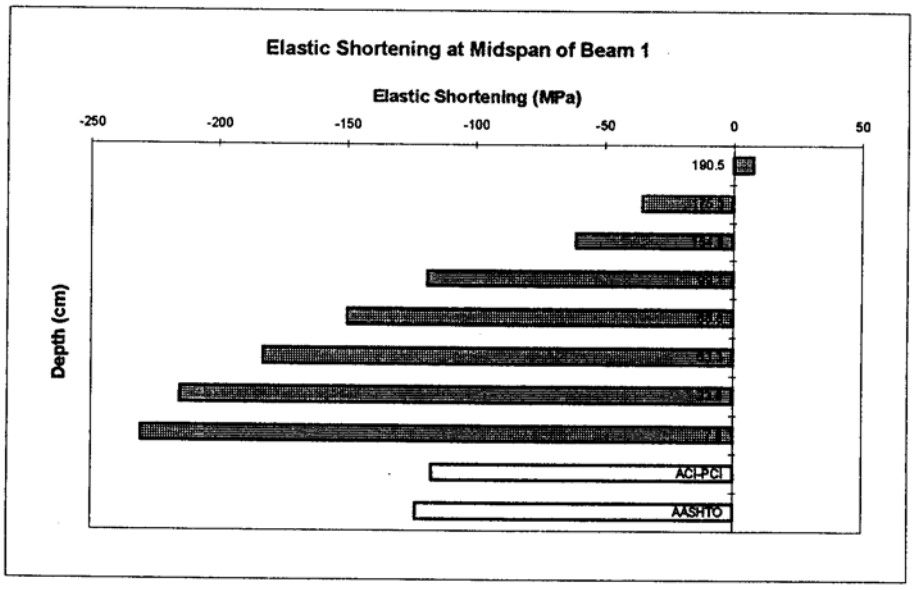

Figure 4-5 Elastic shortening loss for the midspan of Beam 1

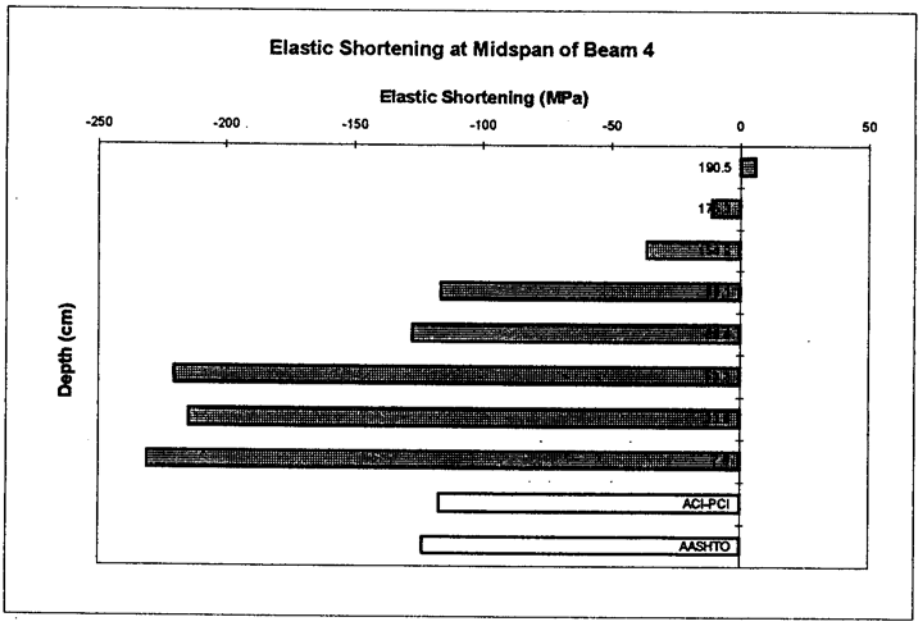

Figure 4-6 Elastic shortening loss for the midspan of Beam 4

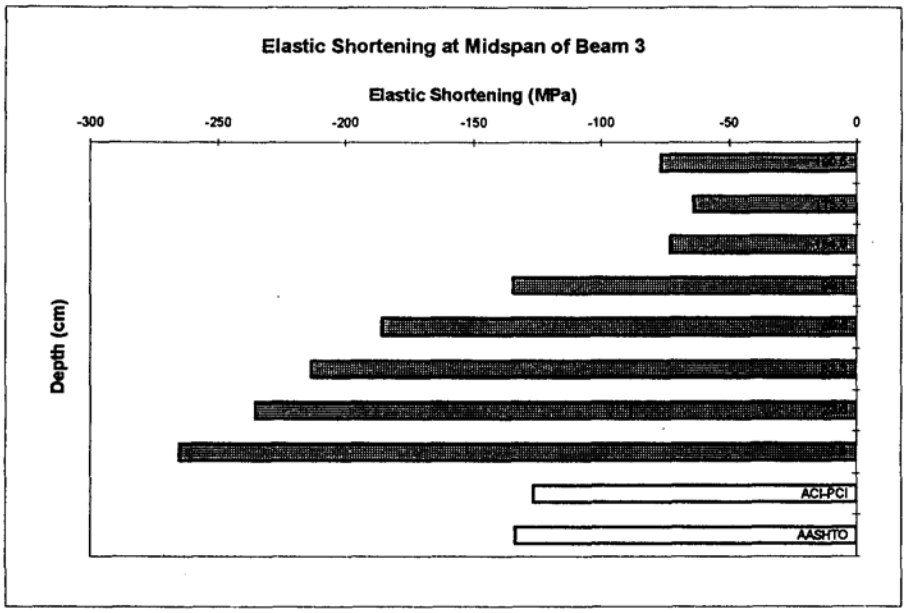

Figure 4-7 Elastic shortening loss for the midspan of Beam 3

Figure 4-8 contains an average of the elastic shortening of the three midspans for five points of interest. At the steel centroid, 23.6 cm, where the average elastic shortening loss is -221.6 MPa. Results for elastic shortening at the concrete centroid, which is at approximately 99.1 cm, is -123.1 MPa. At the future composite centroid, 154.9 cm, the elastic shortening loss was -56.6 MPa. At 175.3 cm which is approaching the top flange, the loss is -36.6 MPa, and at 190.5 cm which is 7.6 cm from the top flange, the elastic shortening loss is -21.0 MPa. The value at the concrete centroid is quite close to that of the Code results. At the steel centroid, however, the elastic shortening loss is much larger.

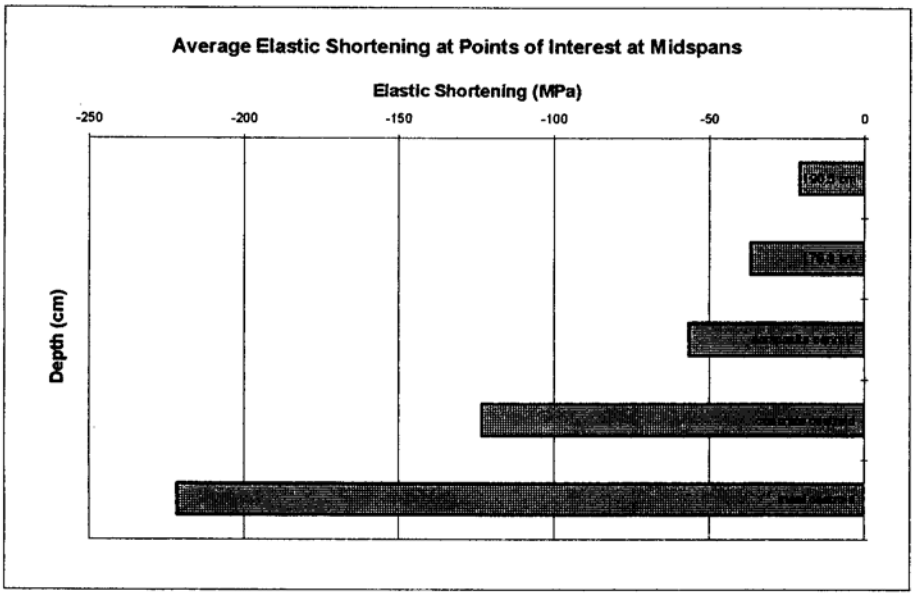

Figure 4-8 Average elastic shortening loss for the midspans.

4.4.3 At Quarter-span and 1.52 m from Support

The results obtained for the quarter span of Beam 3, and at the point 1.52 m from the end support of Beams 1 and 4, can be seen in Figures 4-9, 4-10, 4-11, respectively. These three Figures follow the same trend as the midspan loss, that is the change is relatively small near the top flange, and gradually increases as you move down the crosssection. This trend is consistent with the expectation, that greater values of loss will occur closer to the area where the prestressing strands exist. The magnitude of the loss seems to be smaller, at the quarter span and 1.52 m, when compared to the midspans.

For the quarter-span, four points of interest are 190.5 cm (top flange), 175.3 cm (near the future composite centroid), 84.1 cm (near the concrete centroid), and 18.8 cm

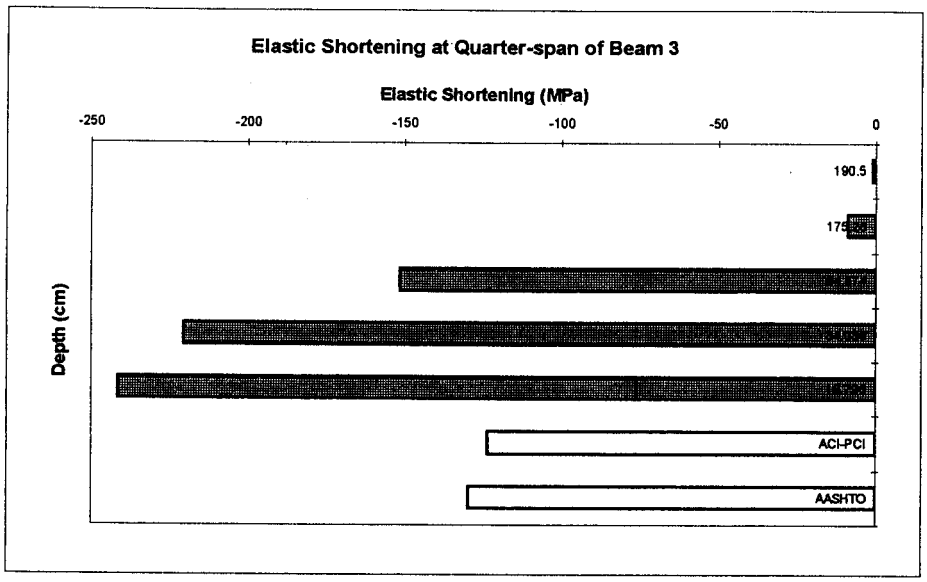

Figure 4-9 Elastic Shoretning Loss for the quarter-span of Beam 3.

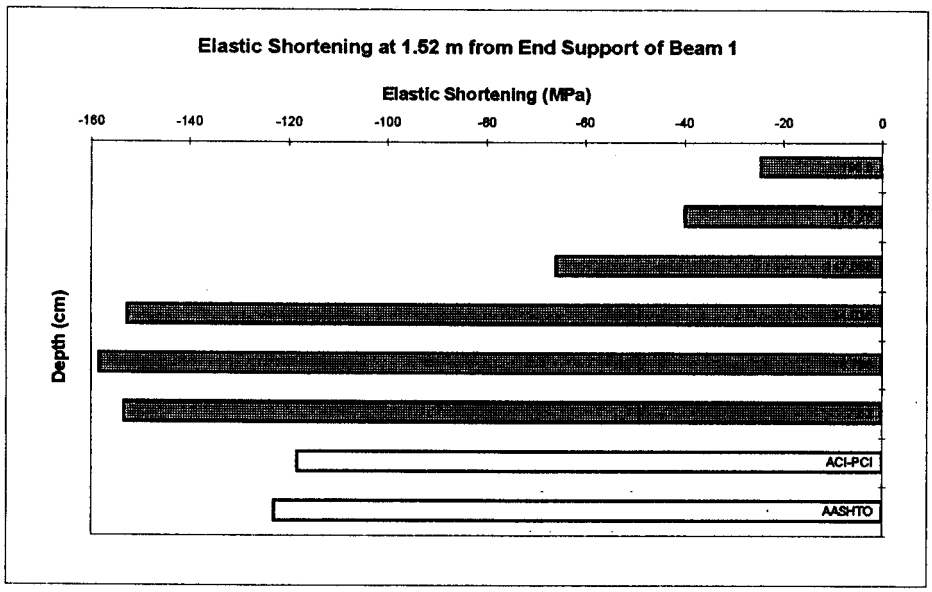

Figure 4-10 Elastic Shortening Loss for Beam 1 at 1.52 m

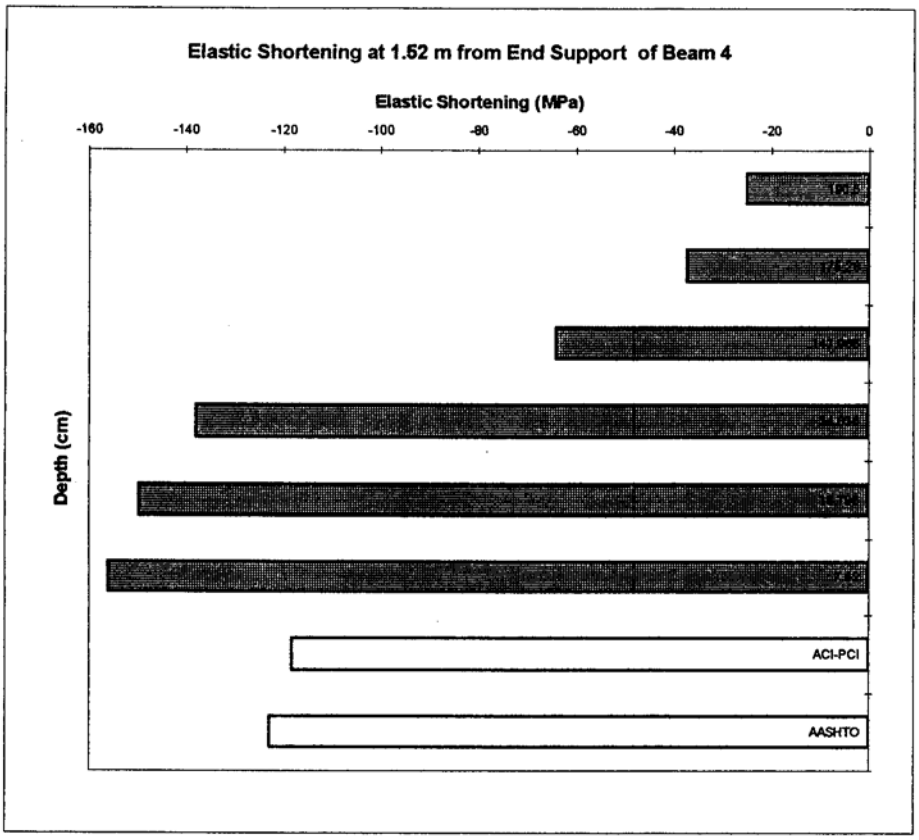

Figure 4-11 Elastic Shortening Loss for Beam 4 at 1.52 m

(straight strand steel centroid). The results for elastic shortening at 190.5 cm, 175.3 cm, 84.1 cm, and 18.8 cm are -0.92, -8.7, -151.4, and -241.4 MPa, respectively.

For the 1.52 m mark, the four points chosen for averaging of Beams 1 and 4 data are 190.5 cm., 175.3 cm, 147.1 cm (near the future composite centroid), and 18.8 cm. The results for the average of Beams 1 and 4 at the 1.52 m mark are shown in Figure 4-12. In that Figure, for 190.5 cm., 175.3 cm, 147.1 cm, and 18.8 cm, the elastic shortening loss is -24.7, -38.6, -65.0, and -154.1 MPa, respectively.

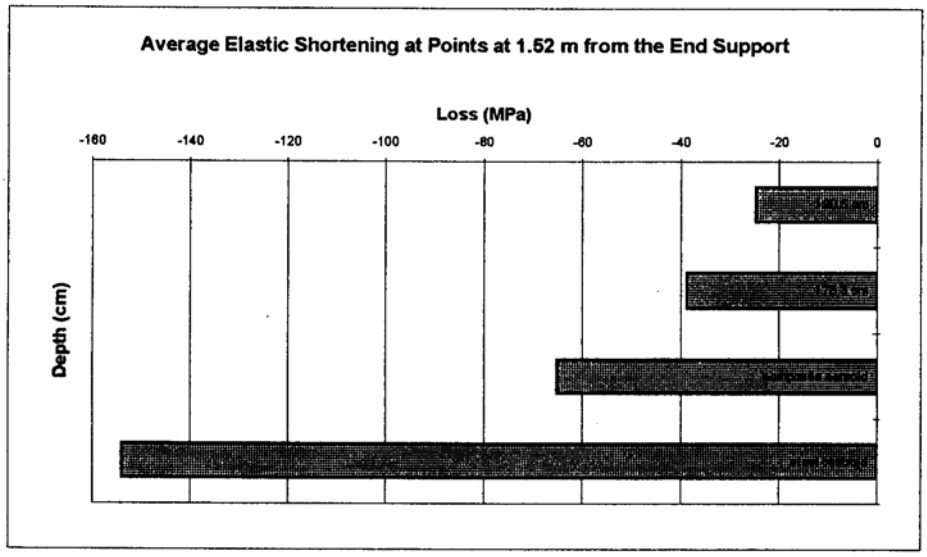

Figure 4-12 Average elastic shortening loss for the 1.52 m marks.

4.4.4 Variation Along the Length of the Beam

The elastic shortening loss has been represented at points within the cross-section without any variation along the length of the beam. The average values at the points of interest will now be plotted with consideration to length as well as depth. Since at the time of this study (150 days), all beams are under similar loading, it is reasonable to superimpose data from the midspan of 21.95 m, quarter-span of 10.97 m, and the 1.52 m from the end support, in order to determine the lengthwise variation of the losses.

Figure 4-13 shows the elastic shortening variation with length for the above mentioned points. It is assumed that at this time, the loading is symmetric so the results from one side can be flipped to the other. The steel centroid loss is larger at the quarterspan than at the midspan, but much smaller at the 1.52 m mark. The concrete centroid

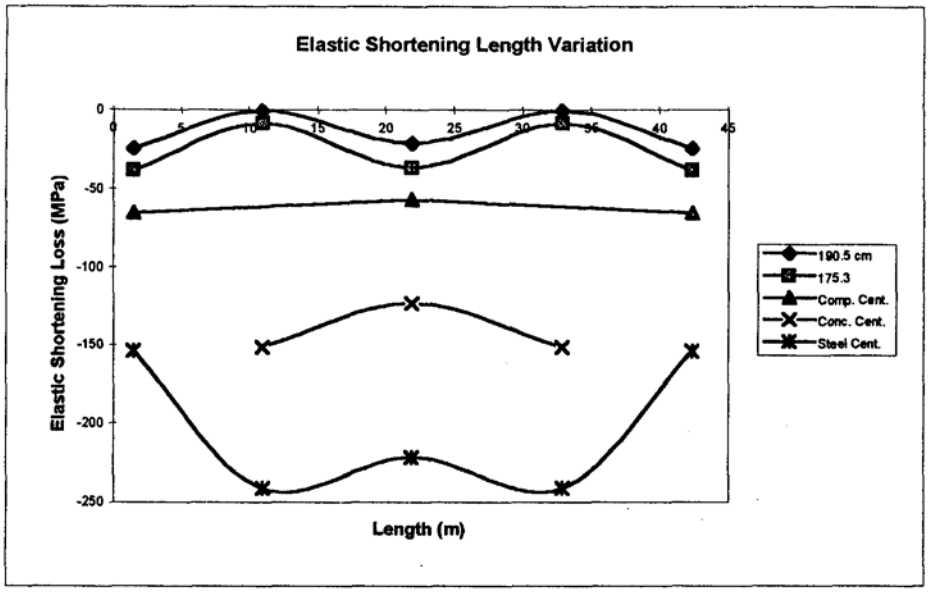

Figure 4-13 Elastic shortening loss variation along the span.

loss is greater at the quarter-span, when compared with that of the midspan. The loss at the level of the future composite centroid seems constant at the 1.52 m and the midspan points (there is no gauge at this location at the quarter-span, although the line is extended through that point). For the 190.5 and 175.3 cm points, the loss is very similar at the 1.52 m and midspans but is less at the quarter-span for these points.

4.5 Time-Dependent Prestress Loss

4.5.1 Introduction

The time-dependent prestress loss is made up of creep, shrinkage of concrete, and steel relaxation. This section does not break the time-dependent prestress loss into its

individual components, but it examines this loss without including the effect of elastic shortening.

It is assumed that the time-dependent portion of the prestress loss begins to occur directly after the immediate losses or when the strands are all cut. This point serves as a reference point to which all time dependent losses will be referred back to. Hence, the loss calculated at any time, t, will encompass all of the time-dependent loss up to that moment in time.

4.5.2 At Midspan

The results obtained for the time-dependent loss at the midspans of Beams 1, 4, and 3, can be seen in Figures 4-14, 4-15, and 4-16, respectively. These plots show data from all gauge locations that occur within the girder cross-sections. There seems to be little or no variation between the slopes of the time-dependent portion of the curves for all the gauges. Also shown are the calculated time-dependent prestress losses from ACI-PCI and AASHTO equations of Chapter 3.

Figure 4-17 contains an average time-dependent loss over the 150 day period, for five points of interest that occur in the midspan. These points are 190.5, 175.3, 154.9, 99.1, and 23.6 cm, and the time-dependent losses are -77.5, -87.1, -96.0, -134.3, and -193.6 MPa respectively. .

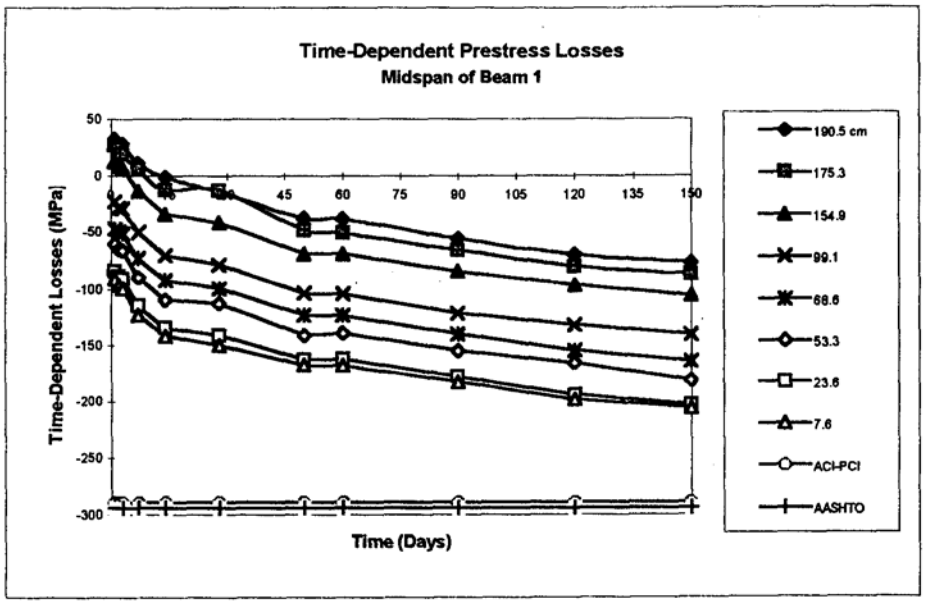

Figure 4-14 Time-Dependent loss at Midspan Beam 1

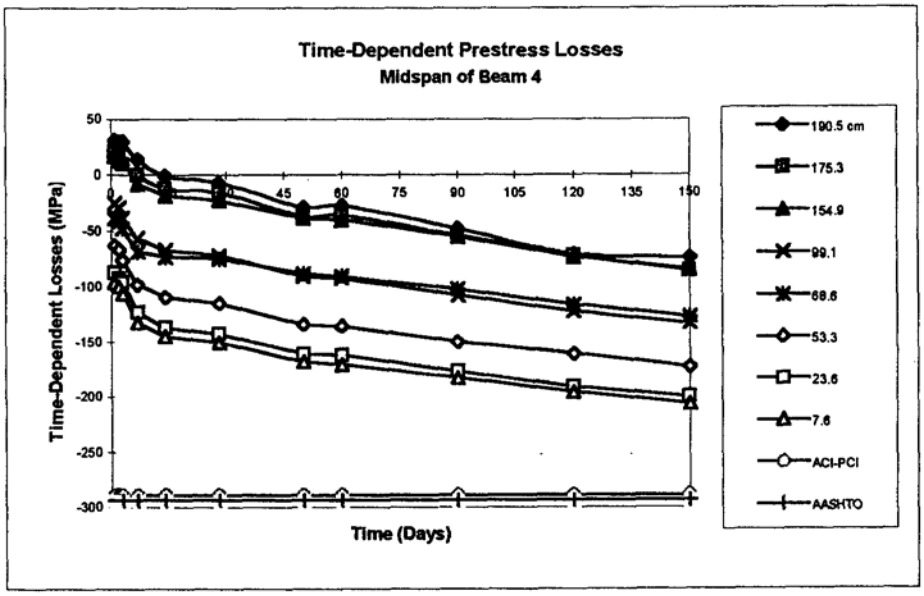

Figure 4-15 Time-Dependent loss at Midspan Beam 4

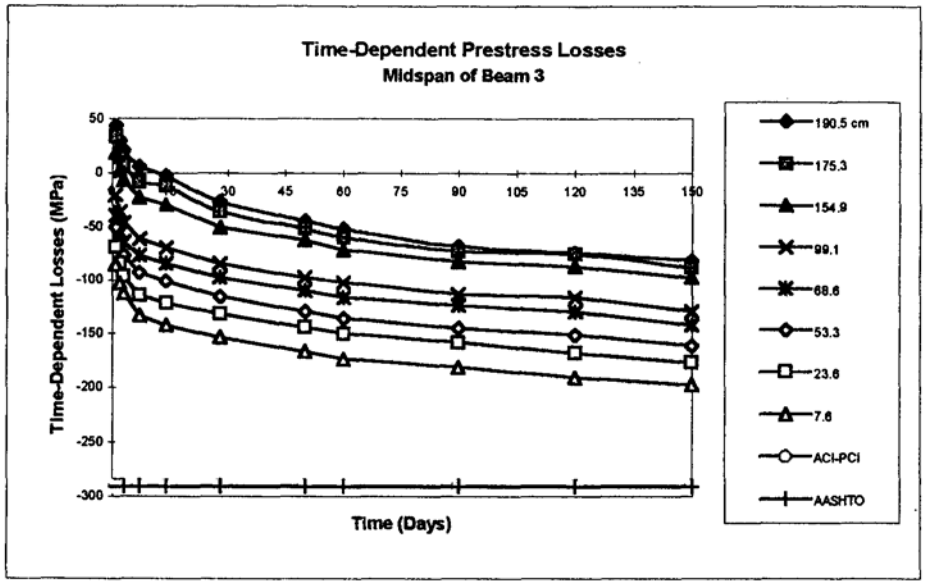

Figure 4-16 Time-Dependent loss at Midspan Beam 3

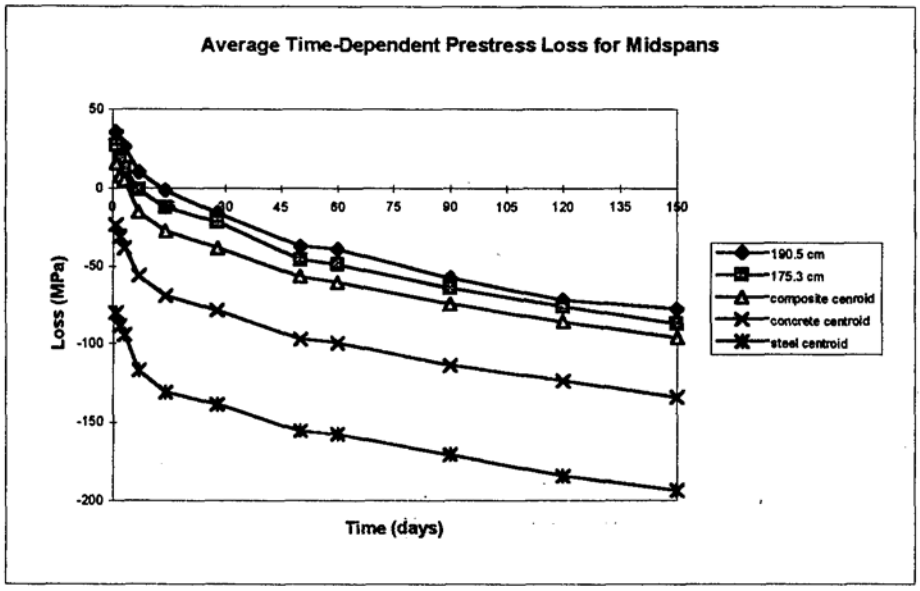

Figure 4-17 Average time-dependent loss at Midspans.

4.5.3 Quarter-span and 1.52 m from Support

The results obtained for the quarter span of Beam 3, and the 1.52 m points in Beams 1 and 4, are Figures 4-18, 4-19, and 4-20, respectively. They follow the pattern whereby they are progressively larger as you move from the top portion of the beam to the bottom. There seems to be little variation between the time-dependent loss at quarterspan and that at 1.52 m.

For the quarter point of Beam 3, the time-dependent loss over the 150 day period for four points of interest are shown in Figure 4-18. For the points 190.5, 175.3, 84.1, and 18.8 cm the time-dependent losses is -80.0. -102.3, -153.3, and -195.9 MPa, respectively. These values are just slightly larger than at 190.5 cm and 175.3 cm of the midspan, and slightly smaller than at the steel centroid (23.6 cm) of the midspan.

The average time-dependent loss for Beams 1 and 4 for the selected points at 1.52 m is shown in Figure 4-21. For 190.5, 175.3, 147.1, and 18.8 cm, the losses are -85.0, -93.7,-104.6, and -164.75 MPa, respectively. The top point losses of the 1.52 m mark are larger than those at quarter-span and midspan, and the bottom point losses are less than at the quarter-span.

4.5.4 Variation Along the Span

The average time-dependent prestress loss variation along the span is plotted in Figure 4-22. The time-dependent prestress loss is very similar for the 1.52 m, quarterspan, and midspan, at the 190.5 cm and the composite centroid levels. At 175.3 cm the

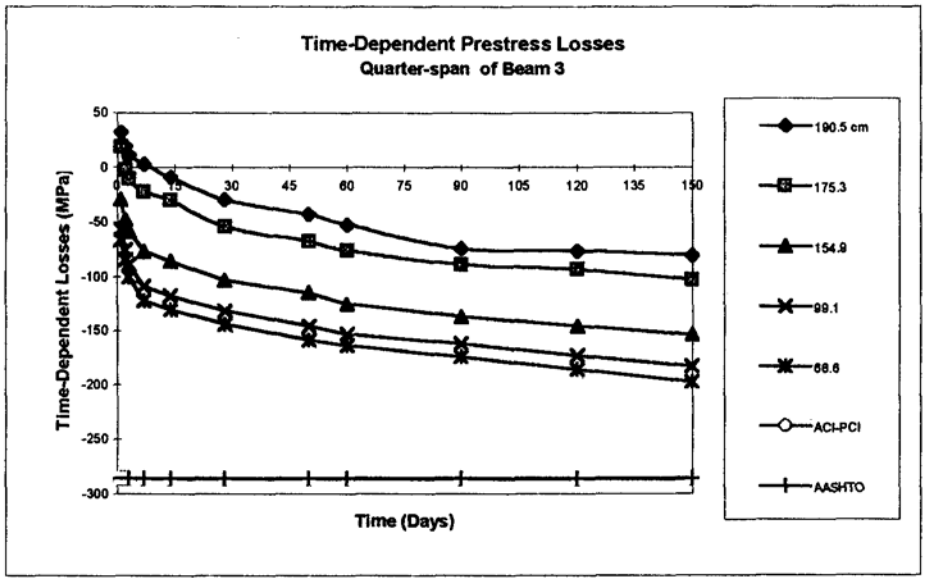

Figure 4.18 Time-dependent loss for the Quarter-span of Beam 3.

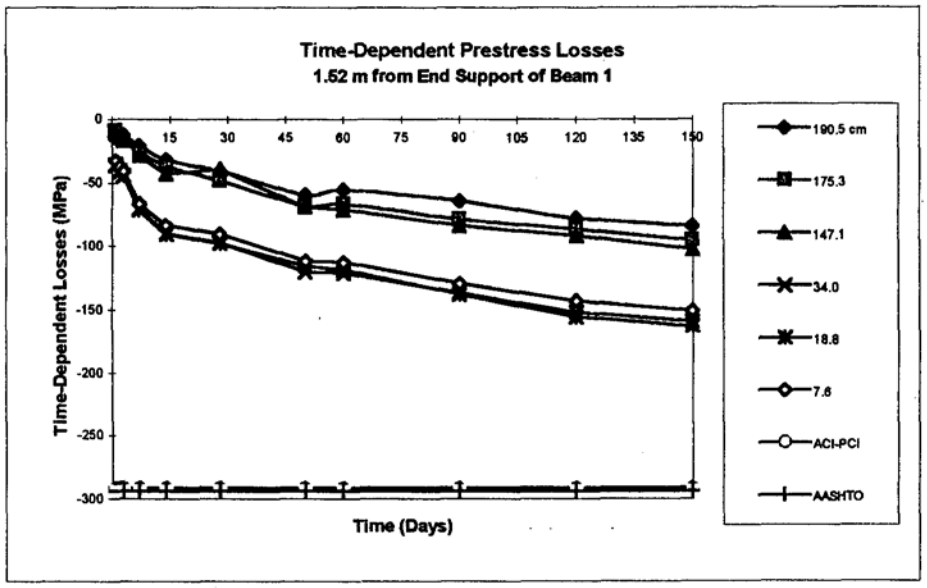

Figure 4.19 Time-dependent loss for the 1.52 m of Beam 1.

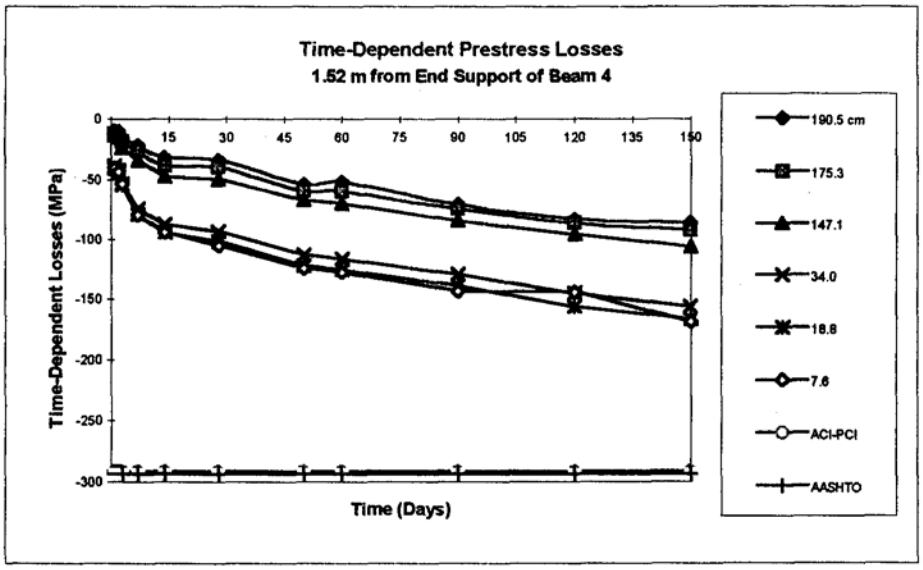

Figure 4.20 Time-dependent loss for the 1.52 m of Beam 4.

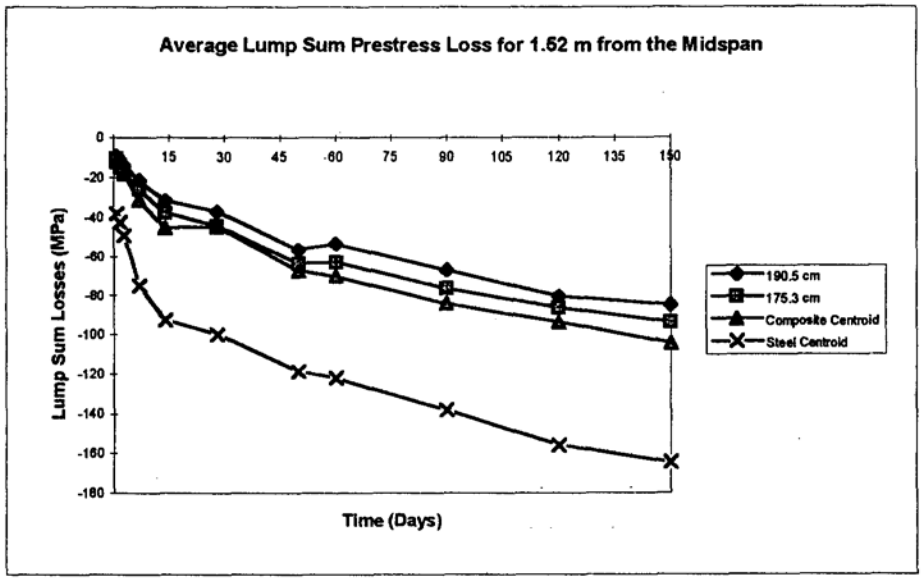

Figure 4.21 Average time-dependent loss for the 1.52 m points.

loss is larger for the quarter-span than the midspan and 1.52 m points. The concrete centroid is larger for the quarter-span than the midspan. The steel centroid level loss is larger for the midspan and quarter-span when compared with the 1.52 m points.

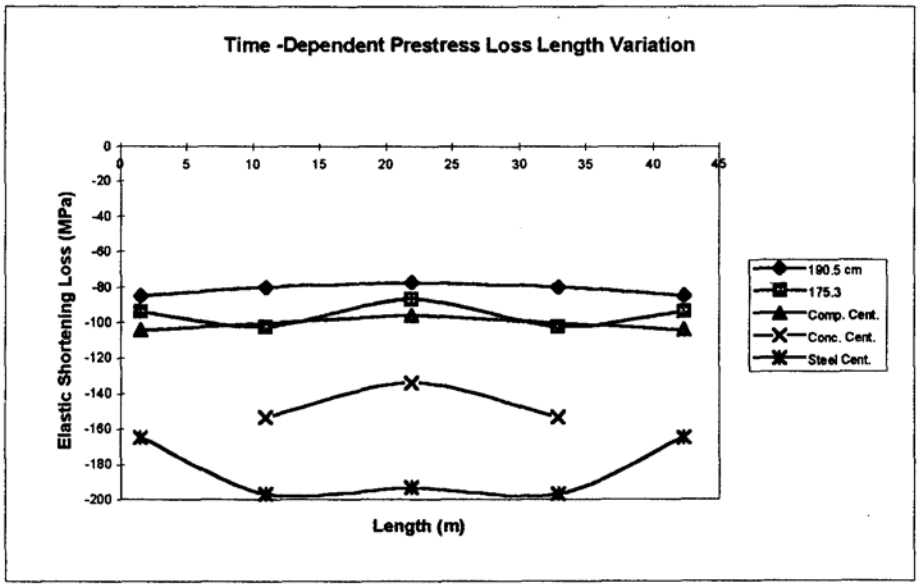

Figure 4.22 Time-dependent loss variation along the span.

4.6 Lump Sum Prestress Loss

4.6.1 Introduction

The lump sum prestress loss is made up of both the immediate and time-dependent prestress loss. This is considered the total prestress loss at any time t. And for this section t is equal to 150 days.

4.6.2 At Midspan

The results obtained for the lump sum loss at the midspans of Beams 1, 4, and 3, can be seen in Figures 4-23, 4-24, and 4-25, respectively. These plots show all gauge locations that occur within the section. There seems to be little or no variation between the slopes of the time-dependent portion of the curves for all the gauges. Also shown are the calculated time-dependent prestress losses from ACI-PCI and AASHTO equations of Chapter 3.

Figure 4-26 contains an average lump sum loss over the 150 day period for five points of interest that occur in the midspan. For the points 190.5, 175.3, 154.9, 99.1, and 23.6 cm, the lump sum loss is -98.6, -123.7, -152.6, -257.4, and -415.2 MPa respectively. The loss at the steel centroid level has already surpassed the ACI-PCI lump sum estimate and is very close to the AASHTO estimate.

4.6.3 At Quarter-span and 1.52 m from Support

The results obtained for the quarter span of Beam 3, and the 1.52 m points in Beams 1 and 4 are in Figures 4-27, 4-28, and 4-29, respectively. They follow the pattern whereby they progressively get larger as you move from the top portion of the beam to the bottom. There seems to be little variation between the lump sum loss at quarter-span and that at 1.52 m.

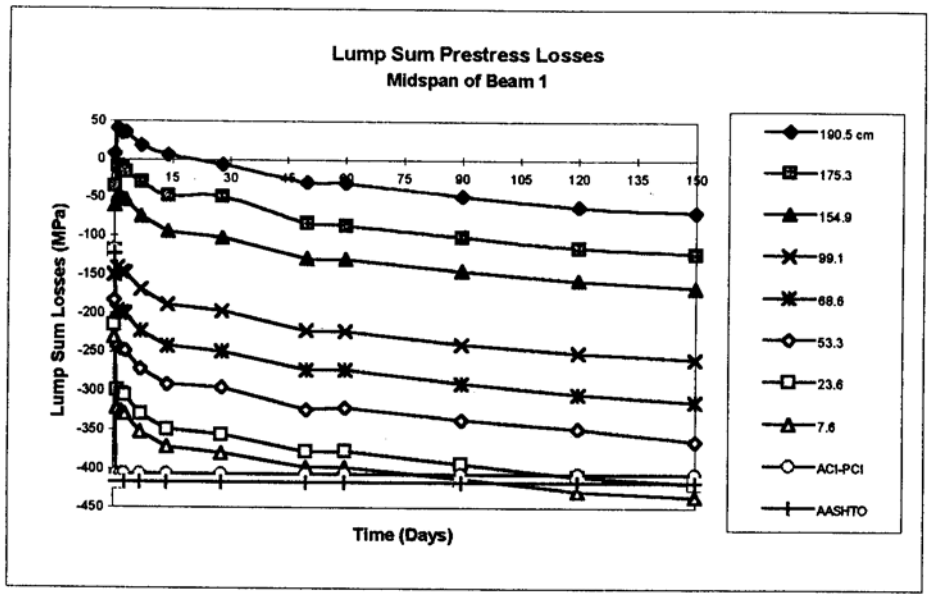

Figure 4-23 Lump Sum Loss at Midspan of Beam 1.

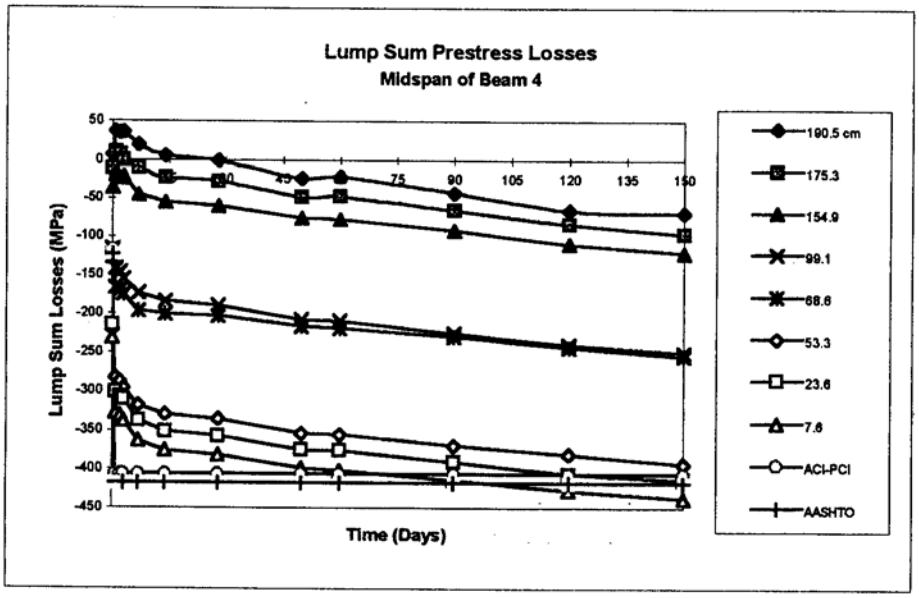

Figure 4-24 Lump Sum Loss at Midspan of Beam 4.

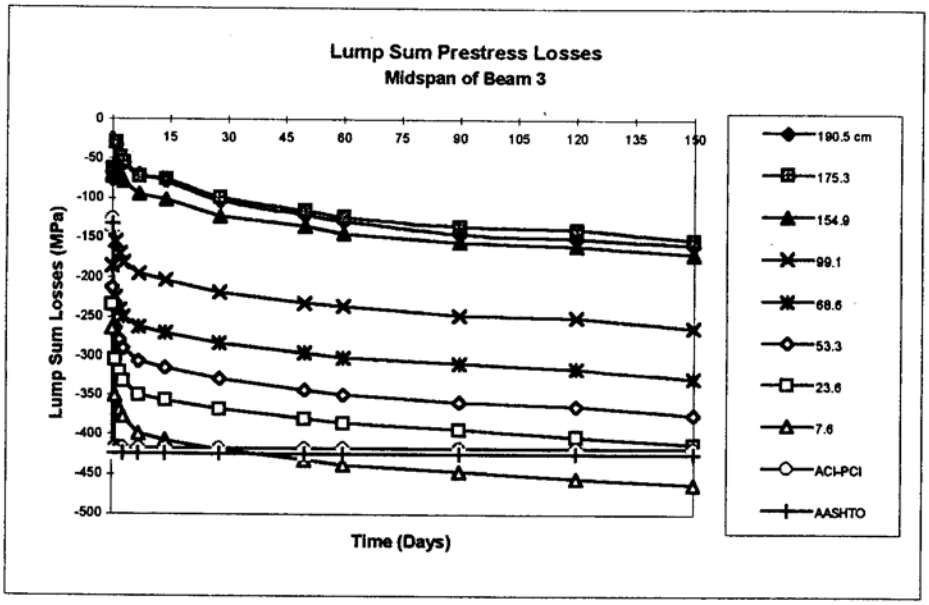

Figure 4-25 Lump Sum Loss at Midspan of Beam 3.

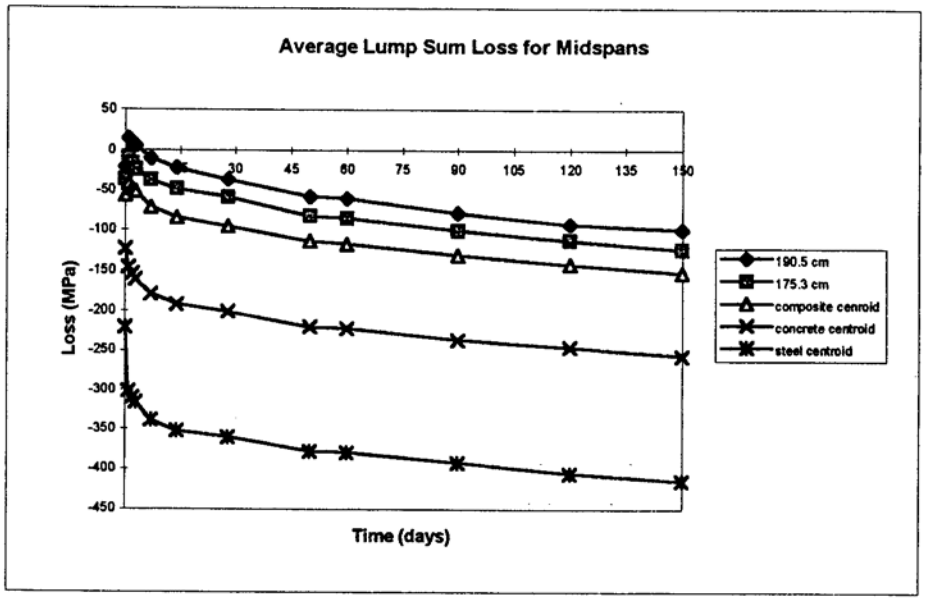

Figure 4-26 Average lump sum loss at Midspans.

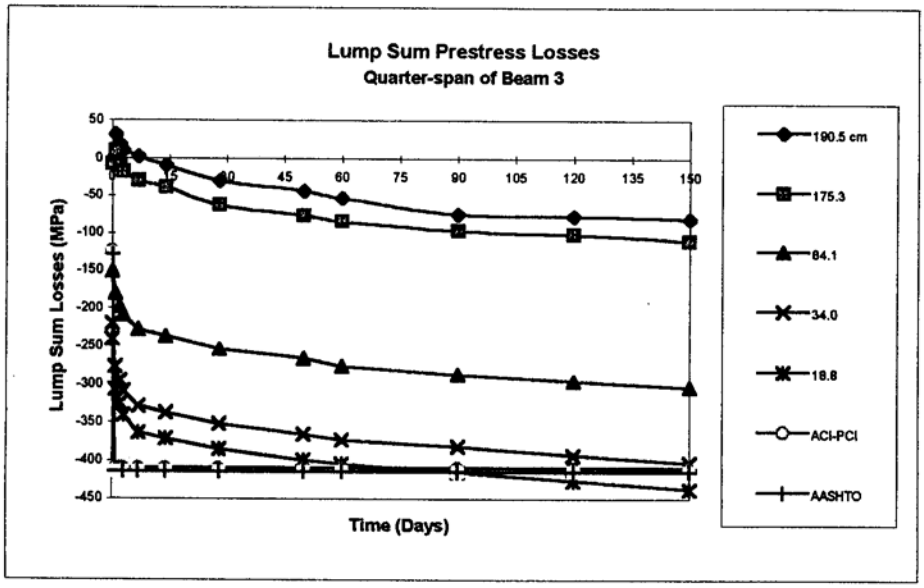

Figure 4.27 Lump Sum loss for the Quarter-span of Beam 3.

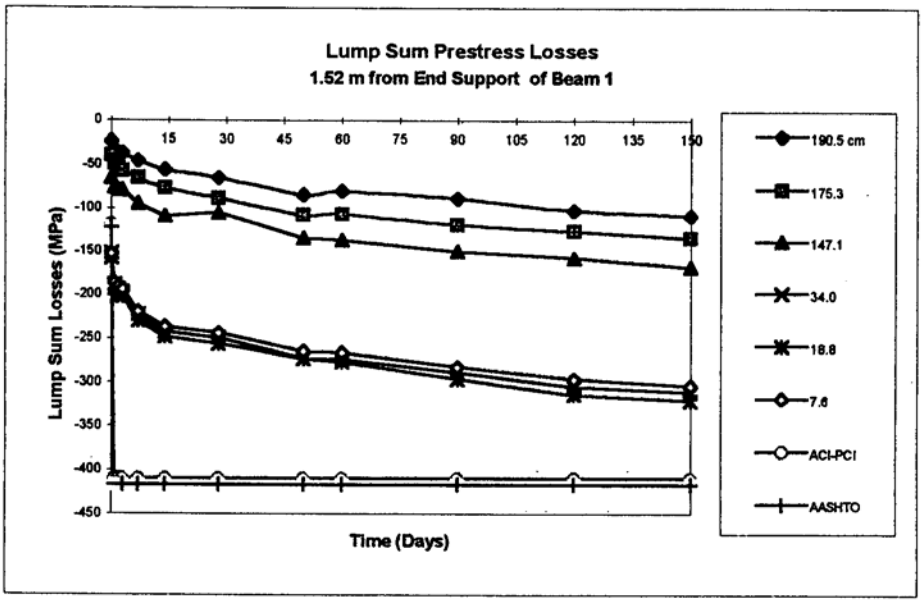

Figure 4.28 Lump Sum loss for the 1.52 m point of Beam 1.

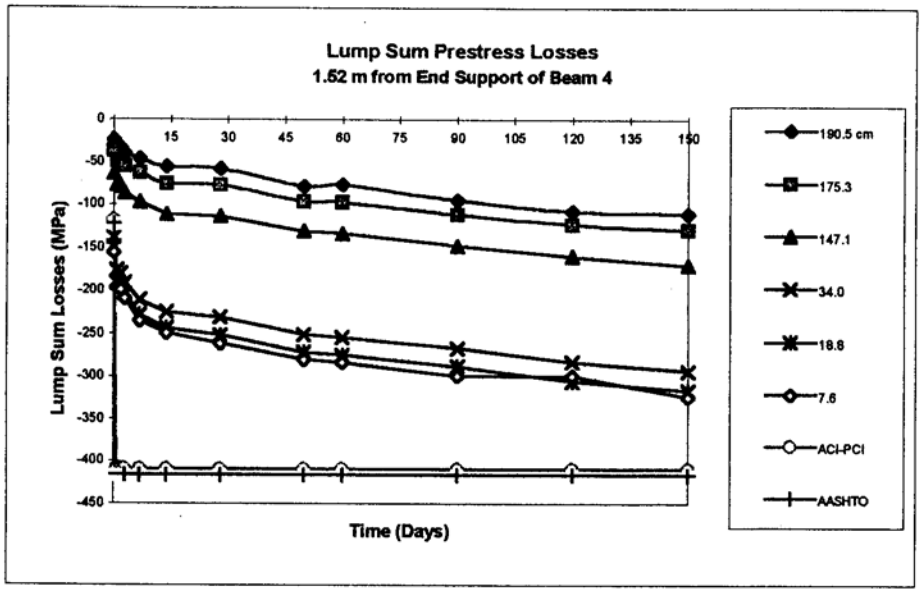

Figure 4.29 Lump Sum loss for the 1.52 m point of Beam 4.

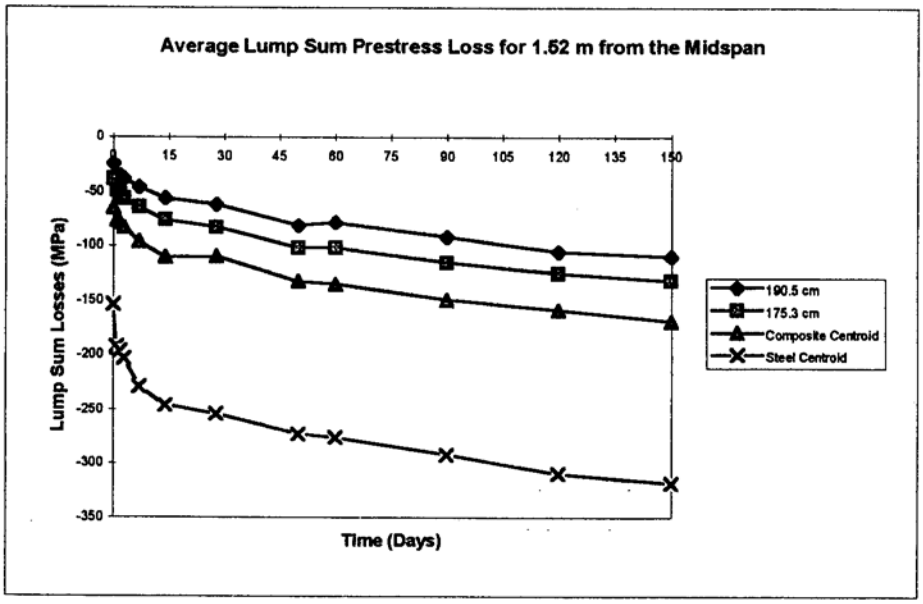

Figure 4.30 Average lump sum loss for the 1.52 m points.

For the quarter point of Beam 3, the lump sum loss over 150 day period for the four points of interest are shown in Figure 4-27. For the points 190.5, 175.3, 84.1, and 18.8 cm, the lump sum loss is -80.9. -111.0, -304.7, and -438.3 MPa respectively.

The average time-dependent loss for Beams 1 and 4, for the selected points at 1.52 m is shown in Figure 4-30. For 190.5, 175.3, 147.1, and 18.8 cm, the losses are -109.8, -132.3,-169.6, and -318.8 MPa, respectively.

4.6.4 Variation Along the Span

The average lump sum prestress loss variation along the span is plotted in Figure 4-31. The lump sum loss is very similar for the 1.52 m, quarter-span, and midspan at 190.5, 175.3 cm, and the composite centroid levels. At the concrete centroid the loss is larger for the quarter-span then the midspan. However, at the steel centroid level, the loss is larger for the midspan and quarter-span compared with the 1.52 m points.

The results observed here will be used to determine the effects of these prestress losses on prestressed concrete bridge design in the next chapter.

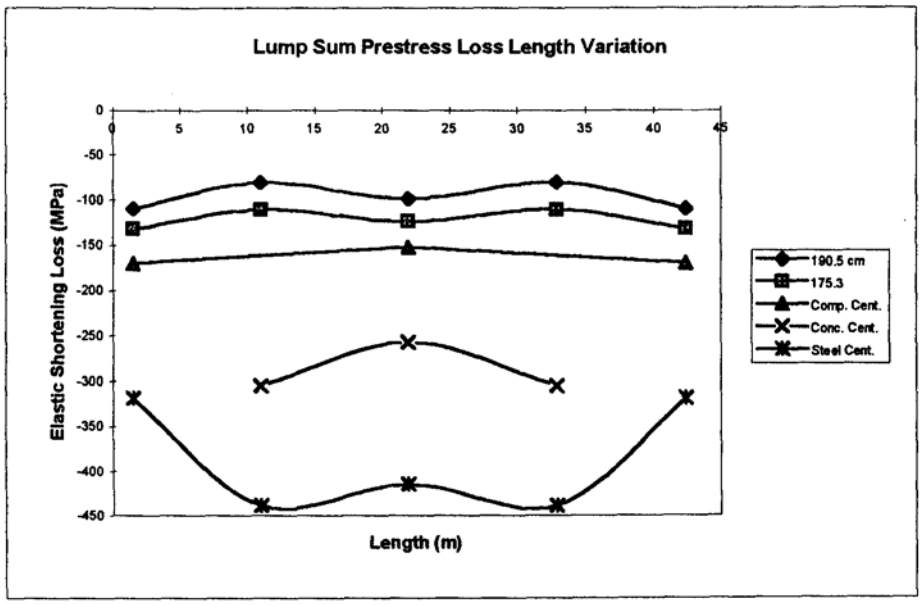

Figure 4-31 Lump sum loss variation along the

CHAPTER 5

EFFECTS OF PRESTRESS LOSS ON BRIDGE DESIGN

5.1 Introduction

In the previous chapter, the methods used to obtain the actual prestress losses were presented and the results shown. In this chapter, the losses are further examined to better understand their effects on bridge girder design. This is important because in design the prestress loss is generally assumed to be constant across the cross-section at any particular location being examined. Since this is not the case in reality, it is necessary to see the effect this has on other areas of design, such as, in other areas such as in the levels of concrete and tendon stresses, as well as, camber and deflection.

This chapter mainly examines three beams, using data at different locations along the span unless otherwise stated. The locations selected are the midspan of Beam 1, the quarter-span of Beam 3, and the 1.52m (5 ft.) from the end support of Beam 4. The results of the other cross-sections are similar.

To begin with, the cross-sectional prestress loss distribution on specific days are superimposed on the same plot for either 3 or 4 different days, to provide continuous time-dependent variation of the losses. Then the various ratios and percentage losses are

shown to further illustrate the effects of the losses throughout the cross-sections. Also, the stresses in both the prestressing tendons and concrete are computed and compared to their allowable values as stated in the ACI Code. Plots of relative humidity and ambient temperature versus loss for the midspan of the all beams studied are presented, and a regression analysis is performed to establish the level of dependency of the losses on these parameters, all things being equal. Finally, the effects of the prestress loss on the camber and deflection of the girders are studied.

5.2 Cross-sectional Prestress Loss Variation

Prestress losses are generally assumed to be uniform across the section of a member being examined during design. In reality this is not the case. The experimentally determined prestress loss varies considerable from the bottom to the top of a member. This variation appeared to be essentially linear within each specified cross-section. Therefore, having a better understanding of the prestress loss variation throughout a cross-section, allows for a more accurate determination of concrete and tendon stresses after transfer, and under service conditions.

The cross-sectional prestress loss results are plotted for the following days: l, 3, 7, 14, 28, 50, 60, 90, 120, and 150 days. These days are consistent with those chosen for the girder design also. There are four plots for each cross-section examined, which will be presented in one figure per cross-section. The plots are in the following sequence: 1.

3, and 7 days, 7, 14, and 28 days, 28, 50, and 60 days, 60, 90, 120, and 150 days. The calculated ACI-PCI and AASHTO prestress, loss results are assumed uniform and are superimposed on each plot as well. Note that the days are measured from when the transfer of stress from the prestressing strands to the concrete occurs.

5.2.1 Midspan of Beam 1

The cross-sectional prestress loss versus depth for the midspan of Beam 1 is plotted in Figure 5-1(a-d). In Figure 5-la, there is only a slight change of the crosssectional loss between 1 and 3 days, but the gap then widens upon 7 days. At 7 days the gauge at 7.6 cm. (3 in.) approaches the ACI-PCI calculated loss. The loss at 190.5 cm. (75 in.) is actually positive signifying the location was becoming less tensile.

In Figure 5-lb, a larger gap appears between 7 and 14 days, but the is little variation between 14 and 28 days. After 14 days, the gauge at 7.6 cm. (3 in.) is beyond the ACI-PCI calculated loss, and the loss at the steel centroid, which is located at 23.6 cm. (9.3 in.), is approaching the ACI-PCI loss. The loss at 190.5 cm. (75 in.) is still positive at 28 days.

In Figure 5-lc, a larger variation is shown between 28 and 50 days with little or no change at all between 50 and 60 days. The value of the loss at the steel centroid goes beyond the ACI-PCI calculated loss by 50 days. The entire loss is now all showing negative values as of 50 days.

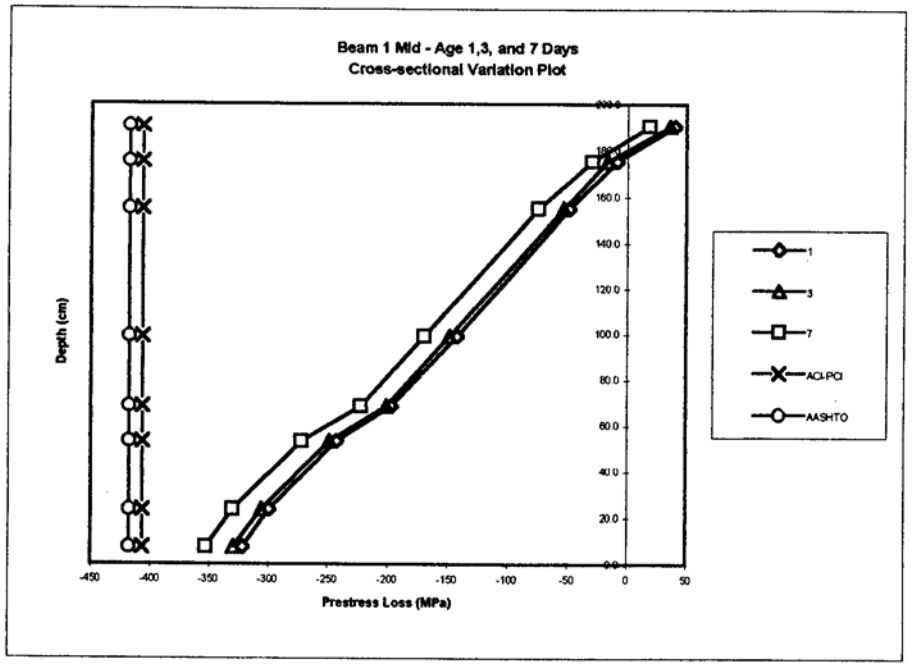

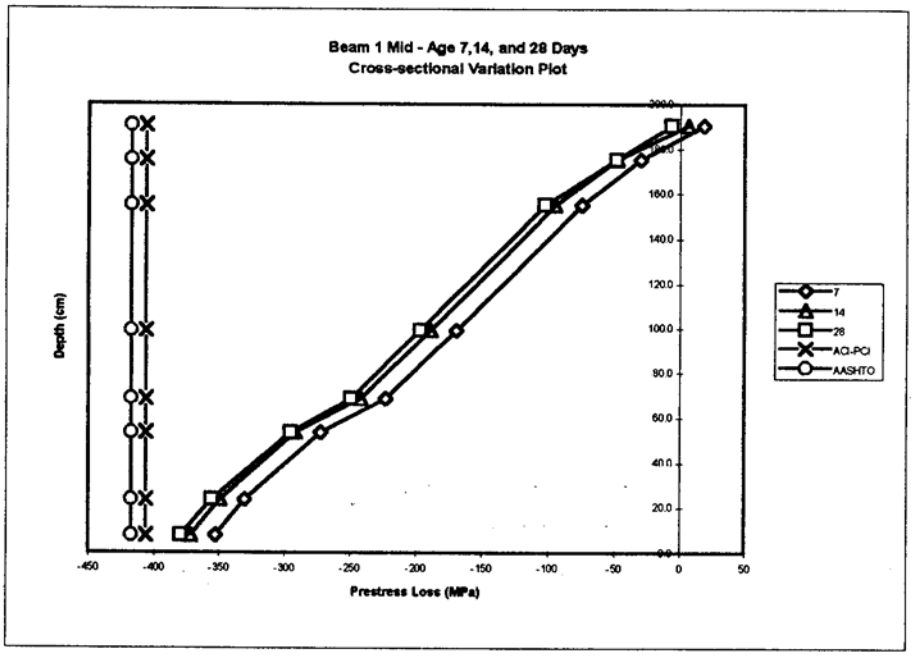

Figure 5-1(a-b) Midspan Beam 1 at (a) 1, 3, & 7 days (b) 7, 14, & 28 days

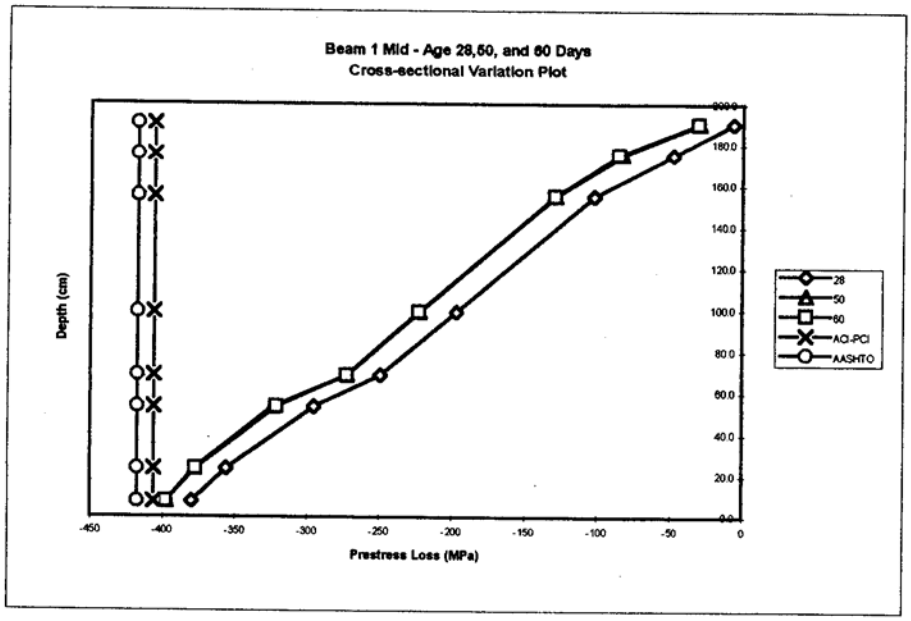

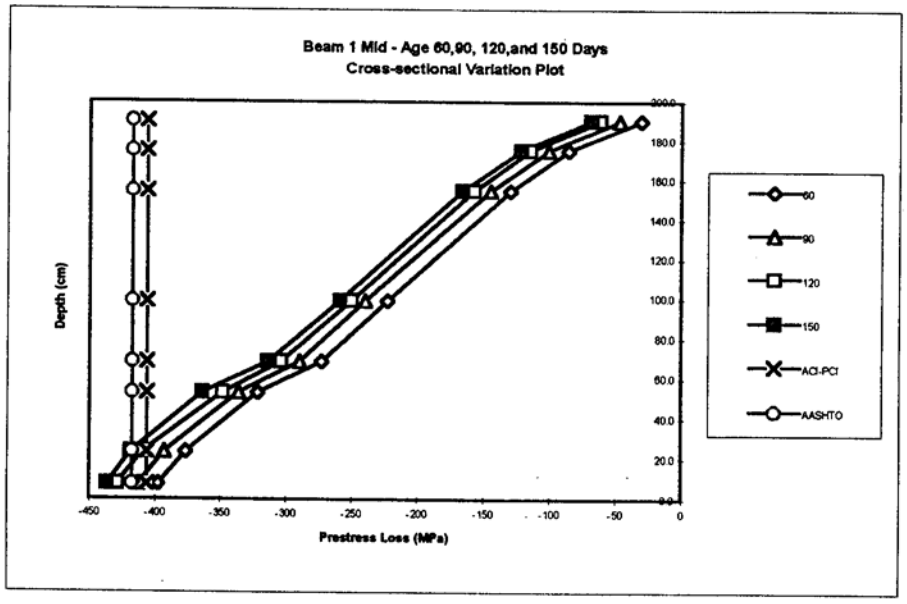

Figure 5-1(c-d) Midspan Beam 1 at (c) 28, 50, & 60 days (b) 60, 90, 120, & 150 days

In Figure 5-1 d, clearly indicates that the loss increases at a decreasing rate, as time elapses This can be seen by the gradual decrement in the gaps between the days shown. The prestress loss for 150 days at location 53.3 cm. (21 in.) is now approaching the ACIPCI calculated loss, and the loss at 7.6 cm (3 in.) is approaching the AASHTO calculated loss.

5.2.2 Quarter-span of Beam 3

The cross-sectional prestress loss versus depth for the quarter-span of Beam 3 is shown in Figure 5-2(a-d). In Figure 5-2a, the change between 1 and 3 days is larger than the change between 3 and 7 days for this cross-section. At 7 days the gauge at the straight prestressing steel centroid, 18.8 cm. (7.4 in.), is equal to the ACI-PCI calculated loss. Initially, at 190.5 cm. (75 in.) and 175.3 cm. (69 in.) the positive loss shows that these locations are becoming less tensile. After 7 days , however, only the 190.5 cm. (75 in) remains in the positive loss zone.

In Figure 5-2b, a smaller gap is shown between 7 and 14 days than between 14 and 28 days. The loss at 34.0 cm (13.4 in.) is gradually approaching that of the ACI-PCI 28 days. The loss at 190.5 cm. becomes negative after 14 days.

In Figure 5-2c, it is interesting to note that the difference between the loss at 50 and 60 days is more pronounced than at the midspan of Beam 1. At 50 days, the value of the loss at 34.0 cm. is equal to the ACI-PCI calculated loss. And at 18.8 cm., the loss is approaching the AASHTO calculated loss.

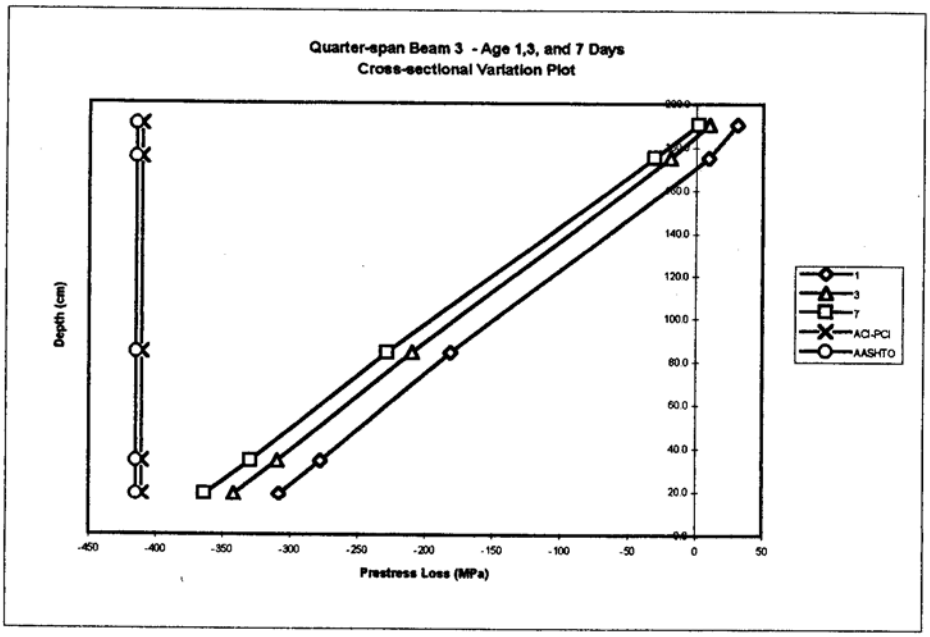

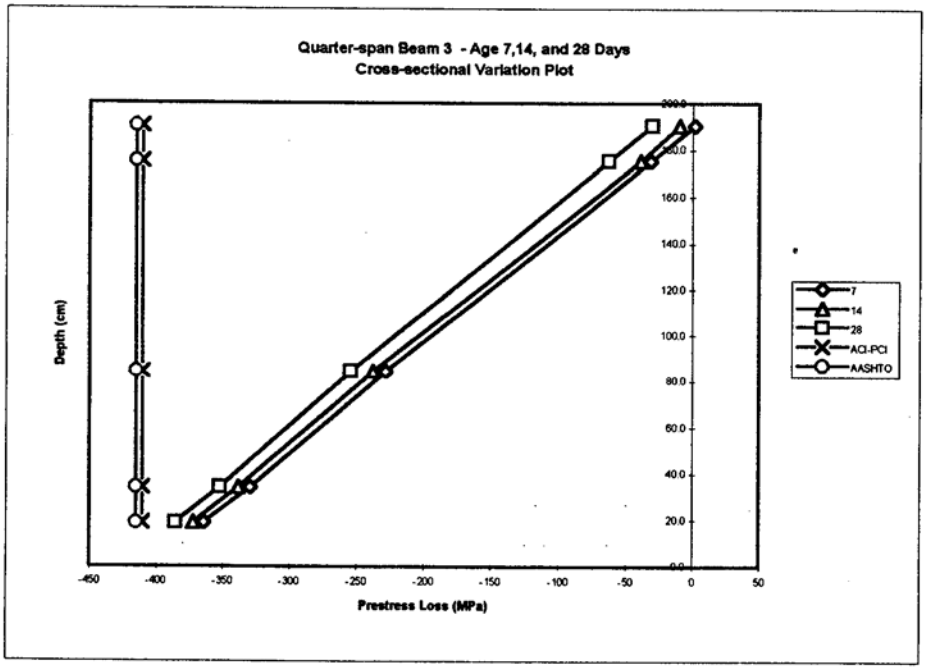

Figure 5-2 (a-b) Quarter-span Beam 4 at (a) 1, 3, & 7 days (b) 7, 14, & 28 days

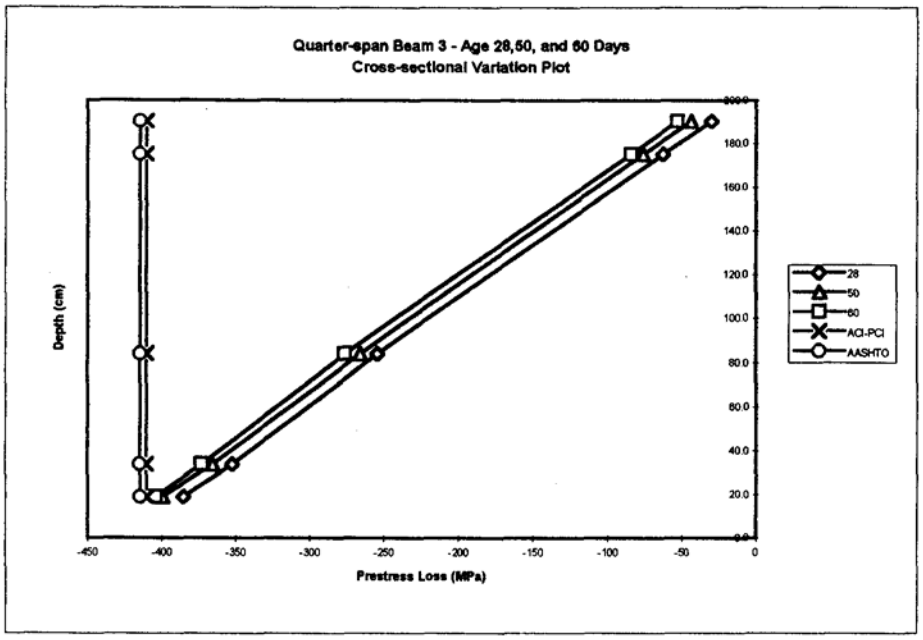

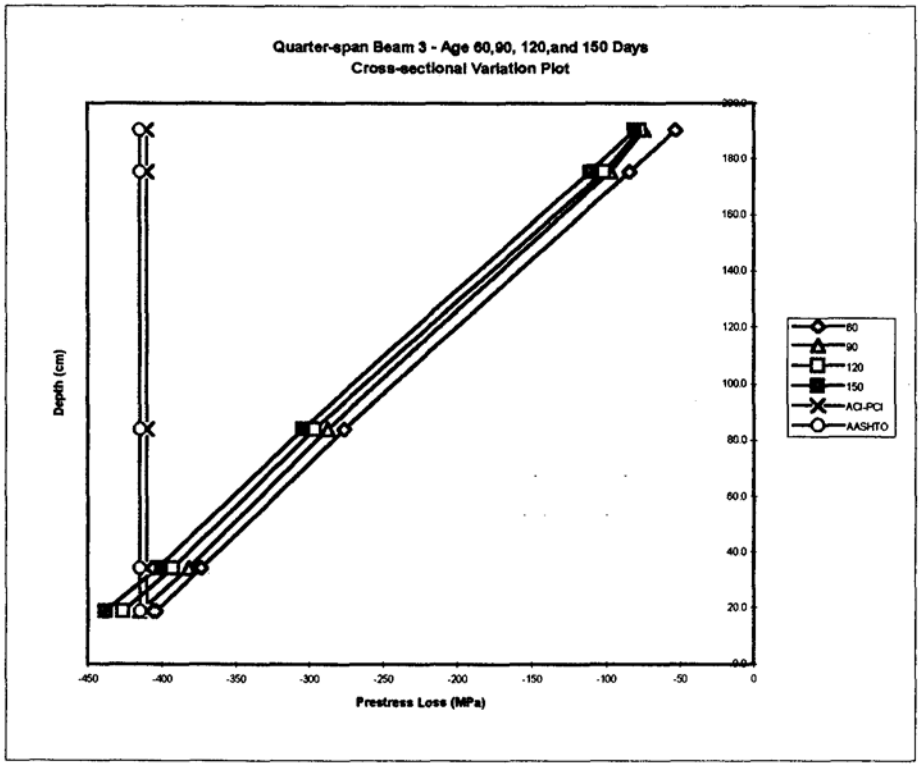

Figure 5-2(c-d) Quarter-span Beam 4 at (c) 28, 50, & 60 days (b) 60, 90, 120, & 150 days

Figure 5-2d is similar to Figure 5-ld in that it shows a decreasing rate of the loss increment between the days. However, the rate at which the decrement occurs is more gradual than at the midspan. The prestress loss by 150 days at 18.8 cm. has reached the calculated AASHTO loss value. These plots are very similar to those of the midspan of Beam 1, but show a more linear variation of the loss over the depth of the beam.

5.2.3 From the End Support (1.52 m) Beam 4

The cross-sectional prestress loss versus depth at 1.52 m (5 ft.) from the end support for Beam 4 is shown in Figure 5-3(a-d). In the first plot, Figure 5-3a, the loss appears to be occurring at higher rate in the lower portion of the cross-section than in the upper. There is no positive loss at this cross-section, suggesting little tensile stresses this close to the support..

Figure 5-3b shows a trend towards a more uniform rate of loss between the top and bottom with little change between 14 and 28 days. However, the change between 7 and 14 days is much greater.

Figure 5-3c is consistent with that of Figure 5.3b except there is a larger change between 28 and 50 days while remaining relatively unchanged between 50 and 60 days. In Figure 5-3d, the loss starts showing a more consistent rate of decrement, and the separation per month going to 150 days is approximately equal. It is interesting to

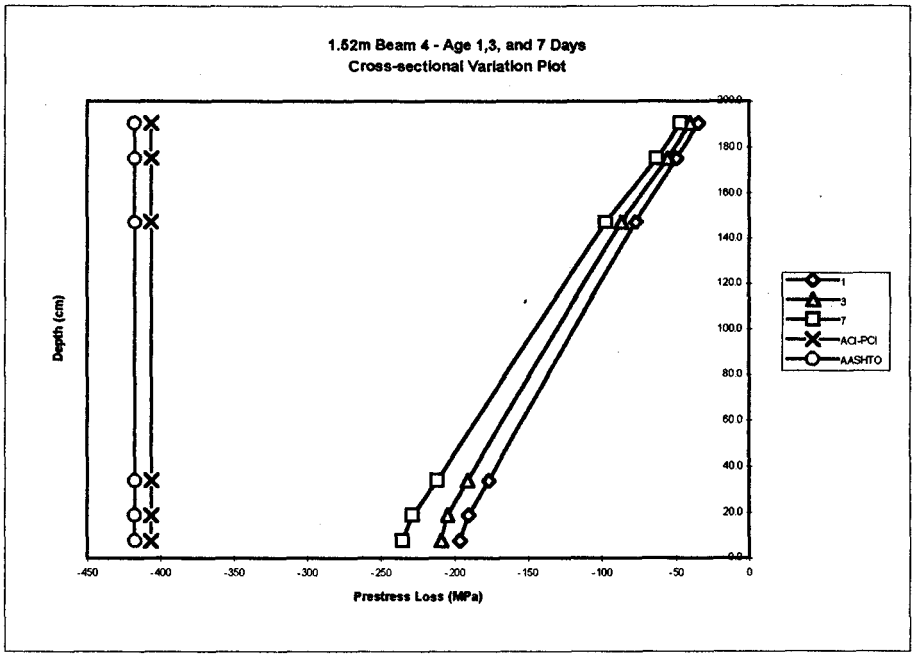

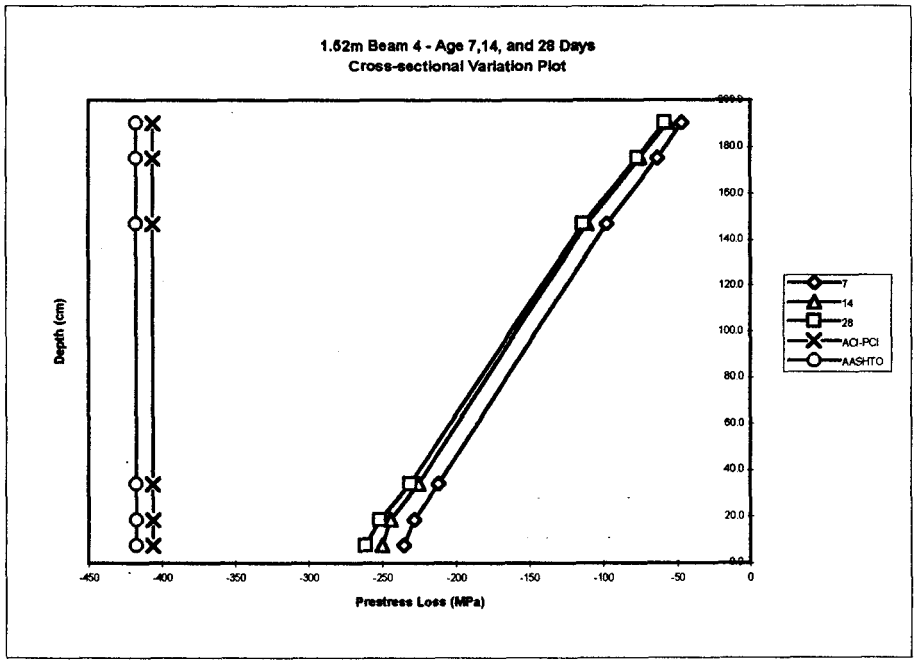

Figure 5-3 (a-b) 1.52 m Beam 4 at (a) 1, 3, & 7 days (b) 7, 14, & 28 days

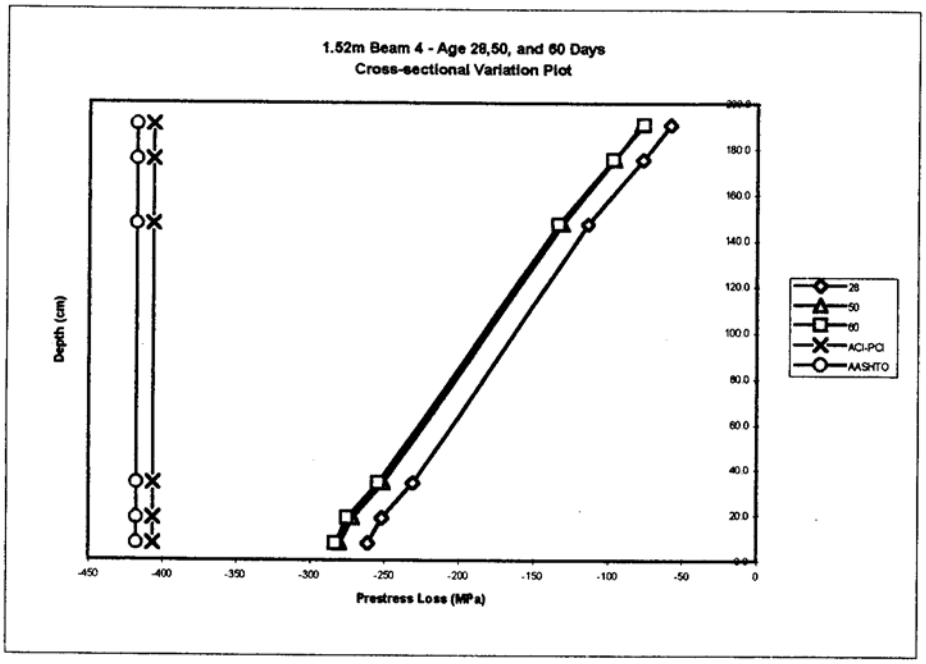

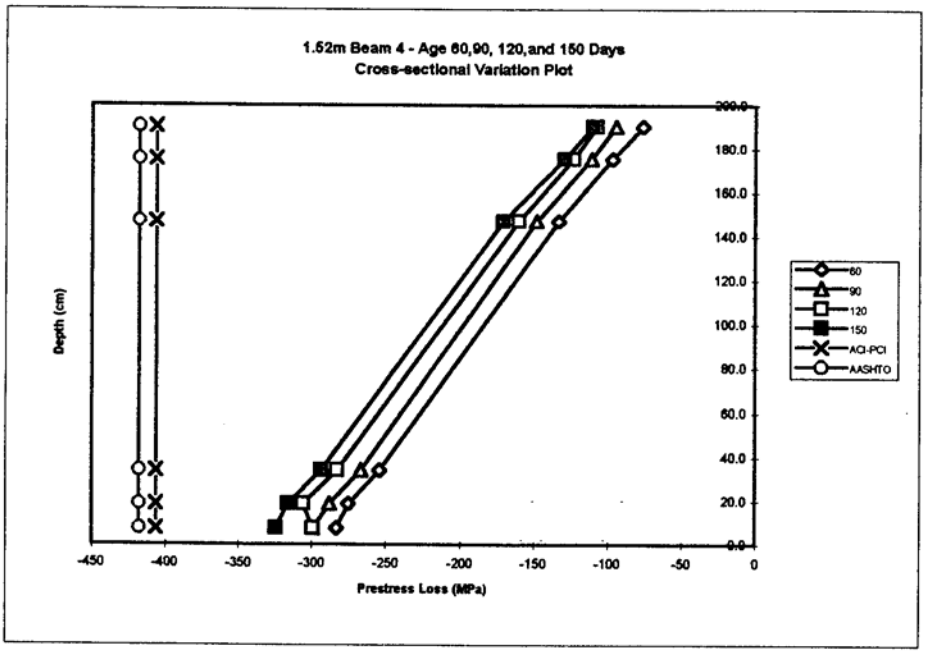

Figure 5-3(c-d) 1.52 m Beam 4 at (c) 28, 50, & 60 days (b) 60, 90, 120, & 150 days

note that the losses for this cross-section are much less than those computed by either ACI-PCI and AASHTO methods.

5.2.4 Discussion

The behavior of the cross-sectional prestress loss variation for the days mentioned is very similar for both midspan of Beam 1 and the quarter-span of Beam 3. Both have locations where the stress is becoming less tensile towards the top. At 7.6 cm from the bottom, they both reach the ACI-PCI computed loss in approximately 7 days and the AASHTO computed loss in about 150 days. The losses at 1.52 m from the end support has no location that is becoming less tensile, and does not even come close to reaching the values of loss calculated by the ACI-PCI and AASHTO methods. The magnitude of the loss is generally greater at the midspan and the quarter-span than, at 1.52 m from the end support.

5.3 Percentage Comparisons of the Prestress Loss

5.3.1 Introduction

So far the prestress loss has been represented by the value actually occurring at a specific location. An example of this is the lump sum prestress loss at the steel centroid of Beam 1 for 150 days is 430.6 MPa. In this section, the prestress loss is taken as

defined ratios to have a better understanding of what all these numbers actually mean, with respect to prestressed concrete girder design.

5.3.2 Initial Prestress to Jacking Stress Ratio

The initial prestress, f_i, is defined as the prestress after all immediate losses have occurred. The immediate losses, in this report, are assumed to be all elastic shortening. The initial prestress can be computed as follows:

$$^{f}i - {}^{f}pi - \Delta f_{ES} \qquad (5\text{-}1)$$

In Equation 5-1, f_{pj} is the jacking stress and Δf_{ES} is the loss of prestress due to elastic shortening. The jacking stress, f_{pj}, was consider uniform throughout the cross-section and was determined as follows:

$$f_{pj} = \frac{P_j}{A_{ps}} \qquad (5\text{-}2)$$

In Equation 5-2, P_j represents the jacking force on one strand and A, is the crosssectional area of one prestressing strand. For the case of the Westbound Gandy Bridge, Pj is equal to 150.4 kN (33.8 kips) and 4 is equal to 1.08 cm^2 (0.167 in). Applying these quantities in Equation 5-2 results for 1395 MPa (202.4 ksi), for the jacking stress.

Now that these parameters have been defined the initial prestress to jacking stress ratio is defined as follows:

$$\frac{f_{pi}}{f_{pj}} = \frac{f_{pj} - \Delta f_{ES}}{f_{pj}} \qquad (5\text{-}3)$$

This ratio tells what percentage of the jacking stress is available after the immediate losses, or in this case after elastic shortening has occurred. This ratio is converted to a percent and plotted versus beam depth for the midspan of Beam l, the quarter-span of Beam 3 and 1.52 m point for Beam 4.

Figure 5-4 shows the results from applying Equation 5-3 across the depth at the midspan of Beam 1. Also included on the plot are the ACI-PCI and AASHTO results obtained using Equation 5-3. The percentages vary with depth similarly to the plots of Section 5-2. The difference in percentages between the top gauge at 190.5 cm (75 in) to the bottom gauge at 7.6 cm (3 in) is 17.1 %. The ACI-PCI and AASHTO Code allow for immediate losses of 9 % o and 11 %, respectively. The Code results for immediate loss compare quite well with that at the girder centroid at 99.1 cm (39 in) of 19 % , but are smaller than at the steel centroid at 23.6 cm (9.3 in) of 16 %.

Figure 5-5 shows the results of initial prestress to jacking stress ratio versus depth for the quarter-span of Beam 3. The difference in percentages between the top gauge at 190.5 cm and the bottom gauge of 18.8 cm (7.4 in) is 17.5 %, which is similar to Figure 54. The Code results compare will with the draped steel centroid at 84.1 cm (33.1 in), which is very close to the girder centroid.

Figure 5-6 shows the results of initial prestress to jacking stress ratio versus depth for the location 1.52 m (5 ft) from the end support of Beam 4. The difference between the top gauge at 190.5 cm and the bottom gauge at 7.6 cm is 8.9 %, indicated a .smaller variation of immediate prestress loss from the top and bottom in the neighborhood of the

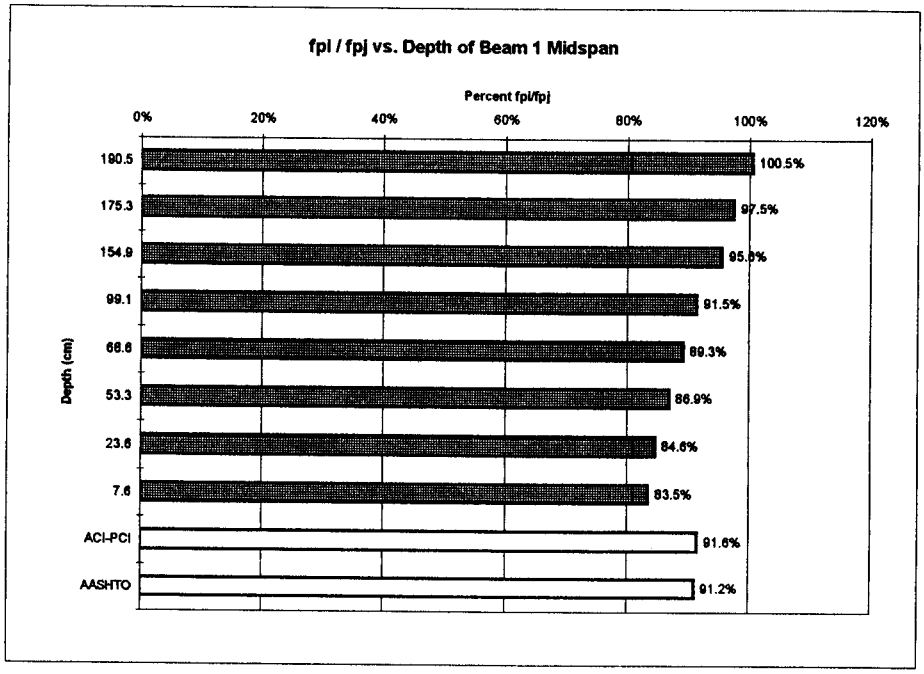

Figure 5-4 Midspan Beam 1, fpi/fpj versus depth

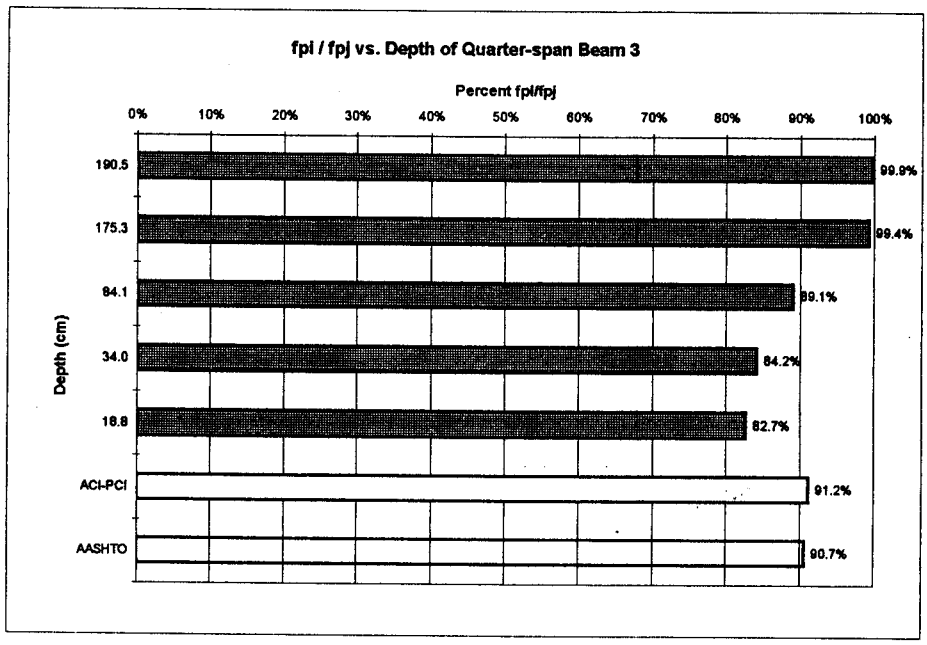

Figure 5-5 Quarter-span Beam 1, fpi/fpj versus depth

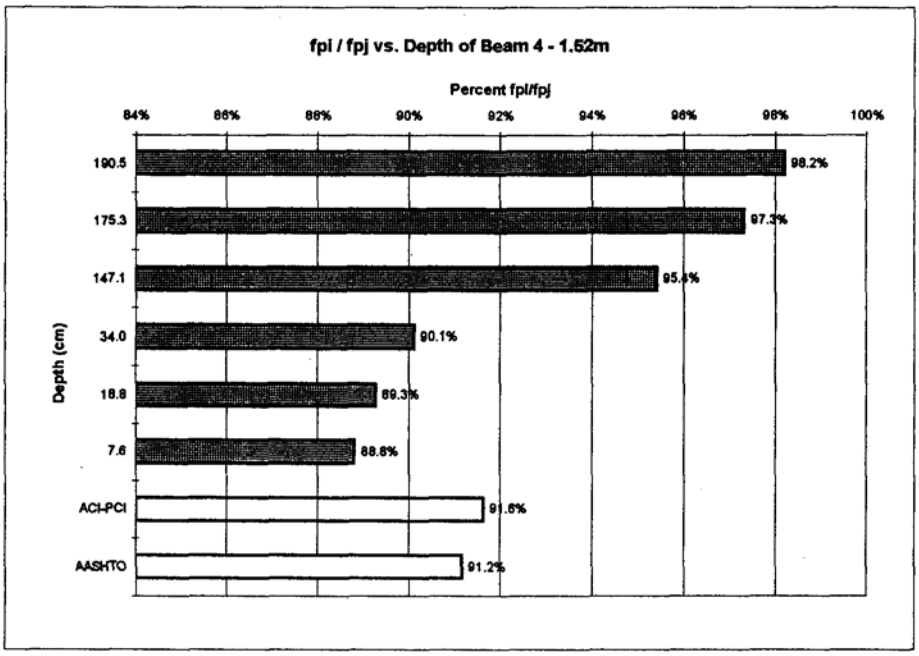

Figure 5-6 Beam 4, 1.52 m, fpi/fpj versus depth

girder support. The Code results correspond quite well with those of the straight steel centroid 18.8 cm.

The girder results compare well with those of the Codes at both the midspan of Beam 1 and the quarter-span of Beam 3. However, the straight steel centroid results at the 1.52 m from the end support compare favorably to the Code values. Although they seem to correspond well at the girder centroid, the straight steel centroid indicates more immediate loss than the Codes suggest.

5.3.3 The Effectiveness Ratio, R

The effectiveness ratio, R, is a parameter defined by Nilson[16] which relates the effective prestress force, P_e, at any time t to the initial prestress, P_i. The effectiveness ratio is as follows:

$$R = \frac{P_e}{P_i} \tag{5.4}$$

This ratio can easily be converted into stress by dividing P_o and P; by the area of prestressing steel A., that corresponds to P_e and P;. Then the effectiveness ratio takes this form:

$$R = \frac{f_{pe}}{f_{pi}} \tag{5-5}$$

In Equation 5-5, f_{pe} can be taken at any time t to determine the effectiveness ratio at that time. The effective prestress, fpe is computed as follows:

$$f_{pe} = f_{pi} - \Delta f_{TD} \tag{5-6}$$

In Equation 5-6, $Af_{,D}$ represents the time-dependent loss occurring up to the time examined. The effectiveness ratio, describes how much prestress in terms of percent of f_{pi} is still available for the use in the girder. Nilson also suggests (1-R) as another interesting quantity to investigate and is represented here in terms of stress as follows:

$$1 - R = \frac{f_{pi} - f_{pe}}{f_{pi}} = \frac{\Delta f_{TD}}{f_{pi}} \tag{5-7}$$

Equation 5-7 relates the time-dependent loss at any time t to the initial prestress. The plots in this section are set with t = 150 days, that means., Af_{TD} is the time-dependent loss occurring up to this time.

Figure 5-7 contains the plots of R and 1-R versus depth for the midspan of Beam 1. The percent difference between the values of R at 190.5 cm (75 in) and 7.6 cm (3 in) is 11.5 %. The values from the ACI-PCI and AASHTO procedures are being approached at the 7.6 cm mark and the steel centroid 23.6 cm (9.3 in), but the value at the girder centroid is some degree higher. The higher the value of R, the more the stress that is still available at the location. From the 1-R plot only 4.8 % of the initial prestress for the location at 190.5 cm has been lossed as opposed to 16.3 % at 7.6 cm. The ACI-PCI and the AASHTO Codes provide for 20 % and 25 % time-dependent losses, respectively.

Figure 5-8 contains the plots of R and 1-R versus depth for the quarter-span of Beam 3. The percent difference between the values of R at 190.5 cm and 18.8 cm is 10.6 %. The value of R at 18.8 cm is somewhat larger than the computed Code values. Forthe 1-R plot, the 190.5 cm location has a time-dependent prestress loss of 5.1 % which differs greatly from the location of 18.8 cm of 15.7 %. These losses are much smaller than the Code suggested values up to this time

Figure 5-9 represents the plots of R and 1-R for the location 1.52 m from the end support. The percent difference between the values of R at 190.5 cm and 7.6 cm is 6.6 %, which is again getting smaller, as was the case for the immediate losses. All values of R throughout this cross-section are far from those of the ACI-PCI and AASHTO computed

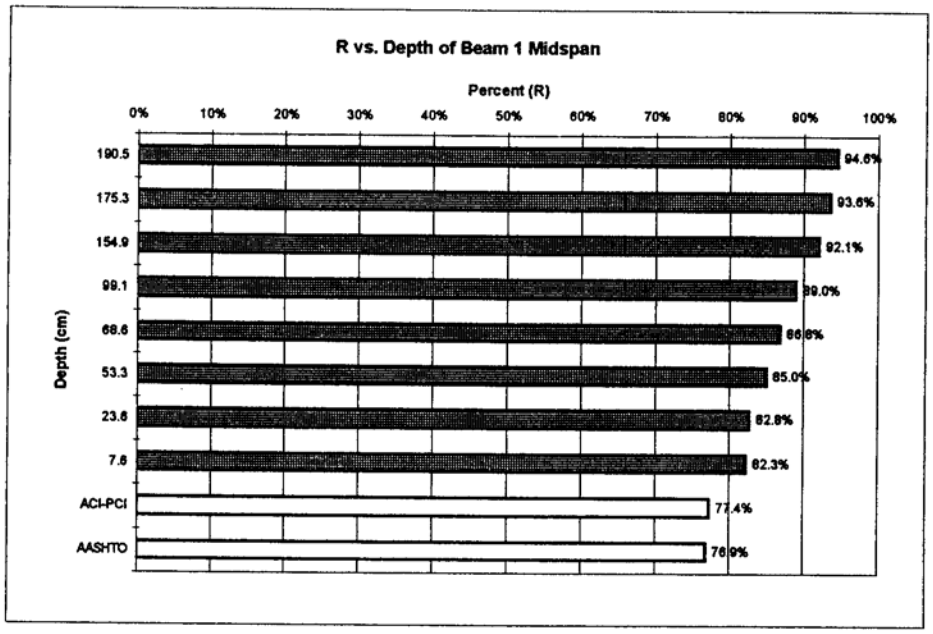

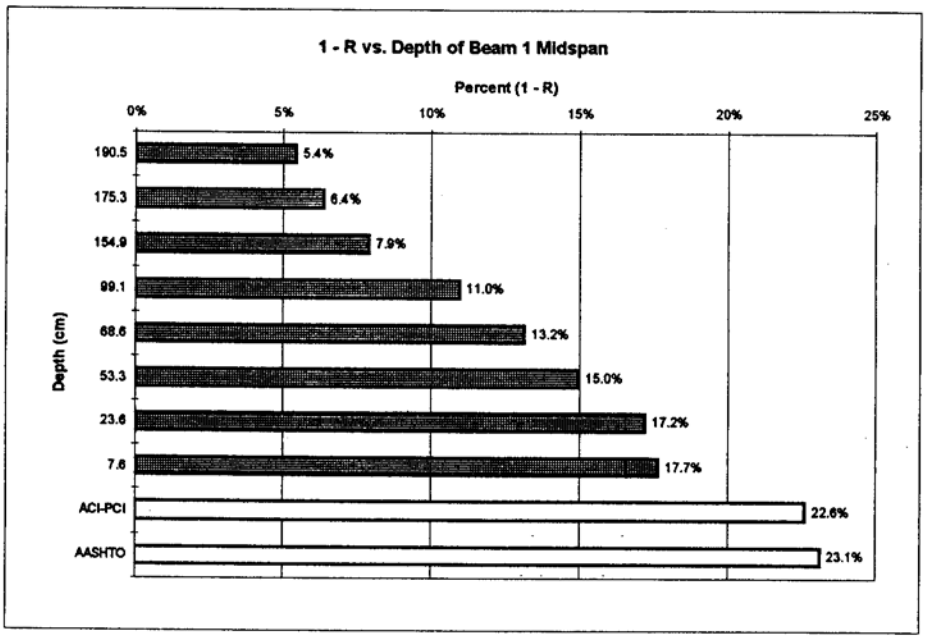

Figure 5-7(a-b) Midspan Beam 1,(a) R (b) 1-R

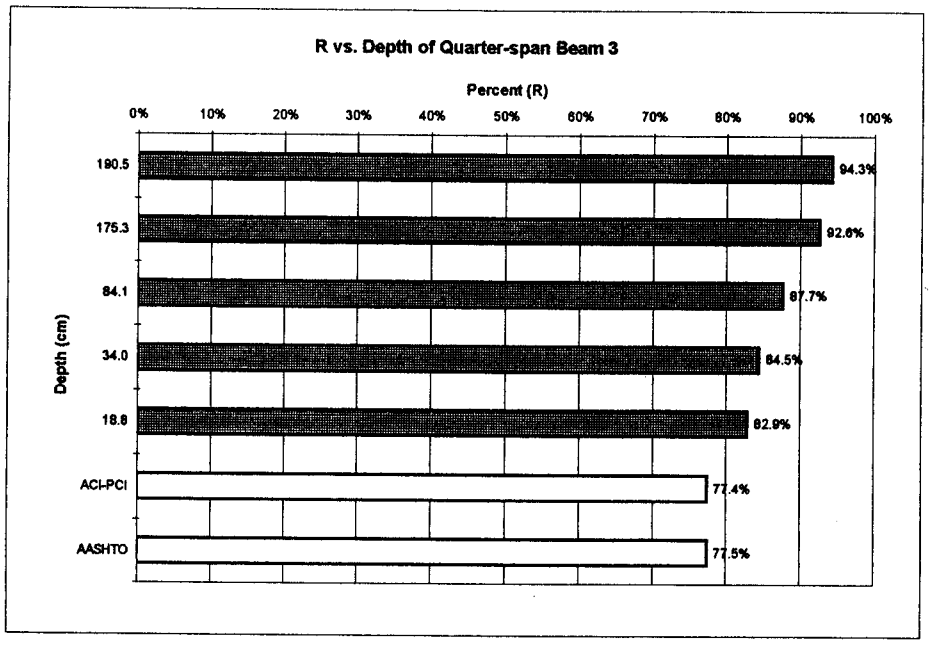

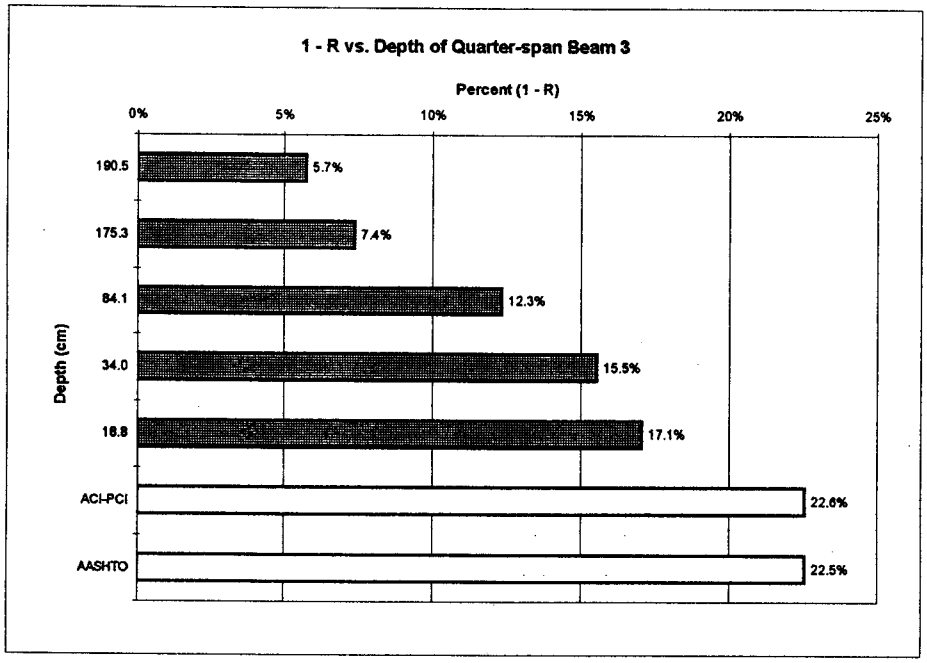

Figure 5-8(a-b) Quarter-span Beam 3(a) R (b) 1-R

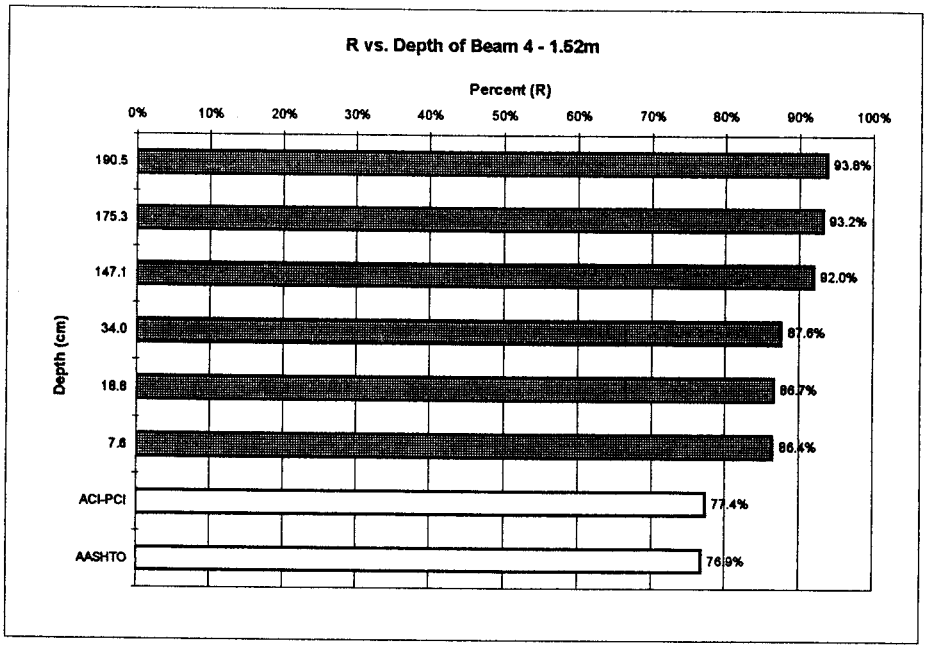

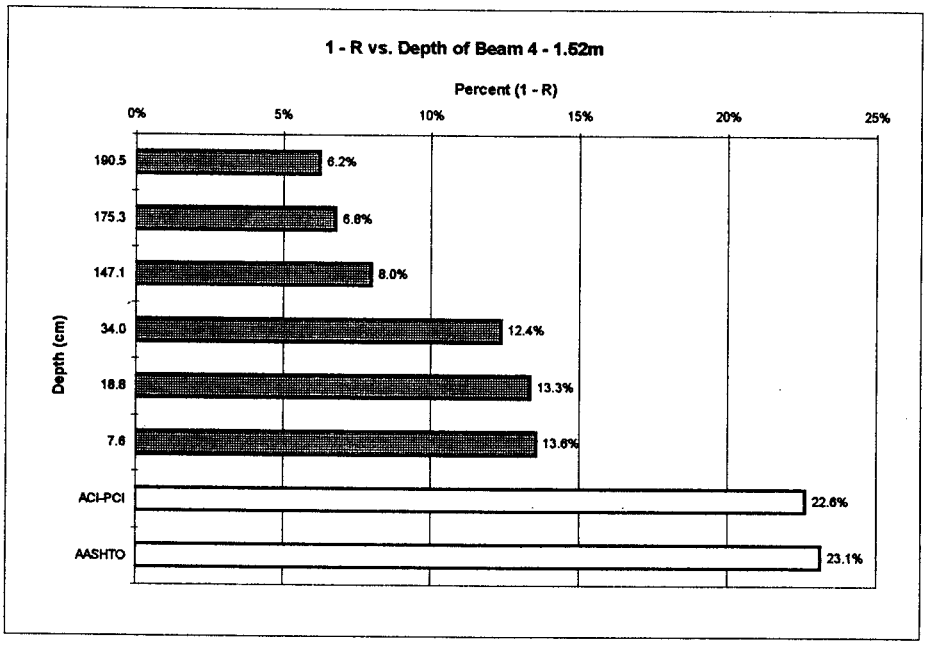

Figure 5-9(a-b) Beam 4 1.52 m,(a) R (b) 1-R

values. For the 1-R plot, 5.7 % of the time-dependent prestress loss has been lost at 190.5 cm compared to 12.3 % at 7.6 cm. If the Code values are to be used as a datum, this suggests that much more time-dependent loss can be expected in the future.

The percent differences for R between the top and bottom, at the midspan of Beam 1 and the quarter-span of Beam 3, are 11.5 % and 10.6 % which are very similar. The location 1.52 m from the end support of Beam 4 shows much less at 6.6 %. This suggests that the support location contains a more uniform loss throughout the cross-section compared to the others. The 1-R values for 190.5 cm were 4.8 %, 5.1 %, and 5.7 % for the midspan, quarter-span and the location 1.52 m from the end support. This trend shows that the time-dependent loss increase slightly in the top portion of the member, the further away you go from the midspan. The steel centroid at the midspan and the straight strand centroid at the quarter-span have almost equal losses at 15.8 % and 15.7 % o respectively. The loss at the level of the straight strand centroid at the location 1.52 m from the end support drops off to only 12.3 %. This suggests that the time-dependent losses are felt greater toward the midspan, than at the supports, and areas with higher concentration of the prestressing steel.

5.3.4 Lump Sum Loss to Jacking Stress Ratio

The lump sum loss to jacking stress ratio tells what percentage of the applied jacking stress is lost. This is important because knowledge of this ratio can be allowed for

in design, so that more realistic service stresses can be obtained. The lump sum loss reported includes immediate losses and the time-dependent losses occurring up to 150 days.

Figure 5-10 shows the lump sum loss to jacking stress ratio versus depth for the midspan of Beam 1. There are significant differences from the top of the cross-section to its bottom. At 190.5 cm, there has only been a 4.9 % loss, compared to 31.2 % loss at 7.6 cm. At both 23.6 and 7.6 cm, the percent loss is already beyond that suggested by the ACI-PCI and AASHTO ratios.

Figure 5-11 shows the lump sum loss to jacking stress ratio versus depth for the quarter-span of Beam 3. There also are significant differences from the top of the cross-section to its bottom. At 190.5 cm, there has only been a 5.8 % loss, compared to 31.4 at 18.8 cm. At 18.8 cm, the percent loss is already beyond that suggested by ACI-PCI and AASHTO ratios, and at 34 cm the ratio is approaching these values.

Figure 5-12 shows the lump sum loss to jacking stress ratio versus depth for the 1.52 m mark of Beam 4. There are as well, significant differences between the top and bottom of the cross-sections, varying from 7.9 % at 190.5 to 23.2 % at 7.6 cm. This difference, however, is smaller than those of the midspan of Beam 1 and the quarter-span of Beam 3. In this end zone, there are no points within this cross-section with percent losses beyond, either the ACI-PCI or AASHTO ratios.

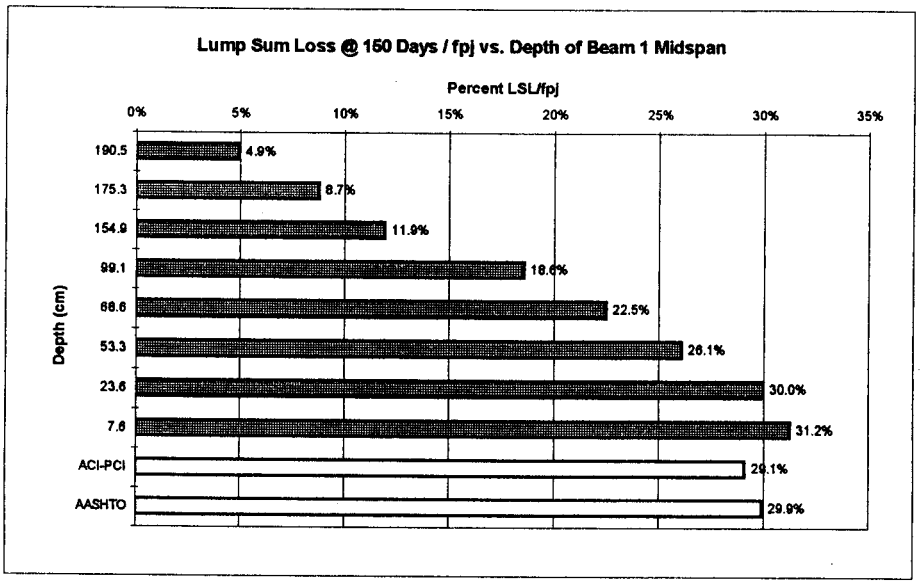

Figure 5-10 Midspan Beam 1, Lump sum loss to jacking stress ratio

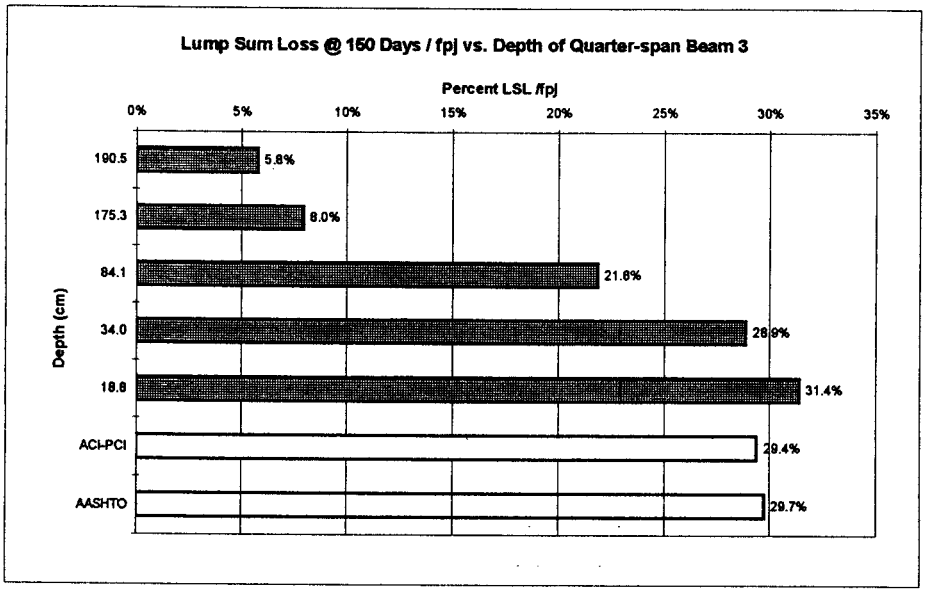

Figure 5-11 Quarter-span Beam 3, Lump sum loss to jacking stress ratio

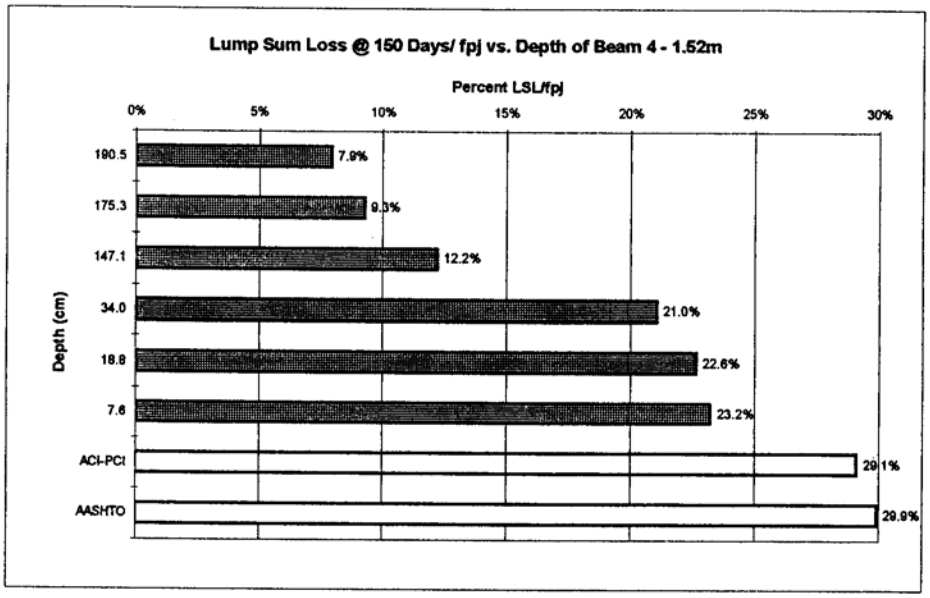

Figure 5-12 Beam 4, 1.52 m, Lump sum loss to jacking stress ratio

5.4 Tendon and Concrete Stresses

5.4.1 Introduction

The ACI Code describes in Chapter 18 the limits for prestressed concrete design. In particular, Section 18.4 and 18.5 of the ACI Code, the permissible stresses in the concrete and the prestressing tendons are discussed. These limiting stresses will be applied to the Westbound Gandy Bridge in this section. In order to do this, it will be necessary incorporate the measured prestress losses in determining the tendon stresses and concrete stresses.

5.4.2 Prestressing Tendon Stresses

In Section 18.5 of the ACI-Code, the allowable tensile stresses for prestressing tendons are stated for two specific stress times. The stress due to the jacking force and the stress immediately after prestress transfer. These stress values will then be compared to those values obtained for the girders that are being investigated. Remember that the available data used in this report covers up to 150 days, which is before the slab and service loads are applicable

The prestressing tendon stress is determined at the steel centroid of the midspan of Beam 1, but for the quarter-span and the 1.52 m from the end support, the tendon stresses will be determined for two different locations. These locations will be where the draped steel centroid occurs in each section and the straight steel centroid, which is the same for both the quarter-span and 1.52 m from the end support location.

In 18.5.1 (a) of the ACI-Code, it states that the tensile stress due to tendon jacking force may not be larger than $0.94f_{py}$, but not greater than the lesser of $0.80f_{pu}$ and the maximum value recommended by the prestressing tendon or anchorage manufacturer because of the jacking force. The quantity f_{py} is the specific yield stress of a prestressing tendon. In the Commentary of 18.5 of the ACI-Code, it suggests that the $0.90f_{pu}$ be used for determining f_{py} for low relaxation wires and tendons, which is the type of tendon used in the Gandy project.

In 18.5.1 (b) of the ACI-Code, it states that the tensile stress may not be larger than $0.82f_{py}$, but not greater than $0.74f_{pu}$, just after the transfer of the prestressing force from

the tendons to the concrete. Table 5-1 has the calculated stress limitations from Section 18.5 of the ACI-Code.

Table 5-1 Limitations on stress in the steel strands.

ACI Code Results for f_{pu} = 1862 MPa (270 ksi)							
18.5.1(a) Due to Jacking Force				18.5.1(b) Immediately After Transfer			
$0.94f_{py}$		$0.80f_{pu}$		$0.82f_{py}$		$0.74f_{pu}$	
MPa	ksi	MPa	ksi	MPa	ksi	MPa	ksi
1575	228.4	1489	216	1339	194.2	1378	200

The stress limit caused by jacking force is controlled by $0.80f_{p,,}$, which is 1489 MPa (216 ksi). The jacking stress f_{pj} was calculated earlier as 13961VIPa (202.4 ksi), which is below $0.80f_{p,,,}$, so this is okay.

The limiting stress immediately after transfer is controlled by $0.82f_{py}$, which is 1339 MPa (194 ksi). The prestressing tendon stresses for the midspan of Beam 1, the quarterspan of Beam 3, and the 1.52 m (5 ft) from the end support of Beam 3 can be seen in Table 5-2.

Table 5-2 Resulting stresses at tendon centroid

Prestressing Tendon Stresses for Steel Centroid Locations				
Beam 1 Midspan	Beam 3 Quarter-span		Beam 4 Location of 1.52 m	
Overall Steel Centroid	Draped Steel Centroid	Straight Steel Centroid	Draped Steel Centroid	Straight Steel Centroid
1171 MPa	1241 MPa	1142 MPa	1332 MPa	1244 MPa
(169.8 ksi)	(180.0 ksi)	(165.6 ksi)	(193.2 ksi)	(180.5 ksi)

The steel stress of 1332 MPa (193.2 ksi) at the draped steel centroid of Beam 4 at the 1.52 m (5 ft) from the end support is dangerously close to the limiting stress of 1339 MPa (194 ksi). All other locations are well within the $0.82f_{py}$ limit.

5.4.3 Concrete Stresses

In this section, the limitations on concrete stress immediately after transfer are presented in Section 18.4.1 of the ACI-Code and will be discussed. Then the crosssectional prestress losses presented in Section 5.2 of this project will be used to determine the concrete stresses throughout the cross-section.. In addition to this, the concrete stress resulting from the uniform loss provided by AASHTO is also computed. These stresses will be determined for two different times. These times being immediately after transfer of the prestress and at 150 days. The ACI-Code limitations will also be superimposed on the plot, for limiting stresses immediately after transfer and at service loads. These plots will

Be done for the midspan of Beam 1, the quarter-span of Beam 3, and the 1.52m (5ft) from the end support of Beam 4.

5.4.3.1. ACI Code Limits onCOncrete Stresses

In section 18.4.1 of the ACI-Code, it states for flexural members the limitations of the allowable stresses in concrete for the extreme fibers immediately after transfer. The limitation in the extreme fiber stress in compression is $0.66f_{ci}$' and for the extreme fiber stress in tension as $3\sqrt{f_{ci}}$' . The tension in th e extreme fiber can be increased to $6\sqrt{f_{ci}}$', if that section being examined is at the end of a simply supported member. Foe all the limitations, the value f_{ci}' is the compressive strength of concrete at the time the prestress is applied to the concrete. Beam 1 and 4 have the same f_{ci}' value, and Beams 2 and 3 have the same f_{ci}'value. Table 5-3 has the f_{ci}' values for the beams and the computed compressive and tensile limits. The ACI-Code in the Commentary to Section 18.4 explians that these limits are concerned with serviceability conditions, and do not ensure that the flexural member will be of adequate strength. It also states that the concrete stress should be computed after immediate losses, but before anytime-dependent losses have occurered.

It is interesting to note that the girders for th e Westbound Gandy Bridge were designed to have f_{ci}' of 34.5 Mpa (5000 psi). Comparing this design with those in the Table 5-3, actural f_{ci}' for Beams 1and 4 are 23% greater, and f_{ci}' for Beams 2 and 3 are 14% greater based upon the design value.

Table 5-3 Compressive strengths and stress limitations for Gandy bridge project.

ACI Code Results for Allowable Stress in Concrete					
Beam 1 and Beam 4					
f_{ci}'		$0.60f_{ci}'$		$3\sqrt{f_{ci}'}$	
MPa	psi	MPa	psi	MPa	psi
42.6	6191	25.6	3714	236	1.63
Beam 2 and Beam 3					
f_{ci}'		$0.60f_{ci}'$		$3\sqrt{f_{ci}'}$	
MPa	psi	MPa	psi	MPa	psi
39.2	5687	23.5	3412	226	1.56

5.4.3.2 Determination of Actual Concrete Stresses

It is now necessary to determine the concrete stresses in a section of the member, based upon the actual prestress loss which occurs within that cross-section. The actual prestress loss has been shown to vary throughout the cross-section of a member at a specified location. To get an accurate representation of the actual concrete stress this cross-sectional variation must be incorporated into the calculations.

The concrete stresses can be computed be computed by the following equations with consistent units:

$$f_{Top} = \frac{-P(t)}{A_c}\left(1 - \frac{e(y - c_2)}{r^2}\right) - \frac{M_0(y - c_2)}{I_c} \text{ for } y \geq c_2 \qquad (5\text{-}8)$$

$$f_{Bottom} = \frac{-P(t)}{A_c}\left(1 + \frac{e(c_2 - y)}{r^2}\right) + \frac{M_0(c_2 - y)}{I_c} \text{ for } y < c_2 \qquad (5\text{-}9)$$

For Equations 5-8 and 5-9, the variables are defined as follows:

f_{Top} = the concrete stress at or above the girder centroid

fB_{ottom}= the concrete stress below the girder centroid

P(t) = the prestressing force at any time t which varies depending on the loss

A_c- = the gross area of concrete

r^2 = the radius of gyration

c_2 = is the distance from the girder centroid to the bottom most fiber

y = is the distance where the stress is being calculated

M_o = the moment created from the self-weight of the girder

I_c = the moment of inertia of the cross-section

Equations 5-8 and 5-9 are based on an uncracked section stressed in elastic regions. Further discussion is necessary for the variable P(t). This value is determined by computing the effective stress f_{pe} at any time t, and multiplying it by the area of one prestressing strand A_{ps} and the total number of strands. The value of P(t) is dependent upon where along the depth of the cross-section the stress is being determined, as well as the location along the span of the girder.

The two times the concrete stresses are determined in this section of the project are immediately after transfer of the stress from the strands to the concrete and at 150 days after transfer. At transfer, only the immediate losses, in our case elastic shortening, is removed from the jacking stress to determine P(t). At 150 days, the total loss, which includes both immediate and time-dependent losses, occurring at that time are removed in order to determine P(t).

For the plots of concrete stress that follow, negative values are considered compressive and positive values are considered tensile. The plots for immediately after transfer contains the actual and AASHTO or design stress distributions, and shows the ACI Code tensile and compressive limits as vertical lines. The plots for 150 days after transfer contain the actual and AASHTO concrete stress distributions. The actual stress distributions take into account the varying of prestress loss along the cross-section. The AASHTO concrete stress distribution uses the same loss throughout the depth of the cross-section.

Figure 5-13 contains the plot for immediately after transfer of stress at the midspan of Beam 1. The concrete stress is well within the limits required by the ACI Code. The entire concrete stress distribution is compressive for the actual and AASHTO according to this plot. The cross-section is much more compressive at the bottom than at the top, which is expected. The actual maximum and minimum concrete stress are -16.9 MPa occurring at 7.6 cm (3 in) and -5.1 MPa occurring at 190.5 cm (75 in). The actual concrete stress tends to be slightly more compressive in the middle portion of the cross

section, and slightly less compressive towards the top of the cross-section compared to that from the AASHTO design requirements. The actual stress distribution is essentially nonlinear as can be seen in Figure 5-13.

Figure 5-14 contains the plot for 150 days after the transfer of stress at the midspan of Beam 1. The actual maximum and minimum concrete stresses are -12.5 MPa occurring at 7.6 cm (3 in) and -5.3 NIPa occurring at 190.5 cm (75 in). The actual concrete stress appears to be virtually constant for the lower portion of the beam. And, the actual concrete stress is much more compressive in the lower portion of the cross-section, and slightly less compressive in the upper portion when compared to the AASHTO results.

Figure 5-15 shows the plot immediately after the transfer of stress for the quarterspan of Beam 3. The stress limits of ACI Code are not in jeopardy at all. The entire concrete stress distribution is compressive for both the actual and AASHTO values. The maximum and minimum actual concrete stresses are -16.5 MPa at 18.8 cm (7.4 in) and - 5.0 MPa at 190.5 cm (75 in), respectively. The upper and lower portions of the actual stress agree quite well with the AASHTO values, but the actual stress is more compressive in the middle portion, as was the case at the midspan.

Figure 5-16 shows the plot for 150 days after the transfer of stress for the quarterspan of Beam 3. The results are very similar to that of Figure 5-14 for the midspan of Beam 1. The actual maximum and minimum concrete stresses are -12.5 MPa

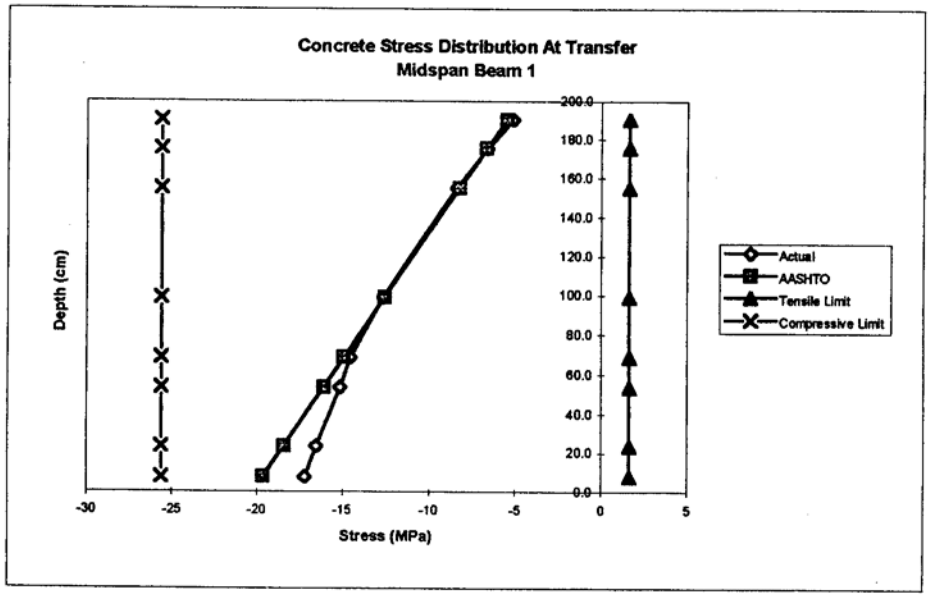

Figure 5-13 Midspan Beam 1 at transfer

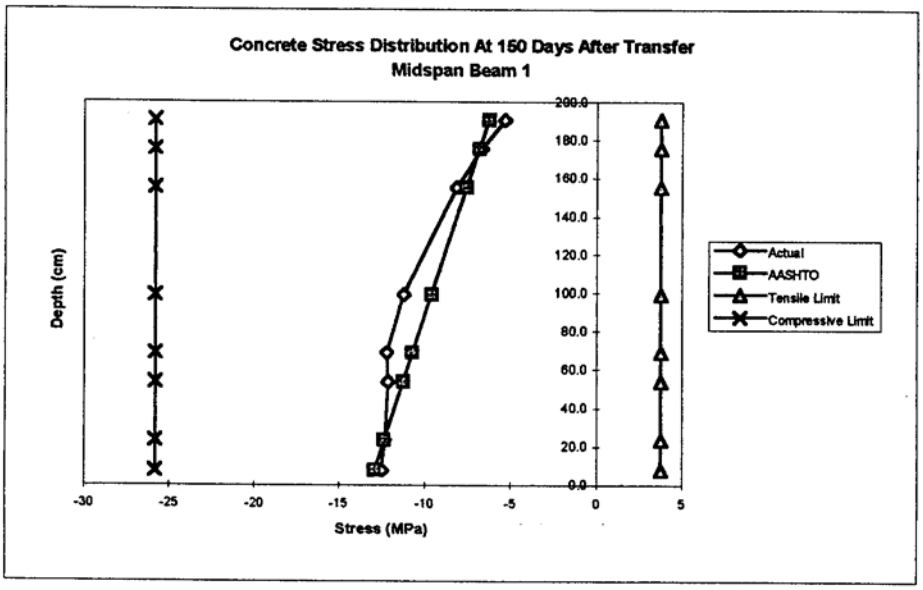

Figure 5-14 Midspan Beam 1 at 150 days

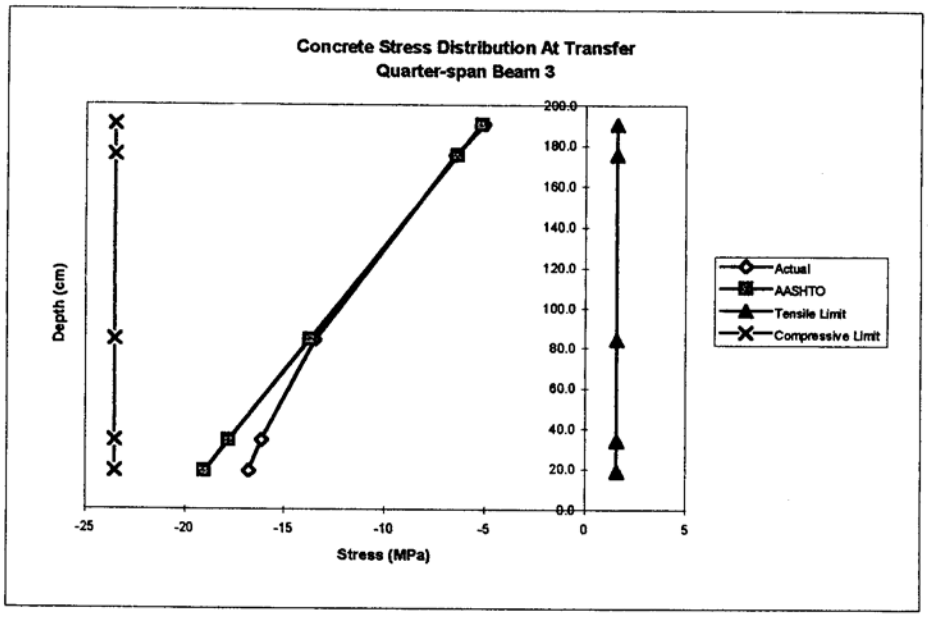

Figure 5-15 Quarter-span Beam 3 at transfer

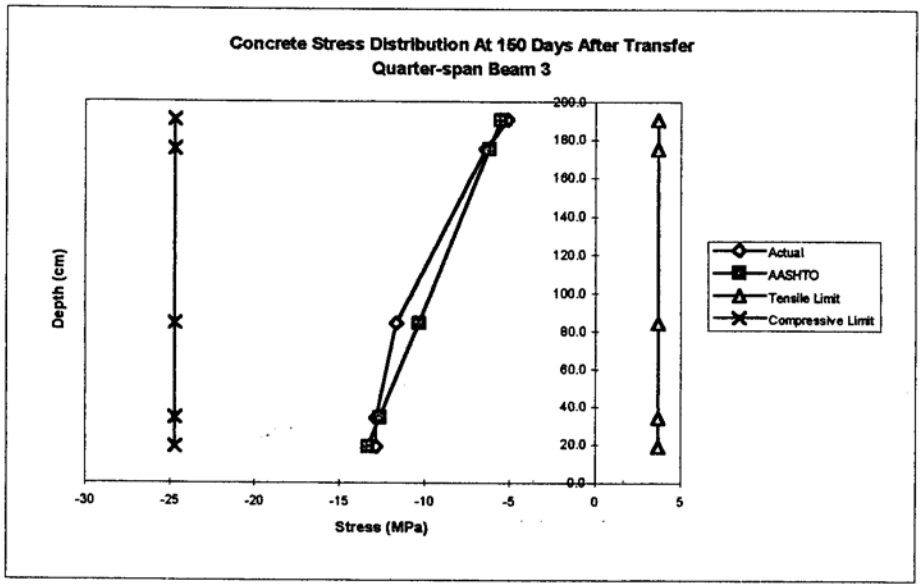

Figure 5-16 Quarter-span Beam 3 at 150 days

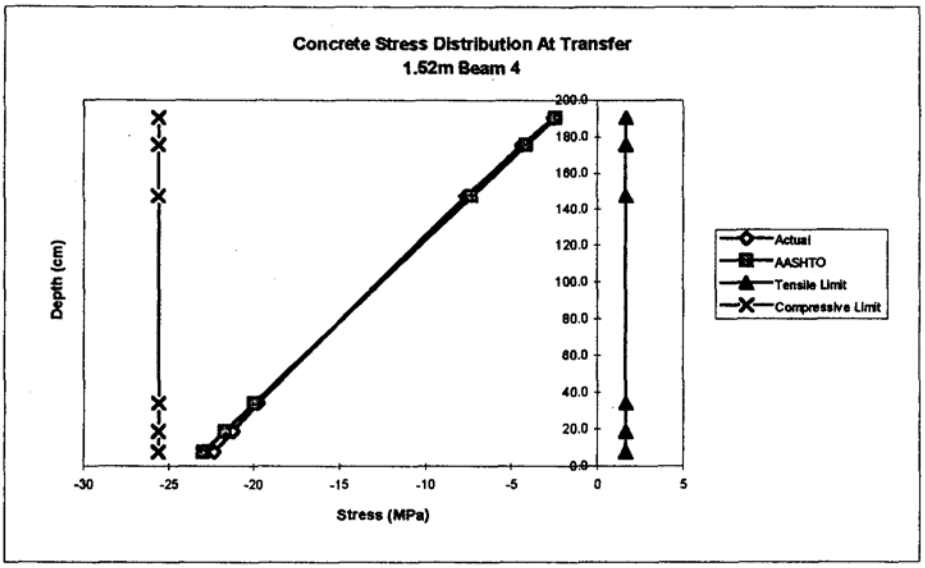

Figure 5-17 Beam 4, 1.52 at transfer

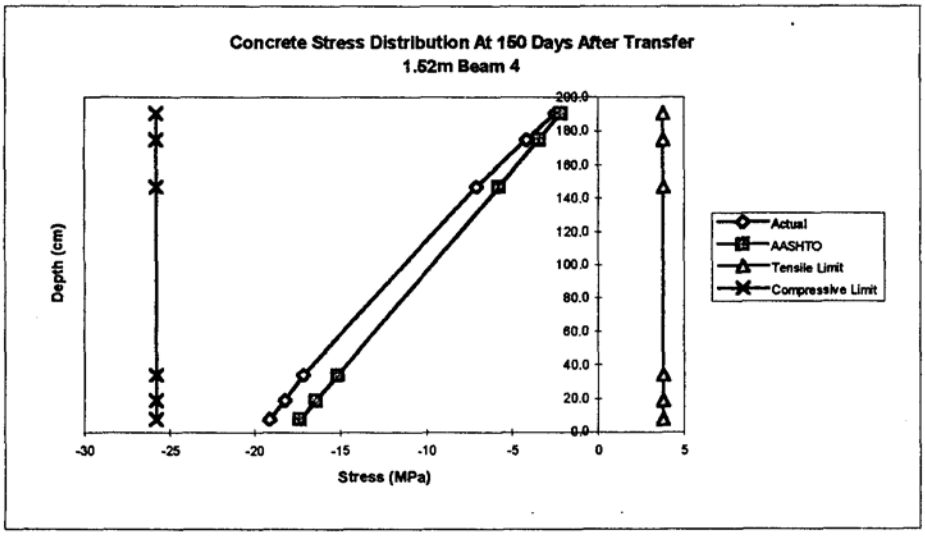

Figure 5-18 Beam 4, 1.52 at 150 days

occurring at 18.8 cm (7.4 in) and -5.1 MPa occurring at 190.5 cm (75 in). The actual concrete stress appears to be virtually constant for the lower portion of the beam. And, the actual concrete stress is much more compressive in the lower portion of the cross-section, and slightly less compressive in the upper portion when compared to the AASHTO results.

Figure 5-17 shows the plot of the concrete stress immediately after transfer Beam 4, at the 1.52 m (5 ft) from the end support. The results for the actual, and the AASHTO concrete stresses are similar, in that they both show almost a straight line distribution. The difference between the two is the slope of the line, the AASHTO has a higher slope. The maximum and minimum of the actual concrete stress are -22.2 MPa at 7.6 cm (3 in) and - 2.5 MPa at 190.5 cm (75 in), respectively. These maximum and minimum values come closer to the limit values than either the midspan or the quarter-span of the previous plots.

Figure 5-18 shows the plot for 150 days after transfer for the 1.52 m (5 ft) from the end support of Beam 4. The actual concrete stress values are much more compressive than the AASHTO values in the lower and middle portions of the cross-section although the gap becomes smaller near the top portion of the cross-section. The actual concrete distribution once again appears to be somewhat linear. The maximum and minimum of the actual concrete stress is -19.1 MPa at 7.6 cm (3 in) and -2.5 MPa at 190.5 cm (75 in), respectively.

5.5 Relative Humidity and Ambient Temperature Effects on Prestress Loss

5.5.1 Introduction

It is a known that relative humidity and ambient temperature effect the shrinkage in a concrete member. In a prestressed concrete member, shrinkage correlates with a loss of prestress for that member. It is important to see how changes in relative humidity and ambient temperature directly relate to the prestress loss of a member. This section does not try to distinguish between what portion of the prestress loss is shrinkage and what is not. Rather, it shows plots of relative temperature and ambient versus lump sum prestress for specific locations within the girder. In addition to these points, a line is presented for each plot using a linear regression to come up with an equation relating relative humidity and ambient temperature to lump sum prestress loss. These regression lines yield absolute value of loss in MPa for inputs of relative humidity in percent and ambient temperature in °C. Four different locations were chosen for this analysis. The midspan of both Beams 1 and 3, the 1.52 m point for Beam 4, and the quarter-span of Beam 3 were selected.

5.5.2 Selection of Points

There are three points chosen for each section. These points are varying through the depth of the section. For the midspan of Beams 1 and 3, the steel centroid at 23.6 cm, near girder centroid at 99.1 cm, and the future composite centroid of 154.9 cm were selected. For the quarter-span of Beam 3, the straight steel centroid at 18.8 cm, the draped steel centroid at 84.1 cm, and a point near the top flange at 190.5 cm were chosen.

For the 1.52 m point of Beam 4, the straight steel centroid at 18.8 cm, the draped steel centroid at 147.0 cm, and a point near the top flange at 190.5 cm were chosen.

5.5.3 Relative Humidity

The relative humidity versus prestress loss for the midspans of Beams 1 and 3 are presented in Figure 5-19 and Figure 5-20, respectively. For the three points examined for Beam 1 midspan, the slopes are positive and less than unity. However, points for Beam 3 midspan, the slopes are negative and are larger in the absolute sense than those of Beam 1 at midspan. Beam 1 has higher average relative humidity values than Beam 3, resulting in positive slope for Beam 1 as opposed to a negative slope for Beam 3. This could mean that less shrinkage was occurring for the days mentioned for Beam 1 than Beam 3, providing all other things being equal.

The relative humidity versus prestress loss for the quarter-span of Beam 3 is presented in Figure 5-21 for the points mentioned. The slopes are negative, which is similar to Beam 3 midspan, for all three points. The slope is highest at the draped steel centroid at 84.1 cm, which is located near the girder centroid. Smaller slopes occur at the straight steel centroid of 18.8 cm and the 190.5 cm mark. These locations are located near the bottom and top flanges, respectively.

Figure 5-22 shows the results of the relative humidity versus depth for the 1.52 m from the end support. The slope of the line is positive gradually increases from the top flange to the draped steel centroid to the straight steel centroid.

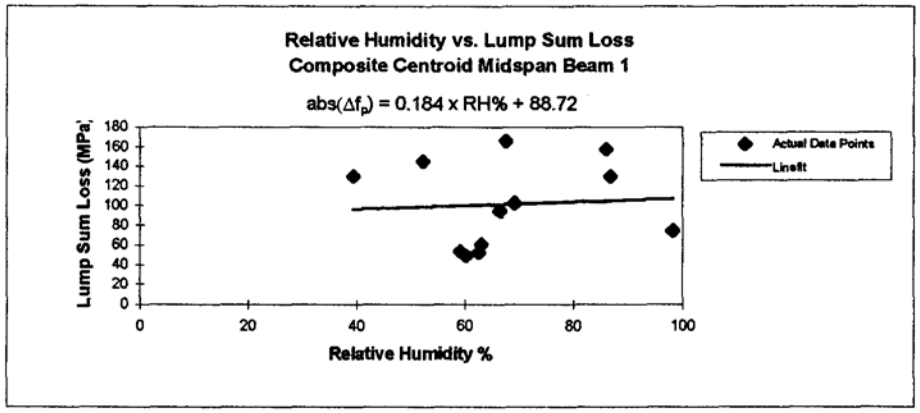

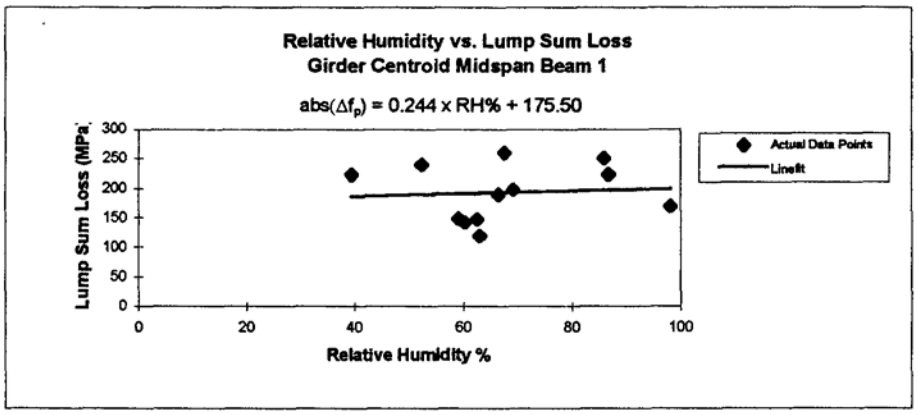

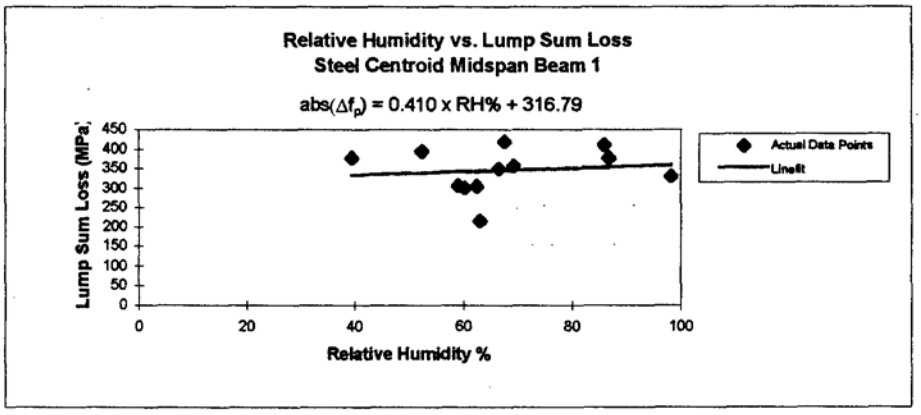

Figure 5-19 Relative Humidity Midspan Beam 1

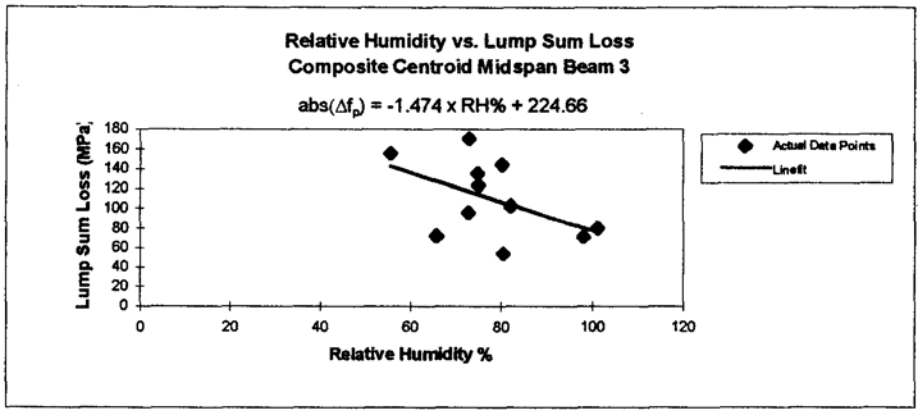

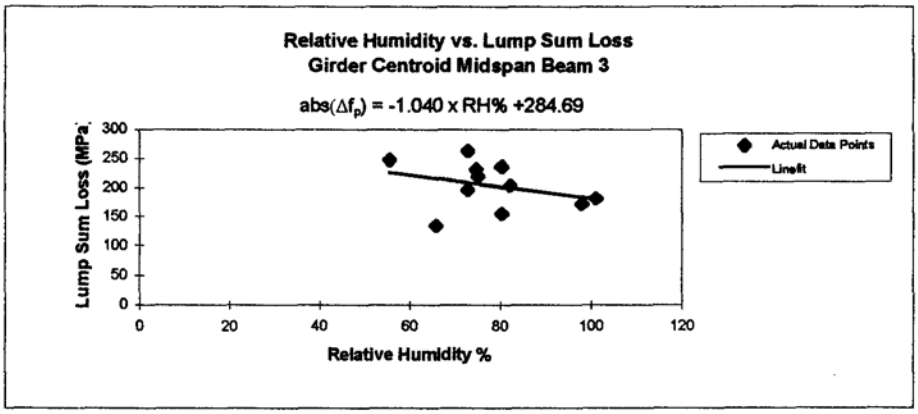

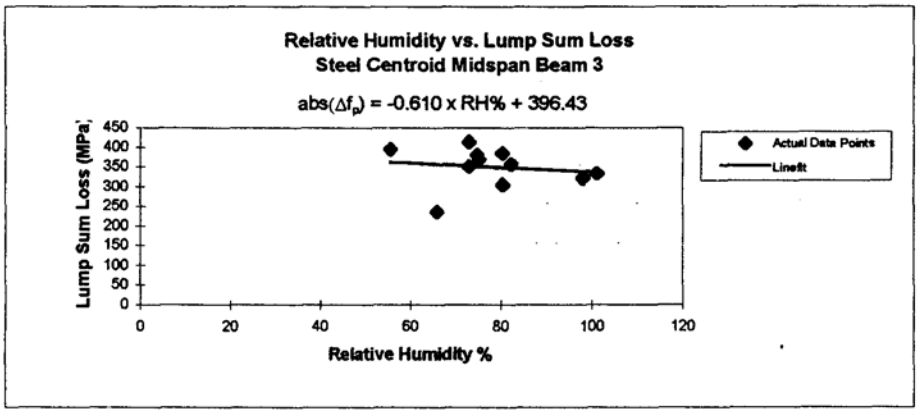

Figure 5-20 Relative Humidity Midspan Beam 1

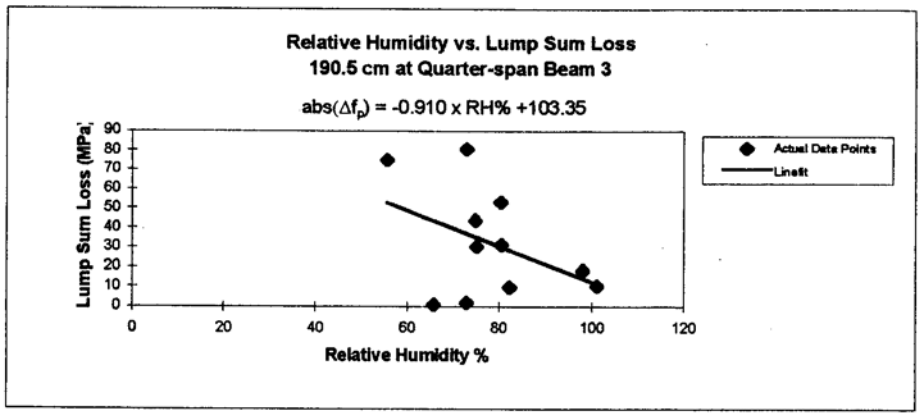

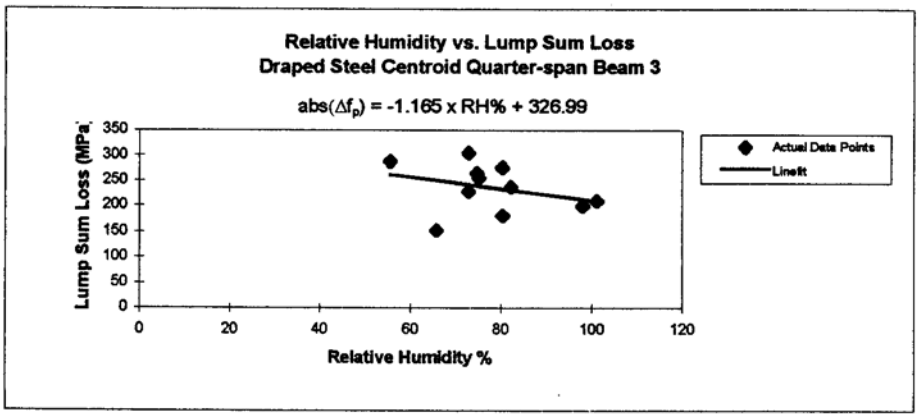

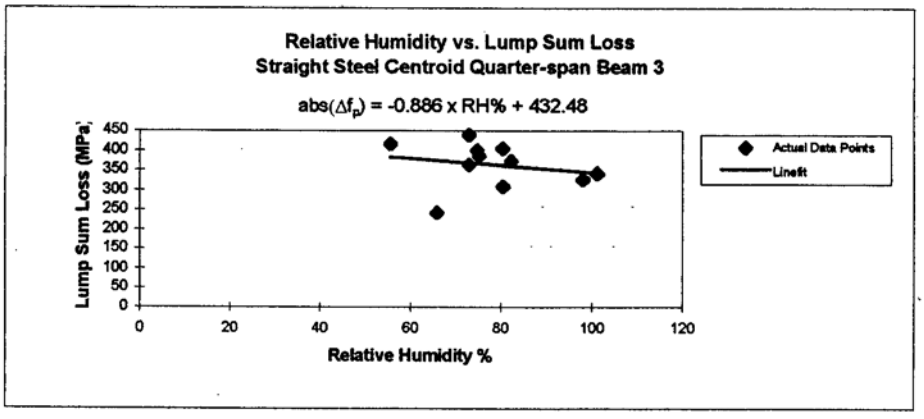

Figure 5-21 Relative Humidity Quarter-span Beam 3

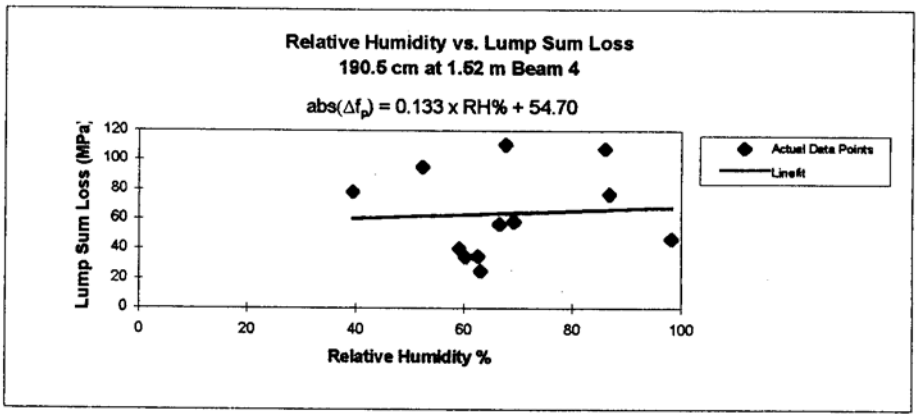

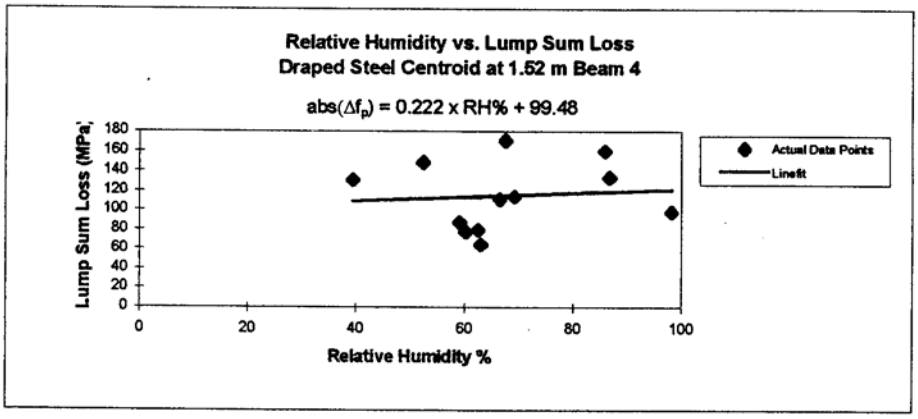

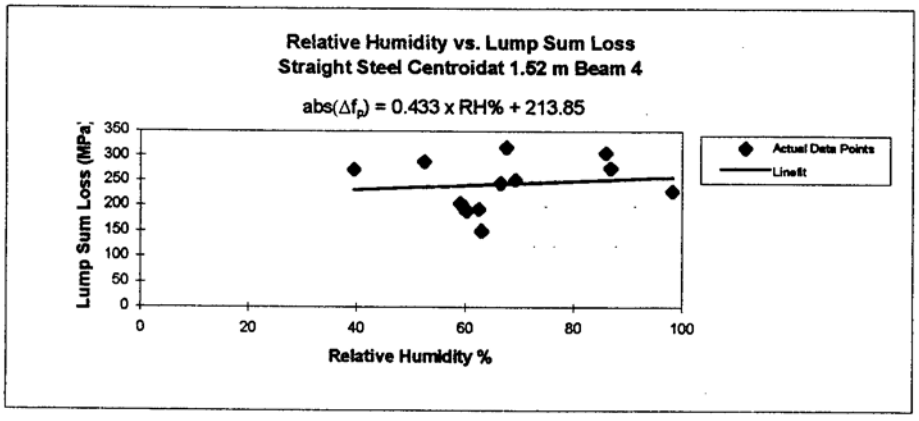

Figure 5-22 Relative Humidity 1.52 m Beam 4

5.5.4 Ambient Temperature

The plots for ambient temperature versus prestress loss are presented in Figures 523 and 5-24, for Beams 1 and 3, respectively. The equations for all three points for both midspans have similar slopes and intercepts. This indicates a smaller dependence of the loss variations on ambient temperature.

In Figure 5-22, the prestress loss versus ambient temperature for the quarter-span of Beam 3 are shown. They have larger slopes the further away from the top of the member and all are positive.

In Figure 5-23, the prestress loss versus ambient temperature is for 1.52 m from the support. Again, larger slopes prevail in the lower portion of the cross-section than the upper portion.

Within the cross-sections, the rate of change of the loss with ambient temperature (the slope) consistently higher in the lower portions of the beam, than the top portion. These plots presented in this section can be enhanced later on to include more points, and may help in extracting the shrinkage losses from the overall prestress loss. The inclusion of more points will help define trends that may be hidden due to limited points used here. In the future, consideration should also be given to gauges located near the surface.

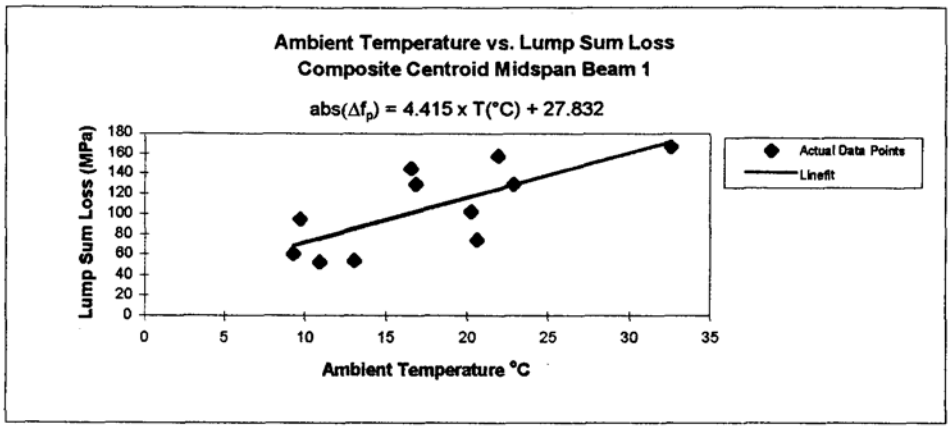

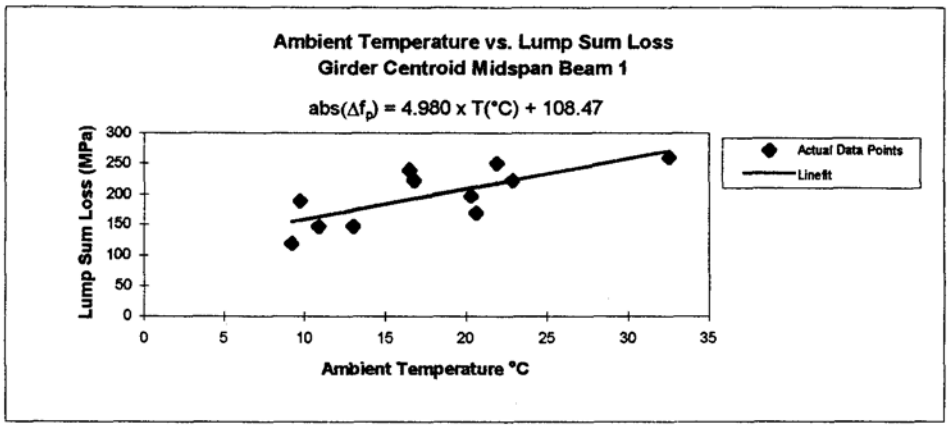

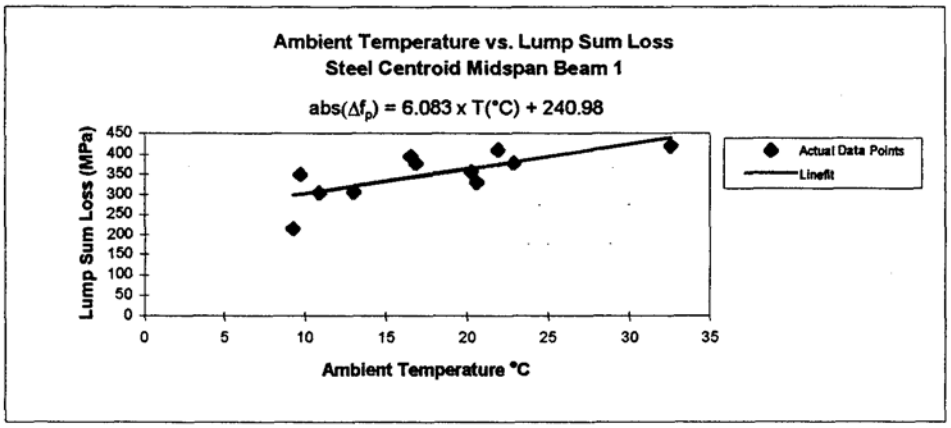

Figure 5-23 Ambient temperature Midspan Beam 1

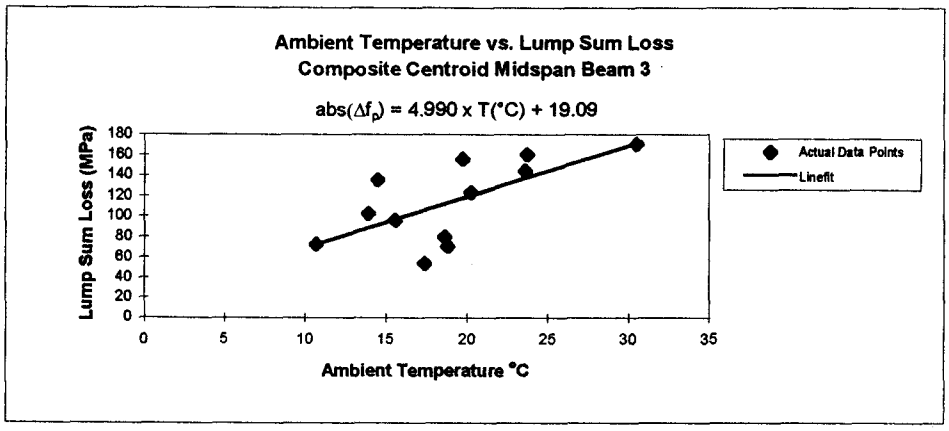

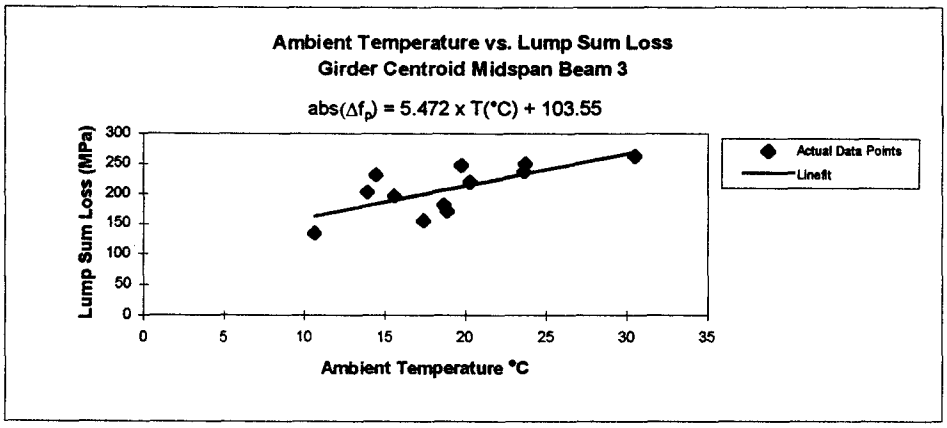

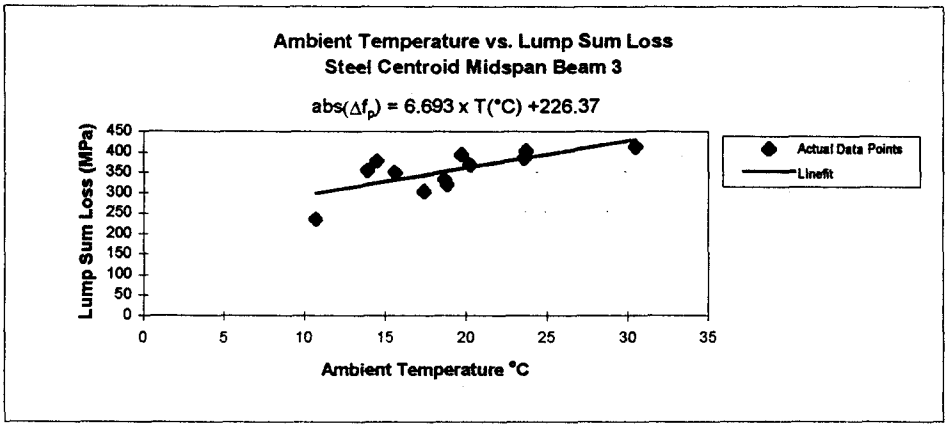

Figure 5-24 Ambient temperaure Midspan Beam 3

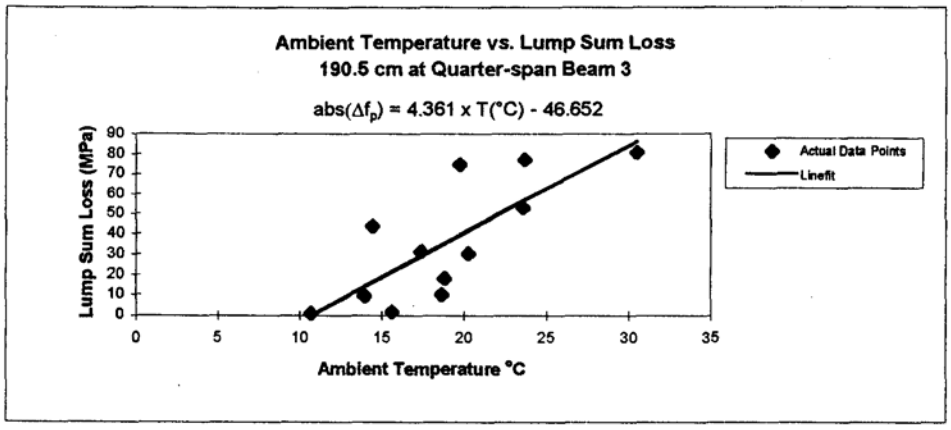

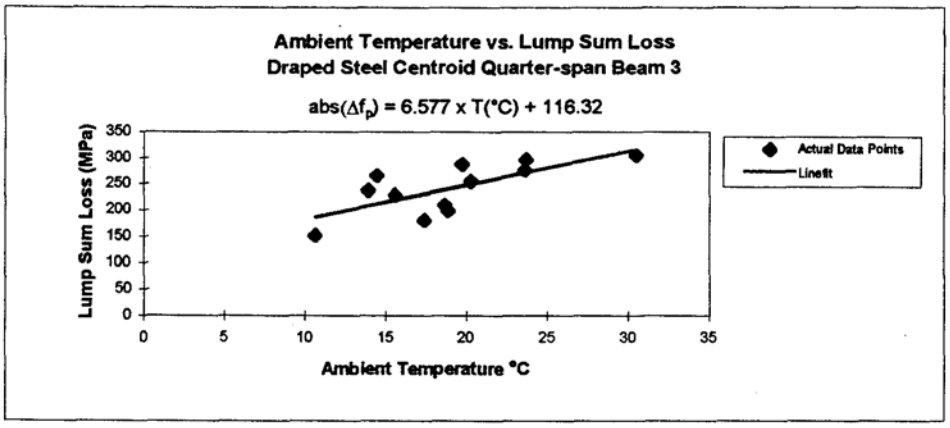

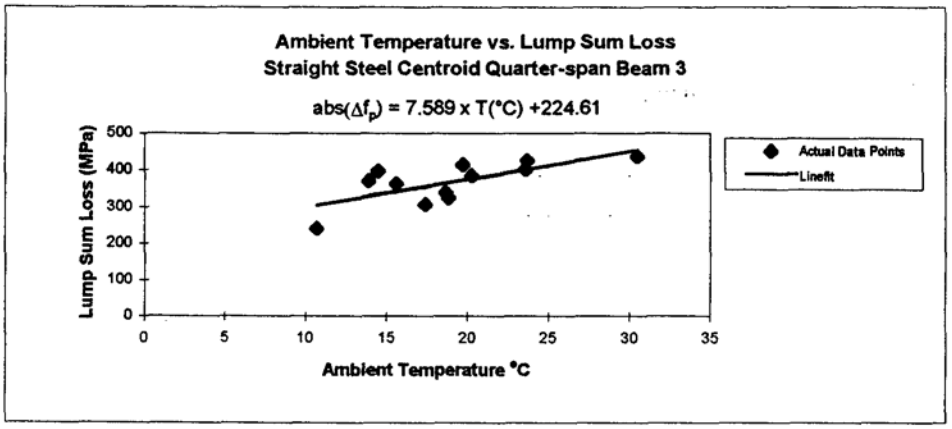

Figure 5-25 Ambient temperature Quarter-span Beam 3

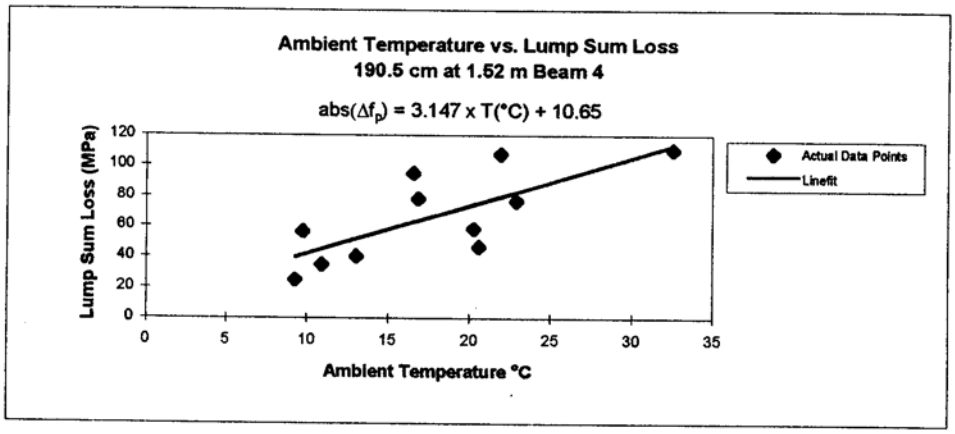

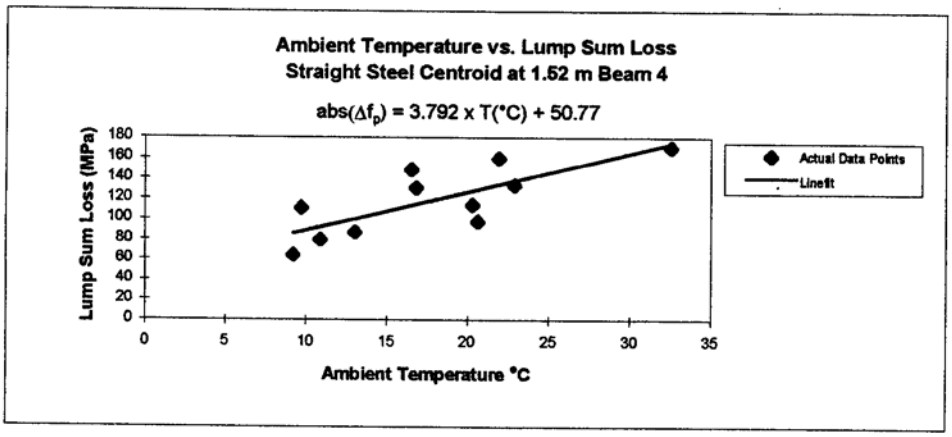

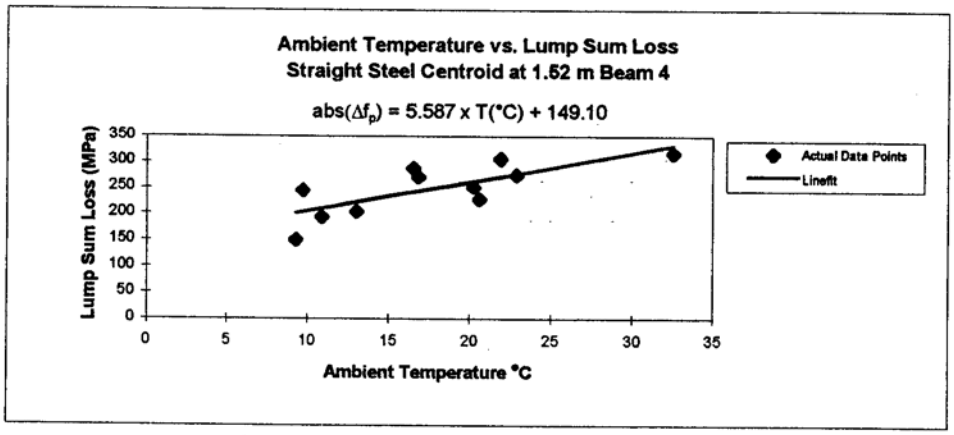

Figure 5-26 Abient temperature 1.52 m Beam 4

5.6 Effects of Prestress Loss on Camber and Deflection

5.6. l Introduction

Camber and deflection of prestressed members are inherently affected by the amount of prestress force at any time, t. With the knowledge of what the prestress loss is at any time, t, a better estimate of the time-dependent camber and deflection can be obtained. Camber and deflection for simply-supported flexural members usually have their maximum values occurring at the midspan.

Typically, in evaluating the equations for camber and deflection of prestressed members, one loss value is assumed at any time and it is considered to be uniform across the cross-section. It has been demonstrated throughout this report, that the prestress loss is not uniform, rather, it varies within an examined cross-section. At what level should the prestress loss within a given cross-section be used in the camber and deflection calculations? Some examples of locations where the loss should be taken are the steel centroid, concrete centroid, and composite centroid.

5.6.2 Field Measurement of Camber and Deflection

The Quality Control personnel, at the Hardaway Company Prestress Division, recorded camber and deflection calculations before the girders were moved to the bridge site. The times at which the readings were taken at the midspan are as follows: immediately after transfer, 28, 60, and 90 days. The values obtained for the midspans

of Beams 1, 4, and 3, can be seen in Table 5-4. These reading will be compared with those calculated using the prestress loss at different levels at the midspan cross-sections of Beams 1, 4, and 3.

Table 5-4 Camber and Deflection Readings

Camber and Deflection Measurements Taken By QC of the Hardaway Company			
Time (days)	Beam 1 (cm)	Beam 4 (cm)	Beam 1 (cm)
Immediately After Transfer (≈0)	6.50	6.03	6.51
28	7.47	7.62	7.14
60	7.62	7.94	7.62
90	7.94	8.26	7.94

5.6.3 Comparing Camber and Deflection Results

The actual measurements obtained in Table 5-4 are compared with the calculated results, based on the actual losses at the steel, girder, and future composite centroids. The method used for calculating the time-dependent camber and deflection is Naaman'S[17] "Simplified C Line Approach." This approach allows for easy incorporation of the effective prestress at any time, t, and assumes uniform loss across the cross-section. The results for the midspans of Beams 1, 4, and 3 can be found in Figure 5-27(a-c). The effective prestress was based on the losses at the steel, girder, and composite centroids, in

order to see which may best model the actual measurements of camber and deflection. From all three of these plots, the camber and deflection are best modeled after the loss at the steel centroid.

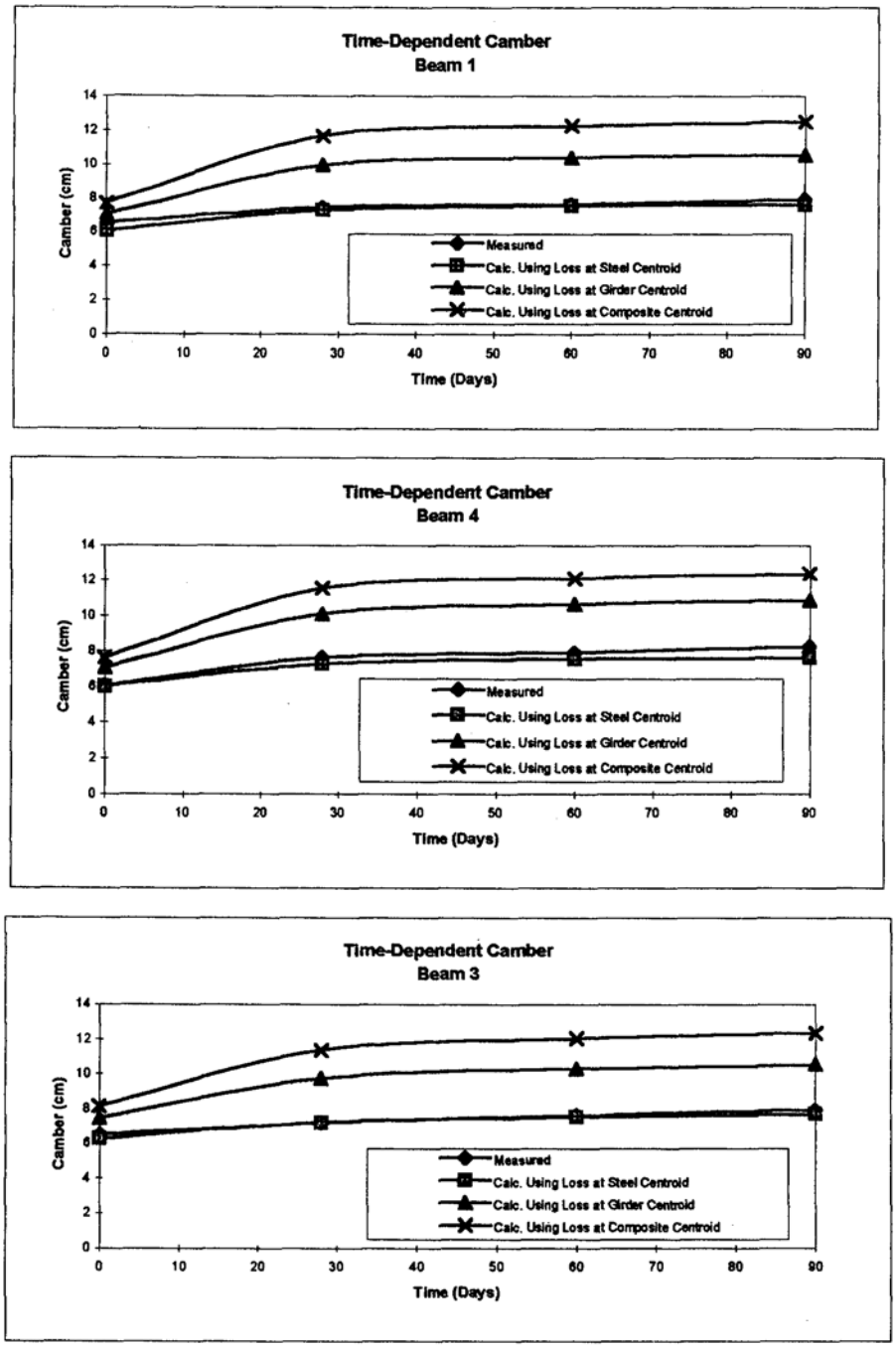

Figure 5-27 Camber (a) Beam 1 (b) Beam 4 (c) Beam 3

APPENDIX A

ACI COMMITTEE 209 METHOD FOR DETERMINING E,(t)

In the text "Concrete Structures: Stresses and Deformations," by Ghali and Farve[18], it suggests a few different methods for determining the time-dependent modulus of elasticity of concrete. The method used here is that which was suggested by the ACI Committee 209.[19] This committee suggests the following equation:

$$\frac{E_c(t_0)}{E_c(28)} = \left(\frac{t_0}{\alpha + \beta t_0}\right)^{\frac{1}{2}} \qquad \text{(A-1)}$$

In Equation A- 1, E,.(to) is the modulus of elasticity of concrete at any time to, a and b are constants based on the type of cement used, and E.(28) is the modulus of concrete at 28 days. The modulus of concrete, E,,(28), can be determined by Equation 2.1, but for high strength concrete ($f_c' > 6000$ psi) it will be overestimated. [20] Carrasquillo, Nilson, and Slate suggest to use the following equation:

$$Ec = 40{,}000\sqrt{f_c'} + 10^6 \text{ psi} \qquad \text{(A-2)}$$

Equation A-2 requires f_c' to be in psi and the corresponding result, E_c will also be in psi.

Table A-1 Modulus of elasticity of concrete calculated according to ACI Committee 209

Design and Calculated Values for E_c			
	Design	Beams 1 and 4	Beams 2 and 3
f_c'	44.818 MPa	57.316 MPa	54.879 MPa
Time (Days)	E_c (MPa)	E_c (MPa)	E_c (MPa)
3	29.138	21.684	21.318
7	30.892	26.874	26.421
14	31.637	30.066	29.558
28	32.030	32.041	31.500
40	32.151	32.873	32.319
60	32.246	33.466	32.901
80	32.293	33.774	33.204
100	32.322	33.963	33.390
120	32.341	34.091	33.516
400	32.409	34.551	33.968
2000	32.432	34.713	34.127
10000	32.437	34.745	34.159

APPENDIX A

ACI COMMITTEE 209 METHOD FOR DETERMINING $E_c(t)$

In the text "Concrete Structures: Stresses and Deformations," by Ghali and Farve[18], it suggests a few different methods for determining the time-dependent modulus of elasticity of concrete. The method used here is that which was suggested by the ACI Committee 209.[19] This committee suggests the following equation:

$$\frac{E_c(t_0)}{E_c(28)} = \left(\frac{t_0}{\alpha + \beta t_0}\right)^{\frac{1}{2}} \qquad \text{(A-1)}$$

In Equation A-1, E,-(to) is the modulus of elasticity of concrete at any time to, a and b are constants based on the type of cement used, and $E_c(28)$ is the modulus of concrete at 28 days. The modulus of concrete, $E_c(28)$, can be determined by Equation 2.1, but for high strength concrete ($f_c' > 6000$ psi) it will be overestimated.[20] Carrasquillo, Nilson, and Slate suggest to use the following equation:

$$Ec = 40{,}000\sqrt{f_c'} + 10^6 \text{ psi} \qquad \text{(A-2)}$$

Equation A-2 requires f_c' to be in psi and the corresponding result, E_c will also be in

Table A-1 Modulus of elasticity of concrete calculated according to ACI Committee 209

Design and Calculated Values for E_c			
	Design	Beams 1 and 4	Beams 2 and 3
f_c'	44.818 MPa	57.316 MPa	54.879 MPa
Time (Days)	E_c (MPa)	E_c (MPa)	E_c (MPa)
3	29.138	21.684	21.318
7	30.892	26.874	26.421
14	31.637	30.066	29.558
28	32.030	32.041	31.500
40	32.151	32.873	32.319
60	32.246	33.466	32.901
80	32.293	33.774	33.204
100	32.322	33.963	33.390
120	32.341	34.091	33.516
400	32.409	34.551	33.968
2000	32.432	34.713	34.127
10000	32.437	34.745	34.159

REFERENCES

'Nilson, Arthur H. Design of Prestressed Concrete. New York: John Wiley & Sons, 1987.

[2]PCI Committee. "Recommendations for Estimating Prestress Losses." PCI Journal July-August 1975: 44-75.

'Lin, T. Y. and Burns, Ned H. Design of Prestressed Concrete Structures. 3rd ed. New York: John Wiley & Sons, 1981.

[4]PCI Institute. PCI Design Handbook: Precast and Prestressed Concrete. 4th ed. Chicago: 1992.

[5]Naaman, Antoine E. Prestress Concrete Analysis and Design Fundamentals. New York: McGraw-Hill Inc., 1982.

[6]Nawy, Edward G. Fundamentals of High Strength High Performance Concrete. Essex, England: Longman Group Limited, 1996.

[7]Finley McNary/Janssen Spaans. State Road No. 600 Westbound Gandy Bridge (Value Engineering Contract). Tallahassee, 1995.

[B]Geokon Inc. Instruction Manual: Models VCE-4200/4202/4210 Vibrating Wire Strain Gages. Lebanon, New Hampshire: 1995.

[9]ACI. Building Code Requirements for Reinforced Concrete (ACI 318-89)S Revised 1992) and Commentary-ACI 318R-89 (Revised 1992,). Detroit, Michigan: American Concrete Institute, 1992.

[10]Ghali, A. and Farve, R. Concrete Structures: Stresses and Deformations 2n[d] Edition. London: E & FN Spon, 1994.

[11]CEB-FIP 1990. Model Code for Concrete Structures (MC-90). London: Thomas Telford, 1993.

[12]AASHTO. AASHTO LRFD Bridge Design Specifications 1st Edition 1994. Washington, D.C.: American Association of State Highway and Transportation Officials, 1994.

[13]See Reference [9]

[14]ACI-ASCE Committee 423. "Estimating Prestress Loses." Concrete International. June 1977: 32-38.

[15]See Reference [2]

[16]See Reference [1]

[17]See Reference [5]

[18]See Reference [10]

[19]ACI Committee 209. "Prediction of Creep, Shrinkage and Temperature Effects in Concrete Structures." 209R-92. ACI, Detroit, Michigan: 47PP.

[20]Carrasquillo, Nilson, and Slate. "Properties of Concrete High-Strength Subject to Short-term Loads." ACI Journal. Vol. 3 1978: 171-178.